SYNTHETIC ANALOGUES OF DINITROSYL IRON COMPLEXES: REACTIVITY STUDIES AND IMPROVEMENTS TOWARDS THERAPEUTIC APPLICATIONS

A Dissertation

by

RANDARA PULUKKODY

Submitted to the Office of Graduate and Professional Studies of
Texas A&M University
in partial fulfillment of the requirements for the degree of

DOCTOR OF PHILOSOPHY

Chair of Committee,	Marcetta Y. Darensbourg
Committee Members,	François P. Gabbaï
	David P. Barondeau
	Gregory D. Reinhart
Head of Department,	François P. Gabbaï

August 2015

Major Subject: Chemistry

ABSTRACT

Dinitrosyl iron complexes (DNICs) are organometallic-like compounds formed endogenously as products of degradation of iron-sulfur clusters by NO or its interaction with the cellular chelatable iron pool. Substantial evidence has accrued on the role of DNICs as endogenous transport and storage agents for the highly reactive NO radical. Such biological significance has led to biomimetic work on such entities in synthetic inorganic chemistry. Recently, such synthetic models have emerged as a new class of potential NO releasing agents. A series of N-heterocyclic carbene (NHC)-stabilized oxidized and reduced DNICs ($\{Fe(NO)_2\}^9$ /$\{Fe(NO)_2\}^{10}$: Enemark-Feltham notation) appeared promising candidates for further investigations on the reactivity of DNICs and on synthetic improvements for possible therapeutic applications.

Planar NHC ligands mimic ligands such as imidazole, itself a surrogate for histidine. A base-promoted conversion was observed of an N-alkyl imidazole bearing, neutral $\{Fe(NO)_2\}^{10}$ DNIC to the NHC-DNIC, while maintaining the $Fe(NO)_2$ unit intact. Subsequent alkylation led to the isolation of the NHC-DNIC product; signifying the integrity of the $Fe(NO)_2$ unit and further establishing that NHCs are 'better' ligands to $Fe(NO)_2$ than imidazoles.

Making use of an NHC-stabilized DNIC $[(NHC)(RS)Fe(NO)_2]$, a RS^-/RS• oxidation process in the presence of added CO was discovered, wherein the oxidized $\{Fe(NO)_2\}^9$ is reduced to $\{Fe(NO)_2\}^{10}$ through carbon monoxide (CO)/RS• ligand substitution. Kinetic studies established a bimolecular rate law and activation parameters

suggested an associative mechanism. Computational results indicated a unique role for the delocalized frontier molecular orbitals of the $Fe(NO)_2$ unit, involving an initial side-on approach of CO to the electron-rich N-Fe-N site.

Attempts to further test the aforementioned computational proposal employed classical Hammett correlations for the elucidation of structure-activity relationships. Hammett correlations were used to monitor the changes in electron density at the $\{Fe(NO)_2\}$ unit and effects on the rate of reaction with CO of a series of $(NHC)(SPhX)Fe(NO)_2$ derivatives with varying *para* substituents at the aryl thiolate. In accordance with the computational mechanistic proposal, rate enhancement was observed with increasing electron donating ability of the substituents.

Although DNICs appear to be promising candidates in the context of nitric oxide releasing therapeutics, their lack of biocompatibility has hindered the progress of such applicability. The first examples of 'sugar appended' monomeric and dimeric DNICs were synthesized, making use of the tuning sites provided by the NHC-DNIC architecture. Such efforts are among the few examples for the synthesis of bio-functionalized DNICs.

DEDICATION

To my parents, who dedicated their lives to making me the person I am today, and to my husband, for always being my comfort and my strength.

ACKNOWLEDGEMENTS

The graduate school experience at Texas A&M University for me has been an extremely valuable and rewarding training. I would like to extend my sincere gratitude to my advisor Dr. Marcetta Y. Darensbourg, for taking me under her wing and training me to become a better scientist. Her great love and passion for her work, her attention to detail and perfection, and the respect she shows to her peers and their work, are values that I will always remember as those of an exemplary scientist. I am extremely thankful to her for the many opportunities I had to present my work at various conferences, for the long hours spent improving my writing and for her valuable advice and guidance regarding my long term career goals. I consider it a great privilege to have been her student.

I would like to thank my committee members, Dr. François Gabbaï, Dr. David Barondeau and Dr. Gregory Reinhart for taking time off their busy schedules to serve on my committee, for their helpful input regarding my work and for teaching some of my favorite classes in graduate school. The work reported in this dissertation was enhanced by the input and expertise of Dr. D. J. Darensbourg. I am extremely thankful to him for this, and also for the opportunity I was given to be his assistant in the green chemistry course, which was a great experience. I wish to thank Dr. Nattamai Bhuvanesh of the x-ray crystallography facility, for always being willing to help, and for his generous advice. I also wish to extend my gratitude to Dr. E. B. Soriaga and Dr. S. M. Lim, for a wonderful teaching experience in the quantitative analysis laboratory.

Thank you to all the members of the MYD and DJD groups, old and new, for making it a welcoming hallway with plenty of food all the time! I must especially mention and thank Dr. Chung-Hung Hsieh (Mark) for being my mentor in the lab, for his patience in training me and for introducing me to the field of dinitrosyl iron chemistry. I was very fortunate to have been trained by such an accomplished synthetic chemist and I thank him sincerely for his support and guidance that helped me achieve this goal. I also thank Tiffany Pinder for being a good friend, for encouraging me to be a part of the many outreach activities, and for all the career advice.

The current MYD group members, Danielle Crouthers, Jason Denny, Pokhraj Ghosh, Allen Lunsford, Rachel Chupik and Shengda Ding, thanks for being there to get my many questions answered and for being willing to help anytime I needed it. I had a great time working with you all! To two wonderful undergraduates whose contributions are a part of the work included in this dissertation; Michael Drummond and Steven Montalvo, thanks for helping me to get things done. Thank you to members of the DJD group, especially Sam, for his contribution that enriched my chemistry, and also for his friendship. Thank you also to Joanna and Andrew, for being such good friends from the start of our time here at A&M. Our wonderful administrative assistant, Ethel, thank you so much for everything you do.

Life outside of school has been exciting thanks to my wonderful friends, and I am thankful to all of them for the support, fun times and the memories. I have been truly blessed to be a part of a loving and supportive family. My grandmother (achchi), thank you for taking care of me and for wishing me nothing but the best in life. My spoilt

sister, Randinu (mawwa), thank you for making my life interesting, and I know you will one day become a better chemist than I am. My parents, the two most wonderful parents one could ever wish for, I thank them for all the sacrifices they made to see me here today. Ammi, thanks for pushing me to be a balanced, disciplined individual, and thaththi, everything about you is what I have always aspired to be. Last, but not least, to my husband, my best friend and my greatest strength, Ramesh; thank you for being the shoulder I cry on and the force that carries me through. I know I have become a better person because of your love, and this journey would not have been possible without you.

TABLE OF CONTENTS

Page

Page

LIST OF FIGURES

FIGURE Page

FIGURE Page

FIGURE Page

FIGURE Page

FIGURE Page

FIGURE Page

LIST OF TABLES

CHAPTER I

INTRODUCTION*

Diatomic ligands in biology

The simplest of ligands in a coordination chemist's toolbox, CO, CN^-, and NO, are known to play extremely important roles in biology. That their fundamental bonding abilities range from strong to weak, and from spectators to "non-innocent" redox assistants of metals, is consistent with nature's amazing ability to manipulate common molecules to achieve the most sophisticated functions. Our knowledge has expanded from recognition of the effects of such diatomics as toxins, to biological research of enzyme mechanisms in which CO and CN^- are deliberately added as inhibitors. As detectors of bioactive metals, the use of CO for its vibrational spectral signature, and of NO as an EPR active spin label, has become the fundamental basis of breakthroughs that identified their endogenous roles as signaling and regulatory agents. Later discoveries that CO and CN^- were biosynthesized in a highly controlled fashion for the purpose of building the hydrogenase enzyme active sites came as a profound (and delightful) surprise to biochemists and organometallic chemists alike.[1]

*Reproduced in part with permission from Pulukkody, R.; Darensbourg, M. Y. *Accounts Chem. Res.* **2015**, *48*, 2049–2058. Copyright **2015** American Chemical Society.

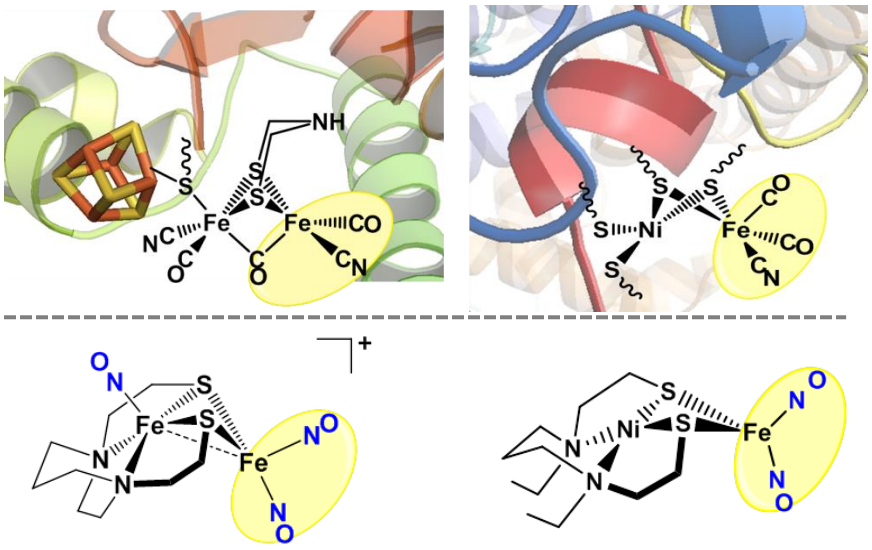

Figure I-1. Top: Depictions (generated using PyMOL) of active sites of [FeFe]-H_2ase[2] and [NiFe]-H_2ase.[3] Bottom: Corresponding $Fe(NO)_2$-containing model compounds.[4,5]

The pyramidal $Fe(CO)(CN)_2$ unit of the [NiFe]-H_2ase active site, and the diiron unit within the H_2-producing, H-cluster of the [FeFe]-H_2ase active site has inspired synthetic modifications of readily accessible small molecule mimics.[6] An isoelectronic analogue of the pyramidal $[Fe^{II}(CO)(CN)_2]$ or $Fe^{I}(CO)_3$ units, the redox active dinitrosyl iron units (DNIUs) $[Fe(NO)_2]^0$ or $[Fe(NO)_2]^+$ were early described as possibilities for building biomimetics of H_2ase active sites (Figure I-1).[5,7] While the first report of a [NiFe]-H_2ase active site model making use of such a dinitrosyliron unit saw no catalytic activity, a recent one purportedly mimicking features of the [FeFe]-H_2ase catalytic site is a modest catalyst for proton reduction (Figure I-1).[4] The latter takes advantage of the two redox levels of DNIUs, described in Figure I-2 according to the Enemark-Feltham electron counting scheme[8] and also by the oxidation state approach of Ye and Neese.[9]

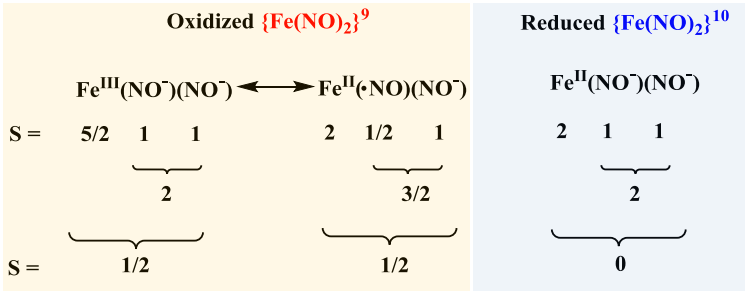

Figure I-2. Correlation of Enemark – Feltham approach[8] to electron count with oxidation states of Fe and NO in oxidized and reduced DNIUs.[9]

Endogenous nitric oxide and the formation of dinitrosyl iron complexes (DNICs)

Nitric oxide (NO), long known as a noxious environmental pollutant, went through a dramatic change in reputation with the discovery of its role as an endogenous messenger. Claimed by *Science* as the molecule of the year in 1992,[10] it was the subject of the Nobel Prize in medicine in 1998[11-13] and is known today to be involved in a variety of physiological processes including blood pressure regulation, neurotransmission and immune response.[14] The endogenous synthesis of NO occurs during the conversion of L-arginine to citrulline by the nitric oxide synthase (NOS) family of enzymes.[15,16] The most widely known biological target of NO is the porphyrin iron of guanylyl cyclase, which catalyzes the formation of the secondary messenger, cyclic guanosine monophosphate (cGMP), by which NO exerts its classical signaling function.[17,18] The myriad chemical reactivity observed of NO *in vivo* suggests the existence, as well as activity of its redox counterparts, oxidized nitrosonium cation (NO^+), or reduced nitroxyl anion (NO^-), through which a variety of reactive nitrogen species (RNS) such as NO_2, NO_2^-, NO_3^- are formed.[14] Many reviews can be found in the

literature on the role of NO as related to bioinorganic chemistry.[19,20] Of particular interest is a comprehensive account of the major areas in NO chemistry found in a special issue of Chem. Review 2002, volume 102, titled 'Nitric oxide chemistry'.

The notable ability of the $Fe(NO)_2$ unit described above to exist as an intact organometallic entity in biology is revealed by the existence of four-coordinate tetrahedral dinitrosyl iron complexes (DNICs), first identified by a characteristic EPR signal at $g_{avg} = 2.03$, and readily related to dithiolates, $(RS)_2Fe(NO)_2^-$.[21] Derived from the action of nitric oxide on the cellular, chelatable iron pool,[22] or by NO degradation of iron sulfur clusters,[23] it has been suggested that there exists equilibria between intracellular protein-bound DNICs and low molecular weight forms, the latter composed of amino acid or small peptide-complexed DNIUs.[24] As a highly reactive radical, free NO has a short life span of 2 ms – 2 s.[25] Stabilization for NO transport and storage *in vivo* is presumed to need small biomolecule-complexed entities. Studies involving the multi-drug resistance protein 1 (MRP1) and the glutathione-*S*-transferase group of enzymes have reported that DNICs are involved in the transport and storage of endogenous NO.[25] This suggestion is supported by a protein crystal structure of the glutathione-*S*-tranferase enzyme containing $Fe(NO)_2$, provided to the transferase in the form of a diglutathione complex, that is imbedded within the glutathione-binding site (Figure I-3).[26]

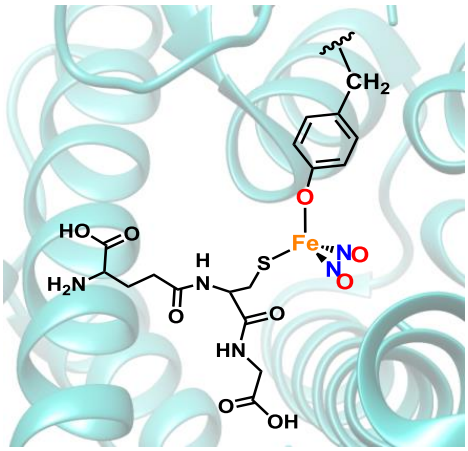

Figure I-3. The glutathione-DNIC trapped within the active site of Glutathione transferase.[15] (Figure generated using UCSF Chimera)

Nitric oxide donors

Therapeutic responses of NO in the cardiovascular, immune and nervous systems have led to extensive studies on exogenous sources of NO, which can release NO *in vivo* or *in vitro* as pharmaceutical agents. Lately, such NO donors have been the subject of several excellent reviews and entire books.[27-31] The importance of such chemical agents particularly lies in the difficulty of delivering gaseous NO into biological systems in a specific and controlled manner. Several NO donors are currently in clinical use, and a selection is shown in Figure I-4. Three kinds of general mechanisms have been outlined by which these compounds release NO. Diazeniumdiolates and S-nitrosothiols are known to release NO 'spontaneously', i.e., through thermal or photochemical decomposition. A second route, known for organic nitrates and nitrites is through chemical reactions with compounds such as thiols, and a third route, applicable to many classes of donors is through enzymatic activation.[28] Only a few metal-containing NO-donors have been reported, among which sodium nitroprusside (SNP) is the first

transition metal-NO complex ever reported. SNP is considered to release NO photochemically, or by reacting with thiols and other biological reductants.[31] Historically, SNP was used to treat hypertension, despite the slow release of CN^- which was detoxified by thiosulfate ions, using enzymatic means. However, the lack of sufficient thiosulfate is known to result in the rapid elevation of CN^- to toxic levels.[19]

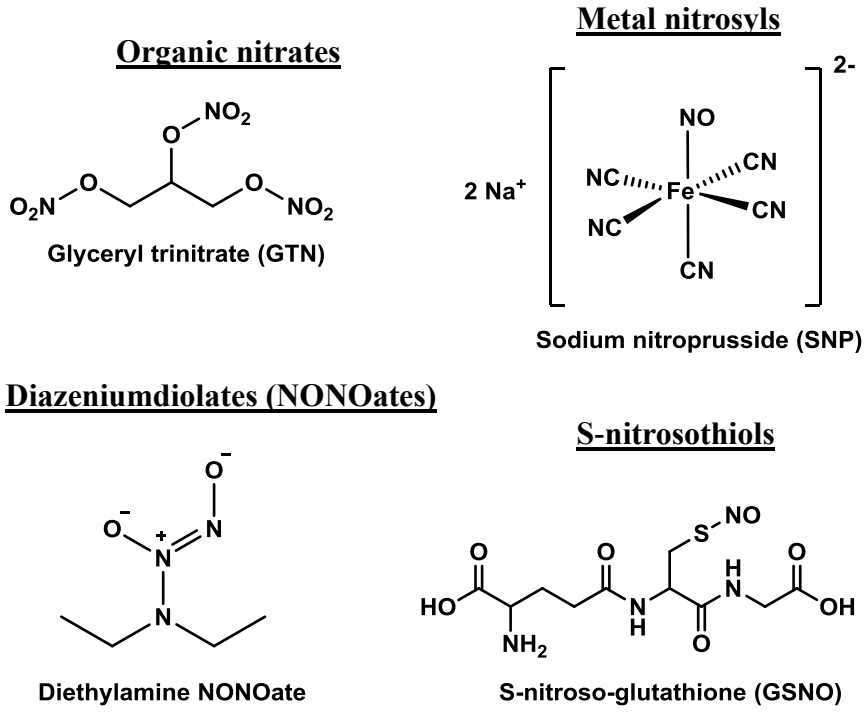

Figure I-4. Selected NO donors currently used in the clinic.[31]

Dimeric DNIU containing compounds are non-heme [Fe-S] cluster nitrosyls commonly known as Roussin's red esters (RRE), $(\mu\text{-RS})_2[Fe(NO)_2]_2$.[32] They have been extensively studied for photo-induced NO release by Ford *et al.* who found that reactivity, optical profile and solubility could be altered by varying the R groups.[33,34] Their potential as efficient NO generators was seen in a study of a series of RREs (where R = methyl, ethyl, benzyl, hydroxyethyl and sulfonatoethyl) that showed photodecomposition into 4 moles of NO per mole of parent compound in aerated solutions. The primary photochemical step of this process was NO dissociation, resulting in a $Fe_2(\mu\text{-RS})_2(NO)_3$ intermediate, which, in the presence of O_2 was proposed to form an unknown species that decomposes irreversibly while releasing the remaining NO.[33] Ford *et al.* also report more elaborate molecular constructs where the RREs have been modified with pendent antennae, as a strategy to enhance visible light photoreaction. Two such modified RREs are shown in Figure I-5. The first (PPIX-RSE) bears a derivative of protoporphyrin-IX and the second (Fluor-RSE) contains two pendant fluorescein dye units attached to the $Fe_2S_2(NO)_4$ core. The photochemistry of these compounds were similar to the other RREs studied, releasing 4 moles of NO per mole of parent molecule, with much higher rates than the simpler RREs.[34] A study by Liaw *et al.* on a water-soluble, RRE, $[Fe(\mu\text{-}SC_2H_4COOH)(NO)_2]_2$ also showed complete NO release (4 moles of NO per mole of RRE) in cell culture media as determined by the Griess assay. Using EPR spectroscopic studies, it was shown that this RRE could be transported into cells and transformed into paramagnetic protein-bound, or low molecular weight, $\{Fe(NO)_2\}^9$ DNICs.[35]

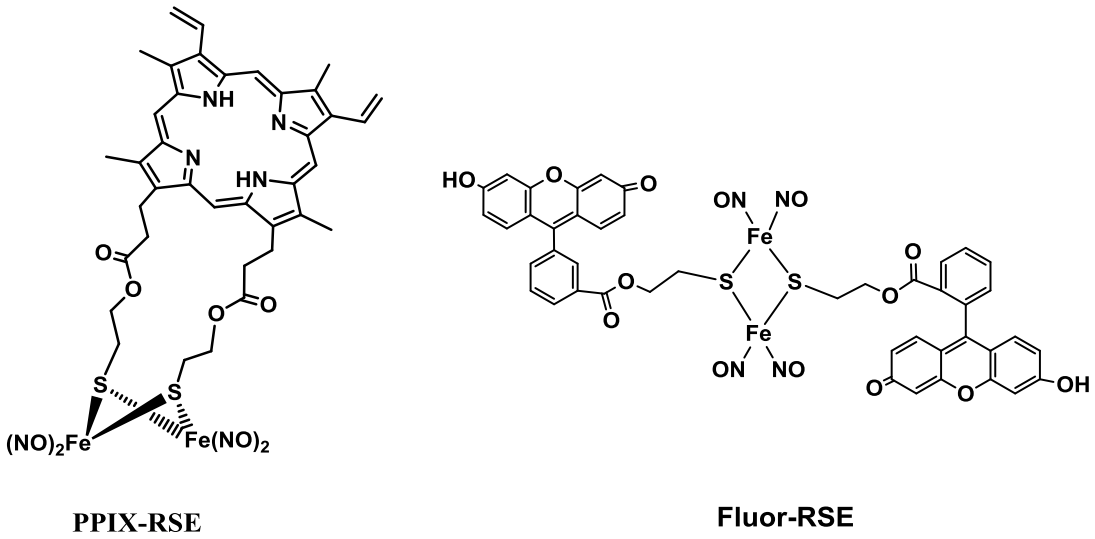

Figure I-5. Structures of Roussin's red esters with strongly absorbing chromophores.[34]

Monomeric DNICs have recently emerged as a potential new class of NO-releasing drugs.[36] Their NO release ability as well as other necessary properties can be modulated by altering the electronic and steric properties of the ancillary ligands, which thereby provide control over the DNIC's NO storage, transport and targeting abilities. Of particular interest are the studies carried out by Vannin *et al.* on simple water soluble DNICs with thiol ligands (cysteine or glutathione).[36] A stable hypotensive preparation of DNIC with glutathione has been formulated as a result of these studies under the commercial name Oxacom®.[37] As a pharmaceutical, it has demonstrated versatile physiological properties including prolonged hypotension, attenuated platelet and erythrocyte aggregation, promotion of skin wound healing and effects on penile erection. Oxacom® is currently in phase II clinical trials.[38] However, details on the mechanism/ triggers of NO release from these compounds are not clearly understood. More recently,

Kim *et al.* reported the use of monomeric synthetic DNICs, [Fe(TMEDA)$(NO)_2$] (TMEDA = *N,N,N',N'*-tetramethylethylenediamine) and [Fe(TMEDA)$(NO)_2$I] where chemical oxidation of the former and removal of the iodide ligand from the latter led to spontaneous NO release through the formation of a putative 4-coordinate $\{Fe(NO)_2\}^9$ DNIC, $[Fe(TMEDA)(NO)_2]^+$.[39] Tests on the use of [Fe(TMEDA)$(NO)_2$I] as a pro-drug candidate of an NO releasing agent showed that upon entering the cell, a cationic DNIC is formed, that readily releases NO.

Synthetic models of monomeric DNICs

Mimicking the reactivity of biological DNICs and the development of DNICs as NO release agents have prompted the synthesis and characterization of a library of monomeric synthetic DNICs, which are typically four coordinate with pseudotetrahedral geometry. An excellent review of this synthetic literature is seen in a recent review by Kim *et al.*[40] An electron-tracking scheme devised by Enemark and Feltham (the E−F notation)[8] described earlier in this chapter, avoids the thorny issue of iron oxidation state assignment in the presence of the highly delocalizing NO ligand and assigns the oxidized DNICs, as a redox active unit with an overall valence electron count of $\{Fe(NO)_2\}^9$, and the reduced form, $\{Fe(NO)_2\}^{10}$.

The oxidized, EPR active form can be found as the more common anionic $X_2Fe(NO)_2^-$ complexes, or neutral $L(X)Fe(NO)_2$ (where for example X = halides, or thiolate S-donors and L = N-donors or the good sigma donor ligands N-heterocyclic carbenes (NHC)).[41-45] The contribution by Liaw, *et al.* to this area has been significant

and has been reviewed recently.[46] They have demonstrated that the dimeric RREs can be cleaved by a variety of thiolates to form anionic bis-thiolate DNICs and numerous reactivity studies have been carried out involving such oxidized DNIC models. For example, Liaw *et al.* reported the first biomimetic study on the degradation and reassembly of a [2Fe-2S] cluster, involving a $(RS)_2Fe(NO)_2^-$ type DNIC with an S_5^{2-} ligand (Figure I-6 (a)). They described the conversion of the [2Fe-2S] cluster into the DNIC by nitrosylation, and reconversion of the DNIC into the cluster by photolysis in the presence of an NO trapping agent.[47] Extending their contributions to this area, Liaw also reported the synthesis and characterization of several rare five and six coordinate DNICs.[48] A study by Kim *et al.* on the O_2 reactivity of $(RS)_2Fe(NO)_2^-$ type DNICs (Figure I-6 (b)) showed the conversion of the DNIC into RREs and other thiol oxidation products including disulfides.[49]

Neutral $\{Fe(NO)_2\}^9$ DNICs are less common compared to the anionic counterpart, and a series of such complexes with NHC ligands have been synthesized by the Darensbourg group and are discussed later in this chapter. Lippard *et al.* have synthesized and characterized a neutral $\{Fe(NO)_2\}^9$ DNIC, (and its reduced analogue, $[(Ar\text{-}nacnac)Fe(NO)_2]^{0/-}$ respectively,[45] where Ar-nacnac = [(2,6-diisopropylphenyl)NC-(Me)]$_2$CH) and showed it was a NO source in the reductive nitrosylation of Fe^{III}(TPP)Cl in the presence of light or elevated temperatures (Figure I-6 (c)).[50]

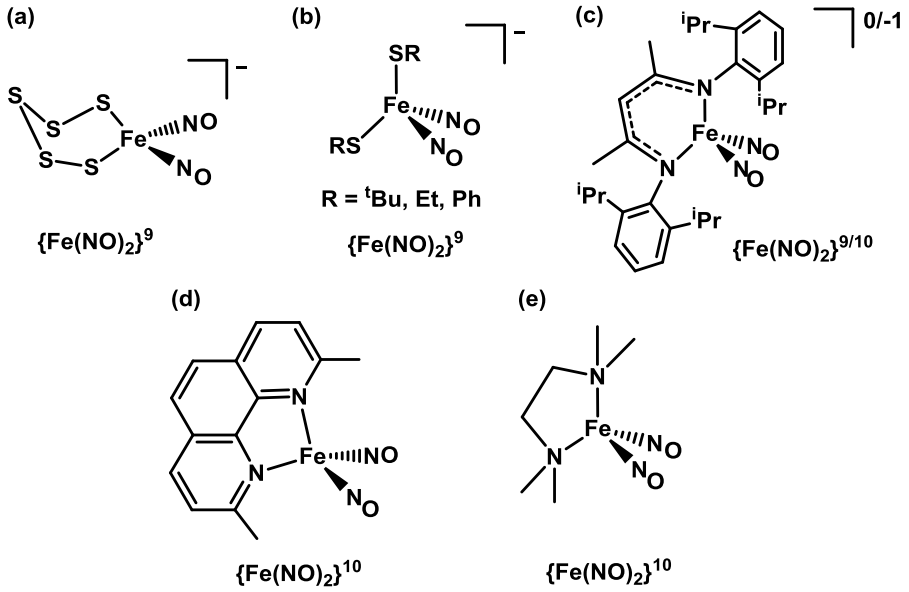

Figure I-6. Representative DNICs of different redox levels.[45,47,49,51,52]

The EPR silent, reduced form of DNICs can be found in $L_2Fe(NO)_2$ complexes, with the paradigm being the 18-electron species, $(OC)_2Fe(NO)_2$, a versatile precursor to $LFe(CO)(NO)_2$ derivatives (L = CO, PR_3, imidazole, NHC etc.).[41,53-55] While the NHC and imidazole-DNICs are discussed later in this chapter, several distinctive reactivity patterns have been observed for other neutral DNICs. For example, Kim *et al.* extended their O_2 reactivity study to neutral N-bound $\{Fe(NO)_2\}^{10}$ DNICs with ligands such as TMEDA and dmp (dmp = 2,9-dimethyl-1,10-phenanthroline) (Figure I-6(d) and (e)).[51,52] These compounds were capable of nitrating phenolic substrates, which was concluded to occur through a peroxynitrite ($ONOO^-$) intermediate. In the absence of substrate, thermally stable nitrato species were formed due to iron-peroxynitrite isomerization, that could be isolated and characterized in the case of the dmp.[52]

Despite the extensive literature devoted to the chemistry and biochemistry of DNICs, the fundamental features that control redox level inter-conversion of the intact $Fe(NO)_2$ unit or NO release in biologically relevant ligating environments remain incompletely defined. The Darensbourg group has employed two main types of unique ligand sets that are able to impart stability on the resulting dinitrosyl iron complexes (DNICs): MN_2S_2 and N-heterocyclic carbene (NHC) ligands. The former has enabled studies of the redox versatility of the DNIU in models of hydrogenase active site mimics. The NHC ligands have been used as analogues of histidine, offering stable models of the biological N-bound, neutral ligands. Thus, the rest of this chapter will review the work done in this area by the M. Y. Darensbourg laboratory.

Metallodithiolate ligands to $Fe(NO)_2$

The stabilization of $Fe(NO)_2$ in its two redox levels by identical donors has been accommodated by only a few ligands.[40,45] The metallodithiolates used involve a contiguous arrangement of nitrogen and sulfur donor sites that mimic the cys-gly-cys or cys-ser-cys peptide motifs and thiolate-S/ amido-N "backbone" binding sites.[56,57] Such N_2S_2 sites, for which an extensive literature is available, are known to ligate Ni^{2+}, iron (as $Fe(NO)^{2+}$, or, by the Enemark-Feltham notation,[8] $\{Fe(NO)\}^7$), and cobalt (as $Co(NO)^{2+}$, or $\{Co(NO)\}^8$) within a largely planar N_2S_2 binding pocket.[58] The cis-dithiolate sulfurs have available lone pairs that are well oriented to further serve as mono- or bidentate ligands to exogeneous metals, and in fact can control aggregation of up to four exogeneous metals per MN_2S_2.[58] The versatility of such metallodithiolate

ligands has been demonstrated in the formation of a variety of heterometallic, S-bridged structures, including those in which the reduced $Fe(NO)_2$ unit, DNIU, has produced heterobimetallic NiFe (Ni(μSR)-$Fe(NO)_2$) and heterotrimetallic $NiFe_2$ (Ni(μSR)-$[Fe(NO)_2]_2$) complexes as well as higher order neutral, cage clusters.[58] The structural analogy to Cu^I bridged moieties that also display open-site, or incomplete, adamantane $[CuN_2S_2]_2[CuCl]_3$ arrangements prompted questions as to the relationship of the Cu^I-d^{10} electronic configuration and corresponding structural propensities to that of the reduced DNIU, also with an electron count of $\{Fe(NO)_2\}^{10}$.[59] This collection of complexes has indicated an intricate interplay of DNIU redox levels and the stability of the MN_2S_2 donor/$Fe(NO)_2$ acceptor adducts.

The Darensbourg laboratory focuses on diazacycles as frameworks for attachment of mercapto-ethane arms that yield stable, readily modifiable, neutral MN_2S_2 metalloligands. Table I-1 lists examples of DNICs in two redox levels, $\{Fe(NO)_2\}^9$ and $\{Fe(NO)_2\}^{10}$, with traditional as well as the NHC and MN_2S_2 ligands. The paradigm for the oxidized DNIC, complex **1**, is found stabilized by PhS^-; another example is the dithiolate/thioether $[S(CH_2CH_2)]_2S]^{2-}$ bound to $Ni^0(NO)^+$, complex **2**.[7] The resultant anionic NiS_2 ligand of **2** is charge neutralized by the cationic $\{Fe(NO)_2\}^9$. In contrast, the Ni(bme-daco)$Fe(NO)_2$ complex **8** demonstrated the ability of Ni^{2+} to produce a thiolate sufficiently "tamed" so as to stabilize the $\{Fe(NO)_2\}^{10}$, i.e., the reduced DNIU.[7] Both neutral complexes, **2** and **3**, have ν(NO) values that place them within the expectations for the DNIU within the respective redox levels.

Table I-1. Selected $\{Fe(NO)_2\}$ complexes containing NHC/MN_2S_2 ligands.

	$\{Fe(NO)_2\}^9$	$\nu(NO)$ (cm^{-1})[a]
1[60]	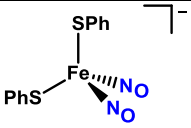	1709, 1744
2[7]	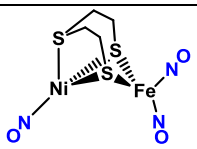	1725, 1767, (1805)
3^{+}[4]	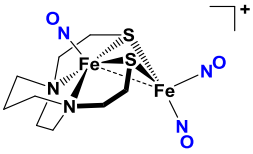	1742, 1796 (1761)
4[41]	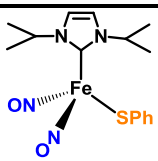	1712, 1757
	$\{Fe(NO)_2\}^{10}$	$\nu(NO)$ (cm^{-1}) [a]
5[53]	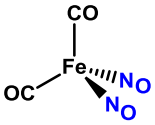	1756, 1810 (2034, 2087)
6[41]	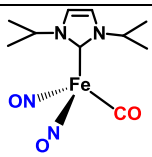	1696, 1738 (1988)
7[41]	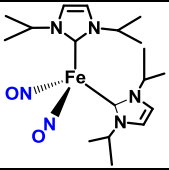	1619, 1664
8[7]		1630, 1677
3[4]	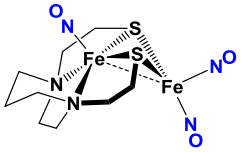	1640, 1690 (1662)

[a] $\nu(NO)$ data for the $Fe(NO)_2$ unit with $\nu(NO)$ or $\nu(CO)$ of additional diatomic in parenthesis

Entries $\mathbf{3}^+$ and **3** of Table I-1 are examples of identical formulations of $MN_2S_2{\cdot}Fe(NO)_2$ in two redox levels. The ν(NO) report of electron densities and π backbonding from the $Fe(NO)_2$ units find a ca. 100 cm^{-1} shift to lower values in the $\{Fe(NO)_2\}^9$ to $\{Fe(NO)_2\}^{10}$ reduction.[4] Consistently, the ν(NO) values of the Fe(NO) unit imbedded in the N_2S_2 binding pocket, are also displaced by ca. 100 cm^{-1} to lower values, implying that less electron density is drained from the $\{Fe(NO)\}^7$ by $\{Fe(NO)_2\}^{10}$ as compared to $\{Fe(NO)_2\}^9$. Notably, the Fe···Fe distances of 2.786 (1) Å in $\mathbf{3}^+$, and 3.006 (1) Å in **3**, as well as spin-spin anti-ferromagnetic coupling in $\mathbf{3}^+$, imply Fe···Fe interaction. Nevertheless, electrochemical, spectroscopic and DFT computations suggest the reduction of $\mathbf{3}^+$ to **3** involves localizing the added electron to the DNIU, generating $\{Fe(NO)_2\}^{10}$.[4] The latter is very air and thermally sensitive, in strong contrast to the stability of the oxidized complex $\mathbf{3}^+$. In fact, several reactions have found the $Fe_2(NO)_3^+$ motif of $\mathbf{3}^+$ to be a common, sometimes unexpected, byproduct, reflecting its thermodynamic stability.

Synthetic approaches to the $MN_2S_2Fe(NO)_2$ platforms

Figure I-7 displays synthetic routes to several DNICs making use of the reduced $Fe(CO)_2(NO)_2$ synthon, especially for $MN_2S_2{\bullet}Fe(NO)_2$ derivatives. Simple mixing with Ni(bme-dach) yields the $NiN_2S_2{\bullet}Fe(NO)_2(CO)$ complex, replacing only one CO with NiN_2S_2 in a monodentate binding mode.[61] A "one-pot" mixture of the [Fe(bme-dach)]$_2$/$Fe(CO)_2(NO)_2$ with NO^+ leads to loss of CO with formation of complex $\mathbf{3}^+$.[4] Addition of I_2 to $Fe(CO)_2(NO)_2$ generates the iodide-bridged, oxidized $\{Fe(NO)_2\}^9$

dimer, which itself can be used to generate $Fe(NO)_2I$ derivatives of the NHC, the vanadyl-N_2S_2, or the NiN_2S_2 metalloligand, Figure 6.[62] Notably, the $(\mu\text{-}I)_2[Fe(NO)_2]_2$ dimer[63] is the analogue of the RRE, $(\mu\text{-}RS)_2[Fe(NO)_2]_2$,[64] described later as a useful synthon for thiolate-containing DNICs.

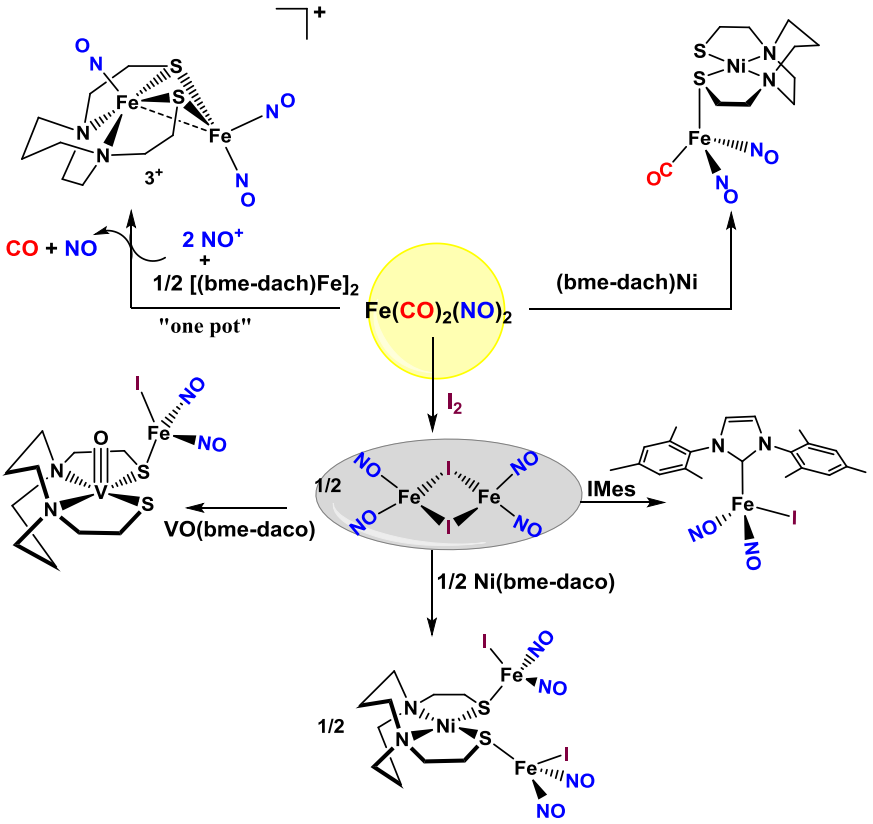

Figure I-7. Synthetic routes *via* the $Fe(CO)_2(NO)_2$ synthon.

An especially useful synthon for the preparation of MN_2S_2-DNIC derivatives has been the NHC stabilized trinitrosyl iron complex, a TNIC, shown in Figure I-8 (prepared by Dr. Chung-Hung Hsieh in the MYD labs and further discussed later). Addition of dimeric $[(bme\text{-}dach)M]_2$, M = Co and Fe, results in NO transfer to the metals of the dimers with subsequent loss of the NHC in the case of Fe, generating the very stable

complex $\mathbf{3}^{+}$.[65] For M = Co, known to be an even better scavenger of NO than the Fe complex, the $Co(NO)N_2S_2$ metallothiolate produces monodentate S-binding (complex **9**), as shown in Figure I-8.[66] The reason why the displacement of the NHC is not favored for this metallodithiolate ligand is not clear, as it has been established to have almost identical spectroscopic and electrochemical properties as its iron analogue, with the exception that the latter $\{Fe(NO)\}^{9}$ unit is paramagnetic, S = ½, while the $\{Co(NO)\}^{10}$, reasonably formulated as a $Co^{III}(NO^{-})$ unit, is diamagnetic.

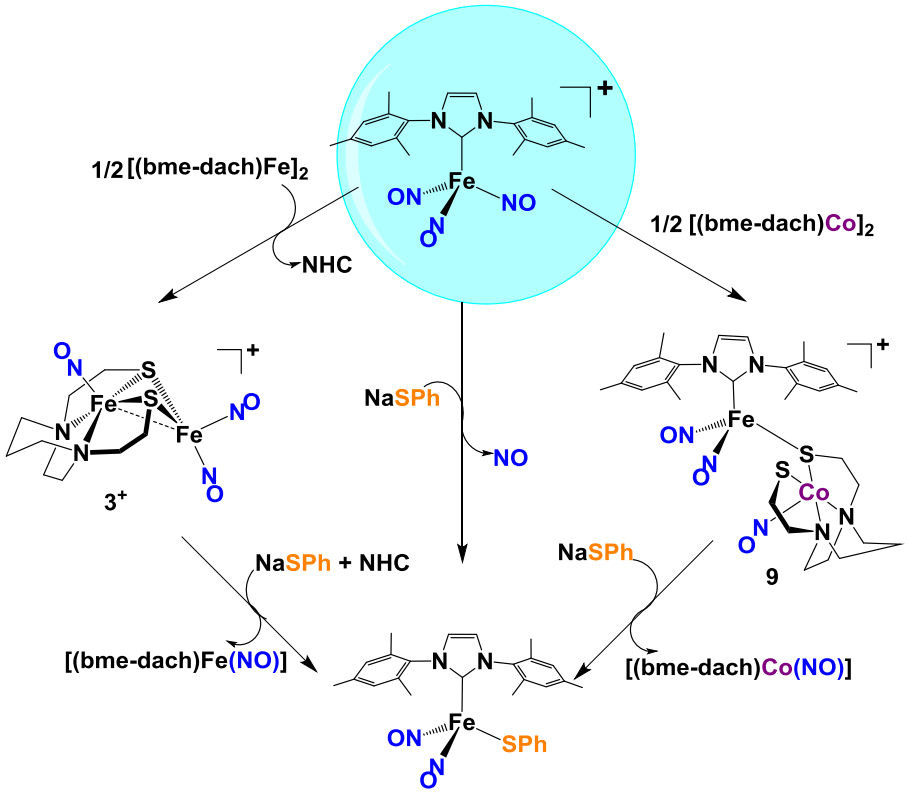

Figure I-8. Synthetic routes *via* the NHC trinitrosyl iron complex.

A biomimetic design

The ability of the N_2S_2 ligand to sequester Fe(NO) was used to advantage in the exploration of NO release from $\{Fe(NO)_2\}^9$. As a biomimetic for protein-bound $Fe(NO)_2$, the protonated bme-daco ligand, with two anionic thiolates available for bonding, was used as an analogue of the sulfurs in -Cys-X_n-Cys- motifs that are expected to account for Vanin's hypothesis[24] for a protein-bound, high molecular weight DNIC, Figure I-9. The (H^+-bme-daco)$Fe(NO)_2$ complex **10**, prepared from the reaction of the free ligand as a dithiol with $[I_2Fe(NO)_2]^-$, was isolated and crystallized at low temperatures, and its structure determined by x-ray diffraction.[67] Solution studies found that in the presence of an NO acceptor, such as an iron porphyrin, serving as a model for the active site of soluble guanylyl cyclase (a primary target of NO in cells), an NO was removed from the DNIC. As indicated in Figure I-9, the remaining Fe(NO) slipped into the N_2S_2 binding site, forming the highly stable $Fe(NO)N_2S_2$.[67,68] To our knowledge, the analogous biochemical process expressed in Figure I-9 (left panel), i.e. the formation of the mononitrosyl derivative as a product concurrent with NO transfer, has not been proposed by others. As the signature EPR signal of the Cys-X_n-Cys•Fe(NO) is expected to be the same as the small molecule $\{Fe(NO)\}^7$ model, g = 2.05, such similarity to the characteristic $\{Fe(NO)_2\}^9$ signal of g = 2.03 might have prevented its discovery.

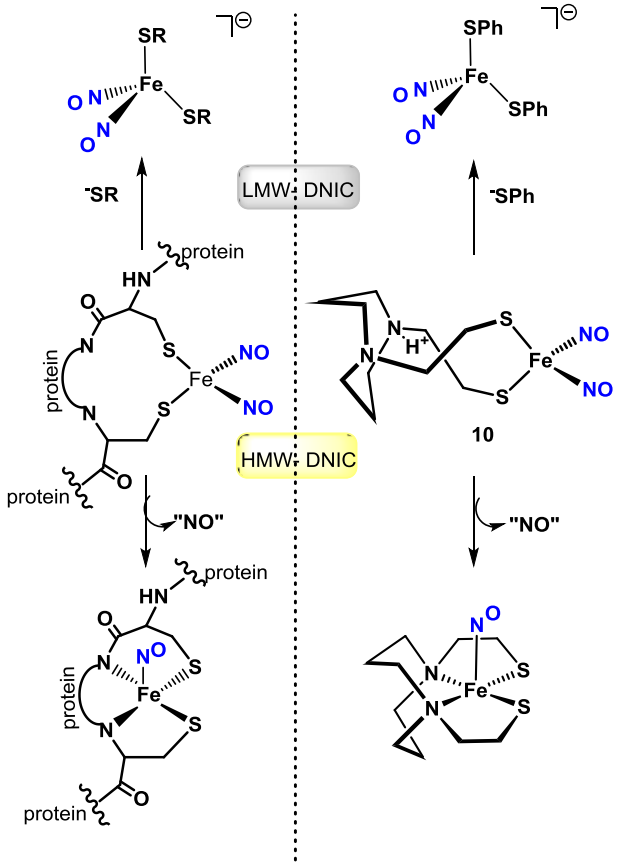

Figure I-9. Right panel: The $(H^+$-bme-daco)$Fe(NO)_2$ complex as a biomimetic for protein-bound $Fe(NO)_2$. Left panel: Proposed analogous biochemical process.[67,68]

The $(H^+$-bme-daco)$Fe(NO)_2$ complex **10** also served to model transfer of the intact $Fe(NO)_2$ unit from the protein bound, high molecular weight DNIC, to a mobile, low molecular weight form, LMW-DNIC, Figure I-9. In the presence of PhS^- as a mimic of thiolates from free cysteine or glutathione, the $(PhS)_2Fe(NO)_2^-$ was obtained within time of mixing.[67]

Synthetic models of histidine bound biological DNICs

The DNICs containing N-donor ligand sets, primarily of the neutral $L_2Fe(NO)_2$ ($\{Fe(NO)_2\}^{10}$) and $L(X)Fe(NO)_2$ ($\{Fe(NO)_2\}^{9}$) types are of interest, as such ligands mimic the coordination of histidine to $Fe(NO)_2$. While the more common cysteine coordination can be considered as a straightforward thiolate ligand binding, histidine coordination to metals is relatively more complex due the possibility of two N-binding sites: a nitrogen base and a second imidazole amine nitrogen that can be deprotonated.

Li *et al.* prepared a series of six imidazole-DNICs as surrogates of histidine-DNICs by reaction with $Fe(CO)_2(NO)_2$, the common starting precursor for $\{Fe(NO)_2\}^{10}$ DNICs.[55,69] Within the series, only $Fe(NO)_2$(1-MeIm)$_2$ (1-MeIm = 1-methyl imidazole) could be isolated and characterized in its reduced, $\{Fe(NO)_2\}^{10}$ form.[55] All derivatives were found to have in solution, EPR signals with a g value of ca. 2.03, indicative of the formation of the oxidized species. Therefore, this study revealed that despite its obvious structural similarity to histidine, imidazole and its derivatives had limited success at stabilizing reduced DNICs.

The versatile and extremely useful N-heterocyclic carbenes are synthesized by deprotonation of the appropriate imidazolium salts.[70,71] One of our studies, driven by the presence of histidine donors in binding sites of Ni-containing biomolecules, explored orientational preferences of such monodentate, flat ligands as imidazoles and NHCs bound to planar [N_2SNi^+] moieties, finding no significant differences in metric parameters and the orientation of the plane of the ligand with respect to the N_2SNi plane.[72] Such fortunate correlations between imidazoles and NHCs prompted us to

investigate the suitability of NHC ligands in the synthesis of stable model DNICs in different redox levels, and reactivity studies thereof.

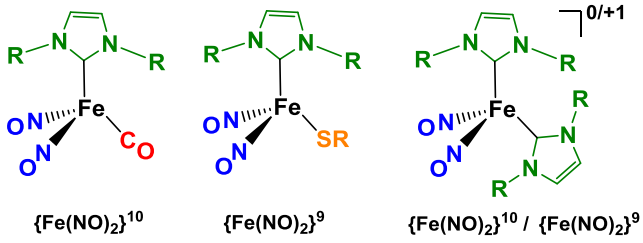

Figure I-10. Prototypic NHC-DNICs in two redox levels.

A new family of N-heterocyclic carbene stabilized monomeric DNICs

Explorations of the suitability of NHC ligands to stabilize the $\{Fe(NO)_2\}^9$ and $\{Fe(NO)_2\}^{10}$ redox levels of DNICs has mainly been based on the prototypes shown in Figure I-10. Figure I-11 summarizes the synthetic design. Among these, the neutral $\{Fe(NO)_2\}^{10}$ compounds are of the $L_2Fe(NO)_2$ type, and can be accessed readily through CO/L ligand exchange for L = NHC, precursor $Fe(CO)_2(NO)_2$. The mono- and bis-NHC-substituted, reduced DNICs can be obtained in this way *via* appropriate stoichiometric control (the steric constraints of bulky NHC ligands such as IMes prevent di-substitution).[41] The cleavage of dimeric $(\mu\text{-RS})_2[Fe(NO)_2]_2$, with the relevant NHC results in stoichiometric conversion of the RRE to neutral, oxidized $L(X)Fe(NO)_2$ type DNICs. While this is the more clearly defined route to oxidized, NHC-bearing DNICs, the reaction of neutral, reduced, bis-NHC DNICs with oxidants such as O_2 and NO^+ also result in the formation of $L_2Fe(NO)_2^+$, $\{Fe(NO)_2\}^9$ compounds.[41]

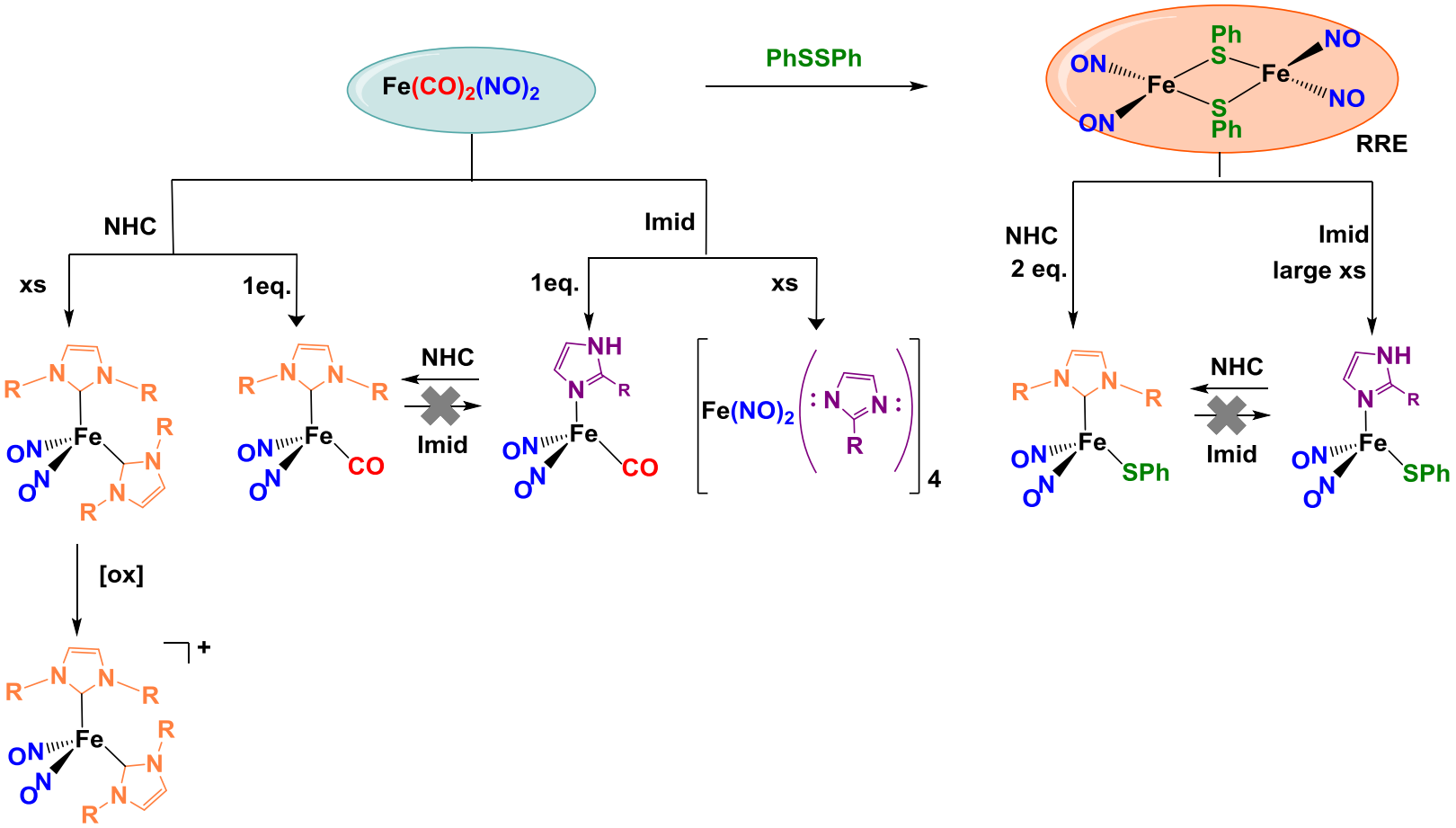

Figure I-11. Synthetic routes to NHC/ Imidazole DNICs.

For comparison to NHC-DNICs, the analogous imidazole bound DNICs were prepared (Figure I-11). The mono-substituted $\{Fe(NO)_2\}^{10}$ complex was obtained using 1 equivalent of imidazole, however, contrary to the NHCs, addition of excess imidazole resulted in the formation of interesting imidazolate-bridged, tetrameric $[(Imid)Fe(NO)_2]_4$ complexes[41,73] with $\{Fe(NO)_2\}^9$ units surprisingly similar to $[(Imid)Cu(tacn)]_4^{4+}$ molecular squares (Figure I-12).[74] Imidazoles could also cleave the RRE to yield the mono-substituted $\{Fe(NO)_2\}^9$ compound as can NHCs. However, unlike the NHCs, the complete conversion of the RRE required a large excess of (>14 eq.) imidazole.[41]

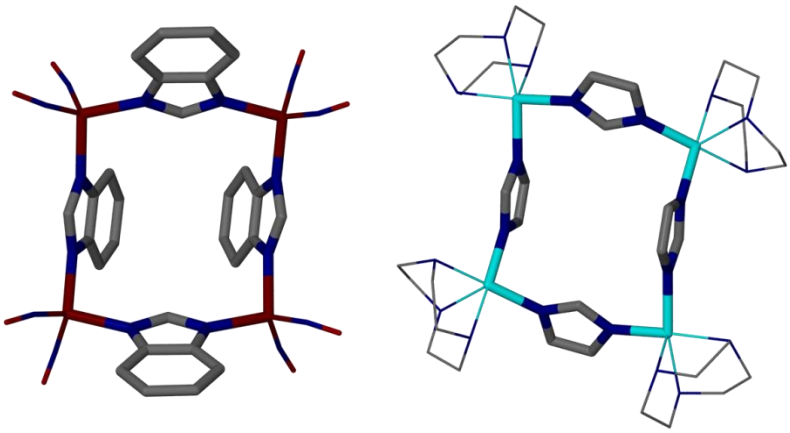

Figure I-12. Capped stick renditions of (left) $[(Imid\text{-}benz)Fe(NO)_2]_4$ and (right) $[(Imid)Cu(tacn)]_4^{4+}$ molecular squares.[73,74]

Structural and spectroscopic standards

All monomeric DNICs containing NHC ligands are four coordinate, pseudotetrahedral compounds with average ∠C-Fe-N_{NO} angles in the range of 107° to 110°. The ∠N-Fe-N values range from 111° to 122°, with the reduced compounds at the larger end of the range.[41,65] These values compare well with the metrics of Li's bis imidazole DNIC, $(Imid\text{-}Me)_2Fe(NO)_2$, in which the ∠$N_{imid}$-Fe-$N_{NO}$ averages to ca. 112.0° and the ∠N-Fe-N is 116.6°.[55] The Fe-N-O angles in the NHC-DNICs are largely linear with the reduced forms averaging to 174° and the oxidized forms slightly less (on average, 6°). The bis-imidazole complex $(Imid\text{-}Me)_2Fe(NO)_2$ has Fe-N-O angles of 168°. In both the oxidized and reduced NHC-DNICs, deviation from linearity is in the form of the NO ligands bending symmetrically towards each other within the planar FeN_2O_2 unit, an orientation termed "attracto" in the metal-dinitrosyl literature (Figure I-13).[75] It is assumed that such a conformation is favored by first-row transition-metal dinitrosyls with supporting ligands that are good π-acceptors.[75] Interestingly, the "attracto" conformation is maintained in bimetallics and clusters that were previously discussed. Observation of other conformations (Figure I-13) are accountable to M-N-O distortions most likely due to an increase in back donation of more electron rich complexes, a classic case being the Eisenberg and Pierpont complex $[Ru(NO)(NO)Cl(PPh_3)_2]^+$, which contains both a linear and a bent M-N-O bond. [19,76,77]

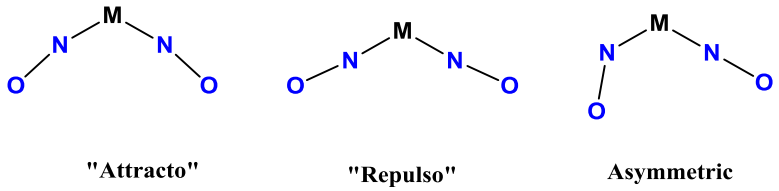

Figure I-13. Conformational orientations of NO ligands in metal dinitrosyls.[75]

The IR stretching frequencies of the diatomic ligands such as NO and CO in selected monomeric DNICs are shown in Table I-1. Extensive compilations of ν(NO) values, of which Table I-1 is a subset, find that ν(NO) values that define the $\{Fe(NO)_2\}^{10}$ NHC-DNICs are in the 1620-1750 cm^{-1} range, shifting to much more positive values in the oxidized $\{Fe(NO)_2\}^9$ form (1710-1790 cm^{-1} range).[41,65] Back-bonding arguments account for these results, which are also consistent with metric data. As with four-coordinate DNICs containing ligands other than NHCs, $\Delta\nu_{NO}$ ($\Delta\nu_{NO}$ = the difference between the ν(NO) band positions) falls into the range around 40 ~ 60 cm^{-1}. Although quite similar, the IR stretching frequencies for the imidazole-containing DNIC counterparts of the NHCs imply that the latter are the better donors.

The presence of the notoriously non-innocent NO ligands gives rise to ambiguity in the assignment of oxidation states to the iron center of DNICs, for which Mössbauer data might be expected to resolve. However, Lippard's reduced and oxidized $[(Ar\text{-}nacnac)Fe(NO)_2]^{-/0}$ complexes (Figure I-6) reported similar isomer shift values (Table I-2).[45] Such an anomaly was the inspiration for the computational studies by Ye and Neese, described earlier.[9] According to their results presented in Figure I-2, the $\{Fe(NO)_2\}^9$ unit is best described by two resonance structures: a HS-Fe(III) (d^5)

antiferromagnetically coupled to two triplet NO^- ligands and a HS-Fe(II) (d^6) antiferromagnetically coupled to an overall quartet from two NO^- ligands, see Figure I-2. The $\{Fe(NO)_2\}^{10}$ species is described as a high spin ferrous center, S = 2, antiferromagnetically coupled to two triplet NO^- ligands, accounting for the observed diamagnetism. Computations further find that counteracting forces of oxidation state of the metal and backbonding abilities of the ligands result in the similar isomer shift values.[9]

In contrast to Lippard's (Ar-nacnac)-DNICs, the Mössbauer spectroscopic parameters of the prototypic NHC-DNICs in Figure I-10 show that the oxidized $\{Fe(NO)_2\}^9$ complexes have larger positive isomer shifts than the reduced $\{Fe(NO)_2\}^{10}$ analogues (Table I-2).[73] For example, the isomer shift of the reduced DNIC [(NHC-iPr)(CO)$Fe(NO)_2$], 0.022 mm/s, is consistent with recorded data for $(Ph_3P)(CO)Fe(NO)_2$ and $(Ph_3P)_2Fe(NO)_2$. In contrast, the oxidized DNIC [(NHC-iPr)(SPh)$Fe(NO)_2$] has an isomer shift of 0.151 mm/s, matching that of the analogous $\{Fe(NO)_2\}^9$ complex, $[(PhS)_2Fe(NO)_2]^-$, δ = 0.18 mm/s. The lower isomer shifts of the reduced compounds (containing CO in place of an $^-$SPh in the above example), are indicative of greater delocalization of the electron density of iron *via* π- backbonding.

These studies involving structural and spectroscopic characterization of the series of NHC-DNICs confirmed the suitability of NHC ligands as mimics of imidazole/histidine in stable model DNICs of different redox levels. A fundamental expectation, and experimentally observed, is that the Fe-NO bond should be stronger in the reduced complexes and NO release is favoured in the oxidized $\{Fe(NO)_2\}^9$ form.

Table I-2. Mössbauer parameters and ν(NO) values of selected DNICs.

	Redox Level	δ (mm/s)	ΔE_Q (mm/s)	ν(NO) (cm^{-1})	Ref
$[(NHC\text{-}iPr)_2Fe(NO)_2]^0$	$\{Fe(NO)_2\}^{10}$	0.045	1.34	1619, 1664	73
$[(NHC\text{-}iPr)_2Fe(NO)_2]^+$	$\{Fe(NO)_2\}^9$	0.114	0.265	1723, 1791	73
$[(Ar\text{-}nacnac)Fe(NO)_2]^{1-}$	$\{Fe(NO)_2\}^{10}$	0.22	1.31	1567, 1627	45
$[(Ar\text{-}nacnac)Fe(NO)_2]^0$	$\{Fe(NO)_2\}^9$	0.19	0.79	1709, 1761	45
$[(NHC\text{-}iPr)(CO)Fe(NO)_2]$	$\{Fe(NO)_2\}^{10}$	0.022	0.818	1696, 1738	73
$[(NHC\text{-}iPr)(SPh)Fe(NO)_2]$	$\{Fe(NO)_2\}^9$	0.151	0.513	1712, 1757	73

A unique subset: NHC-trinitrosyl iron complexes (NHC-TNICs)

Although NHC-DNICs constitute a larger component of the contribution of the Darensbourg group to metal-nitrosyl complexes, success in this area stemmed from the synthesis and isolation of a trinitrosyl iron complex (TNIC), stabilized by an NHC.[65] Previous reports of synthetic TNICs present them as inherently thermally unstable species.[78] Berke *et al.* studied $[(R_3P)Fe(NO)_3]^+$ compounds in the context of nitric oxide releasing pro-drugs, however the overly rapid release of NO would be a drawback in the intended application as pro-drugs.[79] The synthetic work by Dr. Chung-Hung Hsieh showed that a superior possibility, the $[(NHC\text{-}Mes)Fe(NO)_3]^+$ complex, sterically encumbered by the wing-tips of the 1,3-bis(2,4,6-trimethylphenyl)imidazol-2-ylidene (IMes) ligand, could be readily isolated and manipulated in solution under ambient conditions.[65] The trinitrosyl iron moiety is diamagnetic, and can be described as $\{Fe(NO)_3\}^{10}$. This is consistent with the fact that the synthesis of the TNIC was carried

out by isoelectronic replacement of CO in [(NHC-Mes)Fe(NO)$_2$(CO)] by NO$^+$ (Figure I-14). The substitutional lability of one NO ligand rendered the TNICs extremely valuable synthons as previously described.

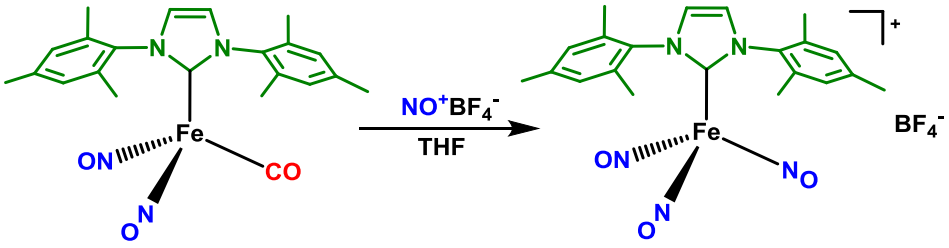

Figure I-14. Synthesis of NHC-TNIC.[65]

As described in this chapter, the use of N-heterocyclic carbenes (NHCs) as ligands to Fe(NO)$_2$ has been established through recent work in the MYD labs, as a successful strategy of synthesizing a library of novel DNICs, in both the oxidized {Fe(NO)$_2$}^{9} and the reduced {Fe(NO)$_2$}^{10} form. It has also been shown that the versatility of these ligands could be extended to the synthesis of stable versions of the rare trinitrosyl analogues. The work reported in this dissertation extends the understanding on this new class of NHC-DNICs through reactivity studies and improvements towards therapeutic applications. Chapter III describes investigations on possible relationships between such compounds and imidazole-DNICs, while Chapters IV and V focus on a system that mimics the reactivity of DNICs with the endogenous gaseotransmitter, CO and mechanistic details thereof. First attempts of manipulating the

design of NHC-DNICs to incorporate desirable properties for their application as NO donors in a biological environment are described in Chapter VI.

CHAPTER II

EXPERIMENTAL SECTION FOR CHAPTERS III-VI

Abbreviations

DNIC = Dinitrosyl iron complex

RRE = Roussin's red ester

NHC = N-heterocyclic carbene

MeMes-NHC = 3-mesityl-1-methyl-imidazol-2-ylidene

sIMes = 1,3-Bis(2,4,6-trimethylphenyl)-4,5-dihydroimidazol-2-ylidene

IMes = 1,3-bis(2,4,6-trimethylphenyl)imidazol-2-ylidene

SPh = phenyl thiolate

Imid-mes = N-mesitylimidazole

(bme-dach)Co(NO) = (*N*,*N*′-Bis(2-mercaptoethyl)-1,4-diazacycloheptane)-nitrosylcobalt

Co(TPP) = 5,10,15,20-tetraphenyl-21*H*,23*H*-porphine cobalt(II)

General methods and materials

Reagent grade solvents were used, further purified and degassed by a Bruker solvent purification system, and stored over molecular sieves. Air-free conditions were maintained during synthesis, isolation, and storage of products through the use of standard Schlenk-line techniques (N_2 atmosphere) and an Ar-filled glove box.

Physical measurements

A Bruker Tensor 37 FTIR spectrometer and CaF_2 solution cells of 0.1 mm pathlength were used to record infrared spectra. EPR spectra were recorded in THF using a Bruker ESP 300 equipped with an Oxford ER910 cryostat operating at 298 K. Elemental analyses of crystalline samples was determined by Atlantic Microlab, Inc., Norcross, GA. ^{1}H NMR and ^{31}P NMR spectra were recorded using a Mercury 300 MHz NMR spectrometer and ^{13}C NMR spectra were recorded on an Inova 500 MHz superconducting NMR instrument. Mass spectrometry (ESI-MS) was performed by the Laboratory for Biological Mass Spectrometry at Texas A&M University. Nanoelectrospray ionization in positive mode was performed using an Applied Biosystems QSTAR Pulsar (Concord, ON, Canada) equipped with a nanoelectrospray ion source. Solution was flowed at 700 nL/min through a 50 μm ID fused-silica capillary that was tapered at the tip.

A Bioanalytical Systems 100 electrochemical workstation with a glassy carbon working electrode and a platinum wire auxiliary electrode was used to conduct the electrochemical analysis of all compounds. A standard three electrode cell under an Ar atmosphere at room temperature was used to obtain all voltammograms. All cyclic voltammograms were recorded in 2 mM THF solutions with 100 mM [*n*-Bu_4N][BF_4] as the supporting electrolyte. All potentials were measured relative to a $Ag^0/AgNO_3$ electrode using a glassy carbon working electrode, and are referenced to Cp_2Fe/ Cp_2Fe^+ ($E_{1/2}$ = 0.00 V vs $Ag/AgNO_3$ in THF).

X-ray crystallography

All samples were run at the X-ray Diffraction Laboratory in the Department of Chemistry at Texas A&M University. Structures included in this dissertation were solved by either Dr. Chung-Hung Hsieh or Dr. N. Bhuvanesh. Suitable crystals of the same habit were identified using a Bausch and Lomb 10x microscope. Each crystal was coated in paratone, affixed to a Nylon loop and placed under streaming nitrogen (110K) in a SMART Apex CCD diffractometer. The space groups were determined on the basis of systematic absences and intensity statistics. The structures were solved by direct methods and refined by full-matrix least squares on F^2. Anisotropic displacement parameters were determined for all nonhydrogen atoms. Hydrogen atoms were placed at idealized positions and refined with fixed isotropic displacement parameters. A list of programs used is as follows: data collection and cell refinement, APEX2;[80] data reductions, SAINTPLUS Version 6.63;[81] absorption correction, SADABAS;[82] structural solutions, SHELXS-97;[83] structural refinement, SHELXL-97;[84] graphics and publication materials, Mercury Version 2.3.[85]

Experimental details for chapter III

Materials. Reagents, including Sodium *tert*-butoxide (NaO^tBu) were purchased from commercial sources and used as received. Standard Schlenk-line techniques (Nitrogen atmosphere) and an Ar-filled glove box were used to maintain anaerobic conditions during preparation, isolation, and product storage. $Fe(CO)_2(NO)_2$,[53] [Na-18-

crown-6-ether][$Fe(CO)_3(NO)$],[86] and 1-mesitylimidazole[87] were prepared according to published procedures.

Synthesis of [$Fe(NO)_2$(Imid-mes)(CO)] (1). In a 100 mL Schlenk flask, 0.50 g (1.10 mmol) of [Na-18-crown- 6-ether][$Fe(CO)_3(NO)$] and 0.13 g (1.11 mmol) of [NO]BF_4 were dissolved in 15 mL of THF and stirred for at least 10 min to produce $Fe(CO)_2(NO)_2$. This was vacuum-transferred to a flask previously loaded with 0.17g (0.9 mmol) of 1-mesitylimidazole (Imid-mes) and immersed in liquid N_2. The reaction mixture was stirred for 1 hour to obtain the product [$Fe(NO)_2$(Imid-mes)(CO)] **(1)** (yield >90%). IR (THF, cm^{-1}) ν(CO) : 1994, ν(NO) : 1747, 1701. Elemental Anal. calculated for $FeC_{13}H_{14}N_4O_3$.THF (found) : C: 50.76 (53.31), H: 5.51 (5.55), N: 13.93 (13.46). ^{1}H NMR (CD_2Cl_2): δ 7.55,7.16 (s, NCH), 7.01 (s, aromatic H on Mes), 3.45 (q, C2H), 2.34 (s, *p*-CH_3 on Mes), 1.99 (s, *o*-CH_3 on Mes).

Deprotonation of [$Fe(NO)_2$(Imid-mes)(CO)] (1). In a separate flask, 0.16 g (1.60 mmol) of NaO^tBu was dissolved in ~10 mL of THF and transferred drop wise into the flask containing the solution of 0.33 g (1.00 mmol) of **1** while stirring. An immediate color change was observed from brown to green. However, the green product **2a/2b** was extremely air sensitive, and decomposed when attempting to dry in *vacuo.*

Synthesis of [$Fe(NO)_2$(MeMes-NHC)(CO)] (3). The solution containing the **2a/2b** was transferred via cannula into a flask containing 0.15 g (1.00 mmol) of alkylating agent, Trimethyloxonium tetrafluoroborate [$(CH_3)_3O^+$ BF_4^-]. A brown product was obtained (yield ~60%), and its formation could be monitored by IR spectroscopy. X-ray quality crystals were grown by cooling a saturated solution of hexanes at -35°C for

three days. IR (THF, cm^{-1}) IR ν(CO) : 1988, ν(NO) : 1743, 1690. Elemental Anal. calculated for $FeC_{14}H_{16}N_4O_3$ (found) : C: 48.86 (49.37), H: 4.69 (4.74), N: 16.28 (16.21). ^1H NMR ($CDCl_3$): δ 7.23, 7.00 (s, NCH), 6.97 (s, aromatic H on Mes), 3.83 (s, NCH_3), 2.33 (s, *p*-CH_3 on Mes), 1.95 (s, *o*-CH_3 on Mes). $^{13}C\{1H\}$ NMR ($CDCl_3$): δ 17.55 (*o*-CH_3 on Mes), 21.01 (*p*-CH_3 on Mes), 33.75 (NCH_3), 123.06, 123.68 (NCH), 128.92 (C3,C5 aromatic C on Mes), 135.25 (C2,C6 aromatic C on Mes), 136.78 (C4 aromatic C on Mes), 138.80 (C1 aromatic C on Mes), 190.69 (Fe-C), 225.12 (CO).

Synthesis of [(MeMes-NHC)$_2$Fe(NO)$_2$] (4). Complex **4** can be directly synthesized in the following manner. A flask was loaded with an excess (1.31 g, 4.00 mmol) of 3-mesityl-1-methyl-imidazolium iodide and 0.39 g (4.11 mmol) of NaO^tBu, dissolved in 10 mL of THF and stirred for ~ 1 hr. The solution was then transferred via cannula to a flask containing $Fe(CO)_2(NO)_2$ freshly prepared and vacuum trapped as described above. The reaction mixture at 22 °C was stirred for 1 week, resulting in a dark brown product; the complete conversion of reactant was monitored by IR spectroscopy. The mixture was filtered through celite to remove impurities and dried in *vacuo*. A brown solid was obtained upon recrystallization with hexanes (yield 63%). IR (THF, cm^{-1}) IR ν(NO) : 1675, 1634. $^+$ESI-MS: Isotope bundle for the parent ion of $FeC_{26}H_{32}N_6O_2$ observed, centered at m/z = 516.19.

Synthesis of [Fe(NO)$_3$(MeMes-NHC)][BF$_4$] (5). A THF solution of complex **3** (0.34 g, 1.00 mmol), prepared as described above, was transferred by cannula to a Schlenk flask loaded with $[NO]BF_4$ (0.116 g, 1.00 mmol) at room temperature. Overnight stirring of the heterogeneous mixture gave a green precipitate. The green solid

thus obtained was filtered off, and dissolved in dichloromethane. Formation of complex **5** was indicated in the IR spectrum. The green solid was washed with pentane to further remove impurities (yield: 72%). X-ray quality crystals of complex **5** were grown in dichloromethane/pentane at -35 °C. IR (CH_2Cl_2, cm^{-1}): IR ν (NO): 1991, 1814 cm^{-1}. Elemental Analysis Calculated (Found): C: 36.06 (36.15), H: 3.72 (3.81), N: 16.18 (16.40). ^{1}H NMR (CD_2Cl_2): δ 7.69,7.39 (s, NCH), 7.02 (s, aromatic H on Mes), 4.02 (s, NCH_3), 2.33 (s, *p*-CH_3 on Mes), 1.94 (s, *o*-CH_3 on Mes). ^{13}C{1H} NMR (CD_2Cl_2): δ 17.88 (*o*-CH_3 on Mes), 21.62 (*p*-CH_3 on Mes), 37.67 (NCH_3), 124.47, 124.94 (NCH), 130.37 (C3,C5 aromatic C on Mes), 130.51 (C2,C6 aromatic C on Mes), 135.22 (C4 aromatic C on Mes), 138.11 (C1 aromatic C on Mes), 142.34 (Fe-C).

Experimental details for chapter IV

Materials. Reagents, including 1,3-bis(2,4,6-trimethylphenyl)imidazolinium chloride ($sIMesH^+Cl^-$), sodium *tert*-butoxide and the phosphine ligands (PMe_3, $P(OMe)_3$ and DMPE) were purchased from Sigma-Aldrich Chemical Co. and were used as received. Standard Schlenk-line techniques (N_2 atmosphere) and an Ar-filled glove box were used to maintain anaerobic conditions during preparation, isolation, and product storage. RRE, $(\mu\text{-SPh})_2[Fe(NO)_2]_2$ was prepared according to published procedures.[64]

Synthesis of (sIMes)Fe(NO)$_2$(SPh) (1). A 0.27 g (0.80 mmol) sample of 1,3-bis(2,4,6-trimethylphenyl)imidazolidinium chloride and 0.12 g (1.2 mmol) of NaOtBu were dissolved in 20 mL of THF and stirred for 30 min prior to transfer to a Schlenk flask containing 1.0 mmol of the Roussin's Red ester $(\mu\text{-SPh})_2[Fe(NO)_2]_2$ in 10 mL of

THF. Stirring for 30 min resulted in a deep purple solution, which was then dried in *vacuo*. The resulting dark purple residue (> 90% yield) was dissolved in 10 mL of ether and filtered through celite. The filtrate was dried and redissolved in THF. X-ray quality crystals were grown from concentrated Et_2O solution at 0 °C. IR (THF, cm^{-1}) ν(NO) 1763(s), 1715(vs). Elemental Anal. calculated for $FeC_{27}H_{31}N_4O_2S$ (found) : C, 61.02 (61.08); H, 5.88 (5.98); N, 10.54 (10.33).

Reaction of 1 with CO(g) to give (sIMes)Fe(NO)$_2$(CO), (2). Carbon monoxide was bubbled into a 20 mL THF solution of complex **1** (c.a 0.5 mmol) in a 100 mL Schlenk flask for 10 min. The flask was sealed under 1 atm $CO_{(g)}$ and the solution was stirred overnight at room temperature. The formation of complex **2** was monitored by IR spectroscopy. A brown colored product was obtained in high yield (> 90%). X-ray quality crystals were obtained from concentrated Et_2O solution at 0 °C. IR (THF, cm^{-1}) ν(CO) 1986(vs), ν(NO) 1747(s), 1705(s). Elemental Anal. calculated for $FeC_{22}H_{26}N_4O_3$ (found) : C, 58.68 (59.18); H, 5.82 (5.96); N, 12.44 (12.17). ^{1}H NMR ($CDCl_3$): δ 6.96 (s, aromatic H on Mes), 4.01 (s, NCH_2), 2.29 (s, *o,m,p*-CH_3 on Mes). The diphenyl disulfide formed as the by-product of the above reaction was characterized by ^{1}H NMR spectroscopy. ^{1}H NMR (CD_2Cl_2): PhSSPh δ 7.53(d, SCCH), 7.27 (m); $FeC_{22}H_{26}N_4O_3$ δ 6.98 (s, aromatic H on Mes), 4.02 (s, NCH_2), 2.29 (s, *o,m,p*-CH_3 on mes)

A ^{1}H-NMR spectrum obtained of a sample of pure $FeC_{22}H_{26}N_4O_3$ (complex **1**) spiked with pure PhSSPh for compared well with that of the reaction mixture.

Reaction of 1 with trimethyl phosphite (P(OMe)$_3$) to give (NHC)((MeO)$_3$P)Fe(NO)$_2$ (10). In a 100 mL Schlenk flask, 0.05 g (0.1 mmol) of

complex **1** was dissolved in 20 ml of THF. Excess $P(OMe)_3$ (0.24 ml, 2.0 mmol) was added to this solution and stirred overnight at room temperature. The formation of complex **10** was monitored by IR spectroscopy. The red product (> 90% yield) was purified by extracting into hexanes, and filtering through celite. X-ray quality crystals were obtained from concentrated solutions of Et_2O solution at -35 °C. IR (THF, cm^{-1}) ν(NO) 1716(s), 1669(s). Elemental Anal. calculated for $FeC_{24}H_{35}N_4O_5P$ (found): C, 52.76 (52.52); H, 6.46 (6.48); N, 10.25 (9.95). $^{31}P\{^1H\}$ NMR (THF): δ 197.4 (s, 1P). The diphenyl disulfide formed as the by-product of the above reaction was characterized by ^1H NMR spectroscopy as described above in the reaction of complex **1** with CO.

Reaction of 1 with trimethyl phosphine (PMe_3) to give $(Me_3P)_2Fe(NO)_2$ (11). Complex **1**, 0.05 g (0.1 mmol) was dissolved in 20 ml THF and reacted with excess PMe_3 (0.20 ml, 2.0 mmol) by stirring at room temperature. Reaction completion and formation of complex **11** was monitored by IR spectroscopy. The reaction mixture was dried in *vacuo* to remove excess PMe_3 and further purification and crystallization was done by similar methods to those described for complex **10** above. IR (THF, cm^{-1}) ν(NO) 1705(s), 1659(s). Elemental Anal. calculated for $FeC_6H_{18}N_2O_2P_2$ (found): C, 29.70 (28.94); H, 7.48 (7.05); N, 9.90 (9.57). $^{31}P\{^1H\}$ NMR (THF): δ 14.3 (s, 2P).

Direct synthesis of Complex 11 using $Fe(CO)_2(NO)_2$ precursor. Complex **11** was also synthesized directly by reacting excess PMe_3 (0.20 ml, 1.9 mmol) with 1 mmol of freshly prepared $Fe(CO)_2(NO)_2$ (In a 100 mL Schlenk flask, 0.50 g (1.10 mmol) of [Na-18-crown- 6-ether][$Fe(CO)_3(NO)$] and 0.13 g (1.11 mmol) of [NO]BF_4 were dissolved in 15 mL of THF and stirred for at least 10 min to produce $Fe(CO)_2(NO)_2$.

This was vacuum-transferred to another 100 ml flask immersed in liquid N_2 at room temperature. The IR monitor showed complete conversion of $Fe(CO)_2(NO)_2$ to $Fe(CO)(PMe_3)(NO)_2$ in 12 hours. IR (THF, cm^{-1}) ν(CO) 1998(s), ν(NO) 1754(s), 1709(vs) cm^{-1}. Continued stirring at 50 °C over 5 days showed complete conversion into complex **11**. IR (THF, cm^{-1}) ν(NO) 1705(s), 1659(vs) cm^{-1}.

Synthesis of $Fe(PMe_3)(sIMes)(NO)_2$ (12). In a 100 ml Schlenk flask, 0.045 g, (0.10 mmol) of complex **2**, $Fe(CO)(sIMes)(NO)_2$ (synthesized directly according to literature procedure for the corresponding IMes analogue)[65] was dissolved in 20 ml of THF. To this flask, 0.11 mmol of PMe_3 (11.3 μl) was added and the flask was exposed to a sun lamp for 12 hours. A red solution resulted, which was purified by pumping down to dryness to remove excess PMe_3 and washing x2 times with hexanes (~95% yield). Red colored crystals of x-ray quality were obtained from concentrated solutions of Et_2O solution at -35 °C. IR (THF, cm^{-1}) *ν*(NO) 1697, 1653 cm^{-1}. Elemental Anal. calculated for $FeC_{24}H_{21}N_2O_2P_2$ (found): C, 57.84 (59.67); H, 7.08 (7.53); N, 11.24 (10.09). $^{31}P\{^1H\}$ NMR (THF): δ 9.6 (s, 1P).

Reaction of 1 with 1,2-Bis(dimethylphosphino)ethane (DMPE) to give $Fe(NO)_2$(DMPE) (13). A portion of 0.09 g (0.20 mmol) of complex **1** was dissolved in 15 ml THF and reacted with DMPE (0.20 mmol, 33.4 μl) by stirring at room temperature. Reaction completion in 2 hours and formation of complex **13** was monitored by IR spectroscopy. The product mixture was completely dried in *vacuo*, redissolved in Et_2O and filtered over celite. X-ray quality crystals of complex **13** were obtained from concentrated Et_2O at -35 °C. IR (THF, cm^{-1}) *ν*(NO) 1703, 1658 cm^{-1}.

$^{31}P\{^{1}H\}$ NMR (THF): δ 56.1 (s, 2P). Complex **13** was also synthesized directly by reacting 0.20 mmol of freshly prepared $Fe(CO)_2(NO)_2$ (as described for complex **11** above) with 0.20 mmol (33.4 μl) of DMPE at room temperature, exposed to the sun lamp. Complete reaction was observed after 48 hours.

Kinetic Measurements. These studies were conducted in collaboration with the D. J. Darensbourg group at Texas A&M University, where the experiments were conducted by Samuel Kyran. *In situ* infrared monitoring was carried out using a Mettler Toledo iC10 ReactIR with an AgX fiber conduit probe having a SiComp ATR crystal. In a typical experiment, a 0.010 M solution of (sIMes)$Fe(NO)_2$(SPh) (**1**) was prepared in a 250 mL 3-neck round bottom flask fitted with the probe by dissolving the compound with 5 mL of CO-saturated toluene under an atmosphere of CO. Once completely dissolved (within 30 s of stirring), the FTIR monitoring was started and the reaction followed until completion. The reactions were conducted over a temperature range from 323 to 348 K; the solubility data of CO was obtained from extrapolation of data in literature.[88,89] The high pressure CO reactions were monitored using an ASI ReactIR 1000 reaction analyses system with a stainless steel Parr autoclave modified with a permanently mounted ATR crystal (SiComp) at the bottom of the reactor (purchased from Mettler Toledo). Kinetic studies with phosphines were conducted in a similar manner, replacing the addition of CO with the appropriate phosphine liquid.

Experimental details for chapter V

Materials. All reagents, including 1,3-bis(2,4,6-trimethylphenyl)imidazolinium chloride ($sIMesH^+Cl^-$) and sodium *tert*-butoxide (NaO^tBu) were purchased from Sigma-Aldrich Chemical Co. and were used as received. Air-free conditions were maintained during synthesis, isolation, and storage of products through the use of standard Schlenk-line techniques (N_2 atmosphere) and an Ar-filled glove box. Roussin's Red esters (**RRE(a-e)**) $(\mu\text{-}(S\text{-}C_6H_4X))_2[Fe(NO)_2]_2$ were prepared according to published procedures.[64]

Synthesis of compounds 1a-1e [(sIMes)(S-C_6H_4X)$Fe(NO)_2$]. The Roussin's Red Esters $(\mu\text{-}(S\text{-}C_6H_4X))_2[Fe(NO)_2]_2$, represented as **RRE(a, b, c** and **e)**, were synthesized by the room temperature reaction of 0.5 mmol of the corresponding 4,4'-XArSSArX disulfide with 1 mmol of freshly prepared $Fe(CO)_2(NO)_2$ (isolated by vacuum transfer to a flask immersed in liquid N_2)[41] in THF solution. (The $-CF_3$ derivative (**RRE d**) was synthesized using similar procedures, but with 1 mmol of 4-(trifluoromethyl)thiophenol in place of the disulfide.) In a separate degassed flask, a 0.34 g (1.0 mmol) sample of 1,3-bis(2,4,6-trimethylphenyl)imidazolinium chloride and 0.12 g (1.2 mmol) of NaOtBu were dissolved in 20 mL of THF and stirred for 30 minutes. This carbene solution was then transferred via cannula into the flask containing the THF solution of the respective RRE. The solution was stirred for 1 h, resulting in a color change from brown to blue/purple. Formation of the product DNIC (**1a-1e**) was confirmed by IR spectroscopy, and the solution was then dried in *vacuo*. The resulting residue (> 85% crude yield) was dissolved in 10 mL of ether, filtered through celite, and

recrystallized in cold hexanes. The solids were handled under inert gas as a precaution against degradation by moisture and air. X-ray quality crystals of **1b** and **1c** were obtained by slow evaporation of concentrated ether solutions, while those of **1a** and **1e** were obtained from solutions of THF/hexanes. Note that complex **1b** co-crystallized with one molecule of cyclohexane, found in low abundance in the hexanes used in the recrystallization process. IR (THF, cm^{-1}) **1a:** *v*(NO) 1759(s), 1713(vs). Elemental Analysis, Found: C, 60.1; H, 6.3; N, 9.4. Calc. for $FeC_{28}H_{33}N_4O_3S$: C, 59.9; H, 5.9; N, 9.9 %. IR (THF, cm^{-1}) **1b**: *v*(NO) 1761(s), 1714(vs). Elemental Analysis, Found: C, 64.1; H, 7.1; N, 8.7. Calc. for $FeC_{28}H_{33}N_4O_2S\bullet$ c-C_6H_{12}: C, 64.85; H, 7.2; N, 8.9 %. IR (THF, cm^{-1}) **1c:** *v*(NO) 1767(s), 1717(vs). Elemental Analysis, Found: C, 57.4; H, 5.5; N, 9.7. Calc. for $FeC_{27}H_{30}N_4O_2SCl$: 57.3; H, 5.3; N, 9.9 %. IR (THF, cm^{-1}) **1d:** *v*(NO) 1769(s), 1718(vs). Elemental Analysis, Found: C, 56.4; H, 5.1; N, 9.0. Calc. for $FeC_{28}H_{30}N_4O_2F_3S$: C, 56.1; H, 5.0; N, 9.35 %. IR (THF, cm^{-1}) **1e:** *v*(NO) 1772(s), 1720(vs). Elemental Analysis, Found: C, 56.6; H, 5.5; N, 11.4. Calc. for $FeC_{27}H_{30}N_5O_4S$: C, 56.3; H, 5.25; N, 12.15 %.

Kinetic Measurements. *In situ* infrared monitoring was carried out using a Mettler Toledo iC10 ReactIR with an AgX fiber conduit probe having a SiComp ATR crystal. These studies were done by Samuel Kyran of the D. J. Darensbourg group at Texas A&M University. In a typical experiment, a 0.0100 M solution of *para* substituted (sIMes)(S-C_6H_4X)$Fe(NO)_2$ (**1a-1e**) was prepared in a 250 mL 3-neck round bottom flask fitted with the probe by dissolving the compound with 5 mL of CO-saturated toluene under an atmosphere of CO. Once completely dissolved (within 30 s of stirring), the

FTIR monitoring was started and the reactions were followed until completion (with exception of **1e**, see chapter V). All reactions were conducted at 333 K; the solubility data of CO was obtained from extrapolation of data in literature.[88,89] The temperature of 333 K was chosen as being apt for this study based on the convenient reaction rates of complex **1** previously investigated (chapter IV). At this temperature, with a $t_{1/2}$ of 3.2 hrs, complex **1** takes close to 20 hrs for complete conversion to complex **2**. Temperatures below 333 K extended the reaction time to more than a day.

Experimental details for chapter VI

Materials. All reagents, including 1,3-bis(2,4,6-trimethylphenyl)imidazolium chloride ($IMesH^+Cl^-$), sodium *tert*-butoxide (NaO^tBu), sodium methoxide (MeONa) 1-thio-β-D-glucosetetraacetate, 1-thio-β-D-glucose sodium salt and CoTPP were purchased from Sigma-Aldrich Chemical Co. and were used as received. Air-free conditions were maintained during synthesis, isolation, and storage of products through the use of standard Schlenk-line techniques (N_2 atmosphere) and an Ar-filled glove box. The NHC stabilized IMes-TNIC, $[(IMes)Fe(NO)_3]^+$ and $[(bme\text{-}dach)Co]_2$ were synthesized according to literature procedure.[65,90]

Synthesis of complex 1. A portion of of 0.10 mmol (0.054 g) of $[(IMes)Fe(NO)_3]^+$ and 0.10 mmol (0.036 g) of 1-thio-β-D-glucosetetraacetate were weighed out and dissolved in 10 ml of THF in a 100 ml Schlenk flask. A color change from green to brown resulted within time of mixing and the formation of complex **1** was confirmed by IR spectroscopy. The solution was filtered through celite, and a brown

powder (83% yield) was obtained by recrystallization of THF solutions of **1** with cold hexanes or pentanes. X-ray quality crystals of **1** were obtained from THF solutions layered by hexanes at -35 °C. IR (THF, cm^{-1}) υ(Me-C(O)O): 1759 (s), 1749 (sh) cm^{-1} υ(NO): 1768 (sh), 1718 (s) cm^{-1}. Elemental Anal. calculated for $C_{35}H_{43}FeN_4O_{11}S$ (found) : C, 53.64 (53.21); H, 5.53 (5.42); N, 7.15 (6.73). $C_{35}H_{43}FeN_4O_{11}S$ (MW = 783 g/mol) $^+$ESI-MS: m/z = 784 $[M + H]^+$. Room temperature EPR measurements showed an isotropic signal at g = 2.03.

Deprotection of complex 1 to give complex 1′ and the direct synthesis of 1′. In a 100 ml Schlenk flask, 0.04 g (0.05 mmol) of complex **1** was mixed with excess (0.40 mmol, 0.022 g) of MeONa and the solid mixture was dissolved in 20 ml of MeOH. The deprotection proceeded with changes in the IR pattern of complex **1**, and was complete in ca. 2 hours. Direct synthesis of complex **1′** was achieved by reacting 0.10 mmol (0.054 g) of $[(IMes)Fe(NO)_3]^+$ and 0.10 mmol (0.022 g) of 1-thio-β-D-glucose sodium salt in THF. The reaction was complete within time of mixing as can be confirmed by IR spectroscopy and a greenish brown product was obtained in powder form in good yield (crude yield > 75%). IR (THF, cm^{-1}) υ (NO): 1768 and 1716 cm^{-1}. $C_{27}H_{35}FeN_4O_7S$(MW = 615 g/mol) $^+$ESI-MS: m/z = 638 $[M + Na]^+$.

Synthesis of complex 2. The Roussin's Red Ester type dimeric complex **2**, $(\mu\text{-}(SR))_2[Fe(NO)_2]_2$, where R = acetylated thiosugar units, was synthesized by the room temperature reaction of 1 mmol of 1-thio-β-D-glucosetetraacetate with 1 mmol of freshly prepared $Fe(CO)_2(NO)_2$ (isolated by vacuum transfer to a flask immersed in liquid N_2)[41] in THF solution. The reaction was complete in about 12 hrs as could be monitored by IR

spectroscopy. A brown powdery product was obtained in good yield (76.3%), by recrystallizing concentrated THF solutions of **2** with cold hexanes. Room temperature EPR measurements showed no signal. IR (THF, cm^{-1}) υ(NO): 1787, 1750 cm^{-1} υ(Me-C(O)O): 1759, 1749 cm^{-1}. $C_{28}H_{38}Fe_2N_4O_{22}S_2$ (MW = 958 g/mol) $^+$ESI-MS: m/z = 959 $[M + H]^+$, 980 $[M + Na]^+$.

NO-trapping experiments. Complex **1** was used in NO trapping experiments with Co(TPP). Into a 50 ml Schlenk flask, 0.06 mmol (0.05 g) of complex **1** was weighed out and dissolved in 10 ml of THF. This was transferred *via* cannula into a different flask containing 0.12 mmol (0.081 g) of CoTPP in 10 ml THF. Loss of NO bands was seen over 48 hours in the IR monitor. In order to isolate the (TPP)Co(NO), the solution was concentrated to ca. 5 ml, and MeOH was added. Careful decanting of the red supernatant showed a dark purple precipitate. The residue was dried in *vacuo* and re-dissolved in dichloromethane. The IR spectrum of this dichloromethane solution showed a strong absorption peak at 1683 cm^{-1} for (TPP)Co(NO). $^+$ESI-MS: m/z = 671 $[(TPP)Co]^+$. UV-Vis (DCM): 410 nm, 534 nm.

Each of complex **1** (0.025 mmol, 0.019 g) and **2** (0.025 mmol, 0.023 g) were reacted with 0.1 mmol (0.056 g) of $[(bme\text{-}dach)Co]_2$ in THF solutions separately. Loss of NO bands in the IR monitor was seen over ~24 hours for complex **1** and over ~12 hours for **2**. The resulting solution was pumped down to dryness and washed x2 with Et_2O. The remaining solid was re-dissolved in dichloromethane, of which the IR showed a strong, broad band at 1601 cm^{-1}, indicating the formation of (bme-dach)Co(NO). $^+$ESI-MS:m/z = 308 $[M + H]^+$, 277 [M-NO].

CHAPTER III

DINITROSYL IRON COMPLEX AS A PLATFORM FOR METAL-BOUND IMIDAZOLE TO N-HETEROCYCLIC CARBENE CONVERSION*

Introduction

While the most famous application of N-heterocyclic carbenes (NHC) as ligands is arguably towards the 2nd generation Grubbs catalyst, it has been described as "one of the most versatile ligands in the toolkit of the synthetic chemist".[91,92] With respect to iron, developments continue to expand in homogeneous catalysis and bio-mimetic chemistry.[91] Within the first coordination sphere the planar NHCs mimic ligands such as imidazole, itself a surrogate for histidine, and in composition and steric character a C_3N_2 heterocycle similar to NHC.[72] Of particular interest in this regard is the study by Li *et al.*, which explored the synthesis and characterization of a series of dinitrosyl iron complexes, DNICs, bearing imidazole derivatives, (e.g., 4-methyl imidazole, imidazole, benzimidazole).[69] In this series, only $Fe(NO)_2(1\text{-MeIm})_2$ (1-MeIm = 1-methyl imidazole), with the DNIC moiety in the reduced, $\{Fe(NO)_2\}^{10}$ (Enemark-Feltham notation)[8] form, could be isolated and characterized by single crystal X-ray diffraction. All derivatives displayed the now classic EPR signature of $\{Fe(NO)_2\}^9$ complexes, an isotropic signal of g = 2.03, indicative of the ease of oxidation of neutral $\{Fe(NO)_2\}^{10}$.[55] To address this difficulty of isolating pure imidazole bound DNICs, Hess *et al.*, found that NHCs supported DNICs at both redox levels, i.e., $\{Fe(NO)_2\}^{10}$ and $\{Fe(NO)_2\}^9$.[41]

*Reproduced in part by permission of The Royal Society of Chemistry. Hsieh, C. -H.; Pulukkody, R.; Darensbourg, M. Y. *Chem. Commun.* **2013**, *49*, 9326-9328.

This ability is uncommon, the [(2,6-diisopropylphenyl)-NC(Me)]$_2$CH (Ar-nacnac) ligand reported by Lippard *et al.* being another such example.[45] Further we have noted that NHCs were superior ligands to DNICs, readily replacing imidazoles in competition studies involving the oxidized and reduced DNICs.[41]

Gas phase calculations of the energetics of the free imidazole molecule have reported that it is ca. 30 kcal mol^{-1} lower in energy than its NHC tautomer,[93] which suggests that tautomerization to NHC is thermodynamically unfavoured. To the contrary, from studies by Crabtree *et al.* addressing the existence of C-bound imidazoles in metalloproteins, it was concluded that this thermodynamic preference may be reversed when each is bound to a metal center.[94] Nevertheless this preference is metal dependent; for largely chloride coordination environments, first row transition metals were found to favor binding via N, while second and third row metals preferred binding via C.[94] Experimental studies by Ruiz, *et al.*, and Lopez, *et al.*, have developed protocol wherein conversion of an imidazole ligand bound to manganese- or rhenium-carbonyls has been effected.[95,96] Similar inter-conversions were reported by Brill, *et al.* and Häller, *et al.* [97,98] Given the aforementioned order of reactivity observed for imidazole and NHC-bearing synthetic DNICs, as well as the biological significance of DNICs, we have pursued the possibility of conversion of an imidazole to an NHC on the dinitrosyl iron platform, when provided with necessary conditions.

Synthesis and characterization

The experimental protocol for conversion of metal-bound imidazoles to NHCs established by Ruiz, *et al.*, was followed (Figure III-1).[95,99] The imidazole containing DNIC **1** (R = -mesityl) was obtained by reacting 1-mesitylimidazole (synthesized via the literature procedure)[87] with $Fe(CO)_2(NO)_2$ in 1:1 ratio,[41] in THF solution, to yield a dark brown product, complex **1**. Its formation could be monitored by IR spectroscopy, ν(CO): 1994 cm^{-1}, ν(NO): 1747, 1701 cm^{-1} (Figure III-2). The product was further characterized by ^{1}H-NMR spectroscopy.

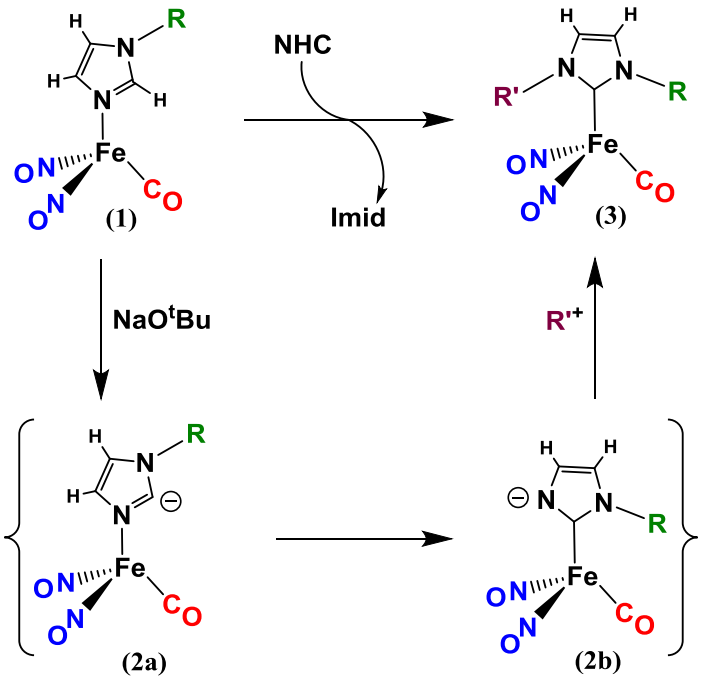

Figure III-1. Conversion of metal-bound imidazoles to NHCs on a DNIC.

Deprotonation of **1** using NaO^tBu results in a color change in the solution from brown to teal green (Figure III-2. IR ν(CO): 1854 cm^{-1}, ν(NO): 1687, 1675 cm^{-1}). We assign the change in the positions and pattern of the IR bands accompanying this color change to the formation of anionic intermediates **2a/2b** (Figure III-1) analogous to those proposed by Ruiz *et al.*[95,99] However, owing to its extreme air sensitivity and instability, we were unable to further characterize the intermediate species.

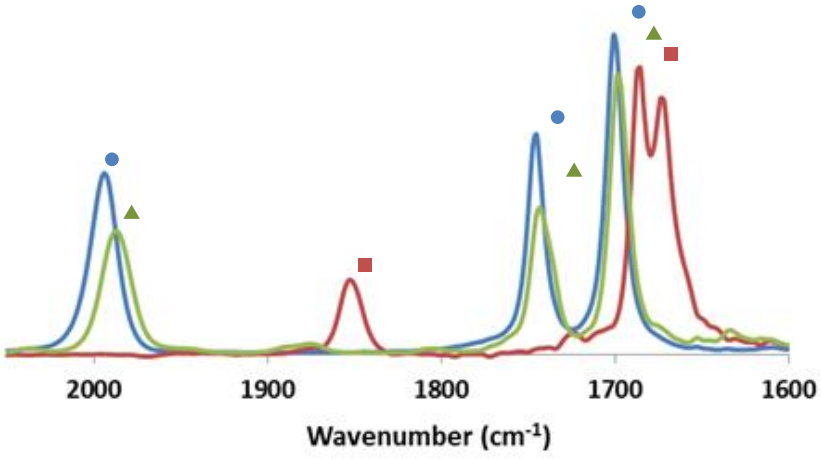

Figure III-2. Overlaid IR spectra of **1, 2a/2b** and **3** in THF. [●, Blue:**1**: ν(CO): 1994 (s), ν (NO): 1747 (s), 1701 (vs)cm^{-1}], [■, Red: **2a/2b**: ν(CO): 1854(w) , ν(NO): 1687(vs), 1675 cm^{-1}(s)], [▲, Olive: **3**: ν(CO): 1988(s) , ν(NO): 1743(s), 1690 cm^{-1}(vs)].

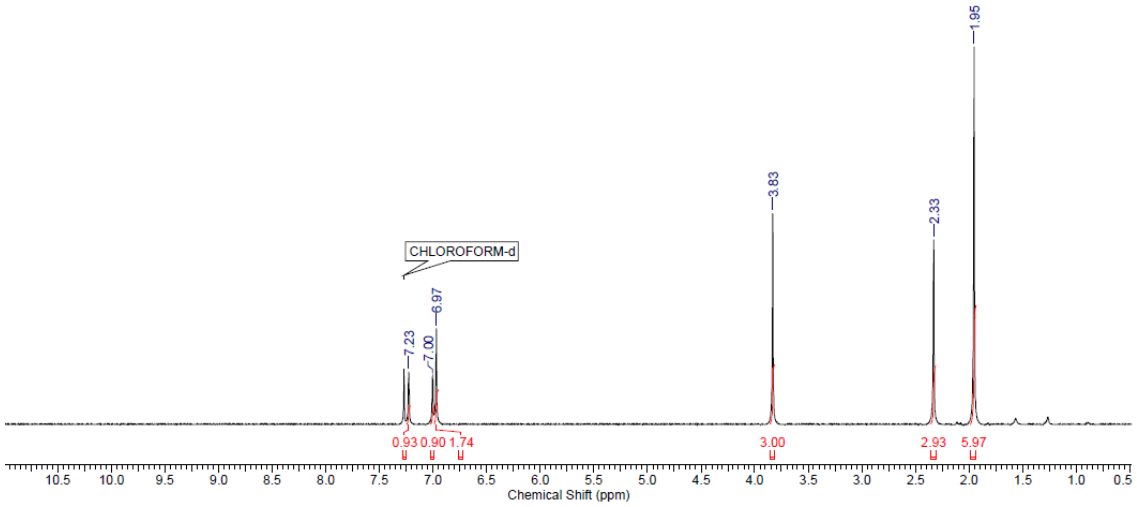

Figure III- 3. ^{1}H-NMR spectrum of [Fe(NO)$_2$(MeMes-NHC)(CO)] **(3)** in $CDCl_3$.

The reaction process is consistent with the calculations of Ruiz *et al.*,[100] as well as our own preliminary DFT calculations conducted by Ryan Bethel of the M. Y. Darensbourg group, wherein it is found that the removal of a proton from the C2 on the imidazole ring produces a 'free carbene' that is unstable and isomerizes to the metal-bound carbene. In the case of the Ruiz study, a *cis* carbonyl at 90° is said to facilitate this process.[100] However, such bond formation is less likely in the tetrahedral geometries of our compounds.

The color of the green solution changed to a dark brown on addition of one equivalent of trimethyloxonium tetrafluoroborate as methylating agent with a corresponding shift in the IR features to ν(CO): 1988 cm^{-1}, ν(NO): 1743, 1690 cm^{-1} (Figure III-2). This can be attributed to the formation of complex **3** (Figure III-1), an NHC-containing species. As expected, the NHC-bound species was seen to possess comparatively lower IR frequencies than the corresponding imidazole, consistent with its higher σ donor ability and earlier studies.[41] X-ray quality crystals were grown by cooling a saturated solution of hexanes at -35°C for three days. The molecular structure of **3** (Table III-1) shows an asymmetric NHC bound iron dinitrosyl compound, which provides conclusive evidence for the ability of the dinitrosyl iron platform to support the conversion of the imidazole to an NHC upon deprotonation. The diamagnetic character of **3** was confirmed by sharp signals in the ^{1}H-NMR spectrum (Figure III-3).

Table III-1. Selected bond distances, angles and molecular structures of **3**, **4** (packing solvent omitted for clarity) and **5**: (top) ORTEP with thermal ellipsoids drawn at 50% probability (H atoms omitted); (bottom) capped stick renditions.

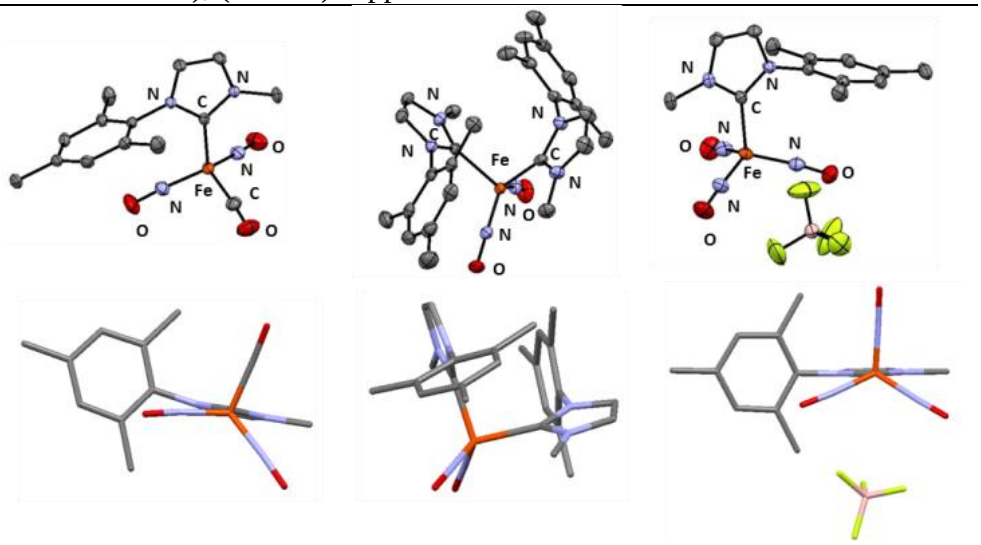

3 **4** **5**

Bond Distances (Å)			
Fe-C_{NHC}	1.991(1)	1.990(1)[a]	2.006(2)
Fe-NO[a]	1.660(1)	1.651(2)	1.695(2)
Fe-CO	1.834(2)	-	-
N-O[a]	1.179(2)	1.203(2)	1.148(2)
Bond Angles (deg)			
N-Fe-N	120.3(1)	118.5(1)	113.0(1)[a]
Fe-N-O[a]	174.8(2)	172.2(2)	173.1(2)
C_{carb}-Fe-NO[a]	107.5(1)	110.3(1)	105.6(1)

[a] Average distance or angles (The maximum deviations from the average distances and angles are shown in the table)

Its CO lability, as established for symmetric NHCs,[41] accounted for decomposition during attempted crystallization by slow evaporation of a concentrated diethyl ether/hexanes solution (1:1) at -35°C over a period of 3 weeks. From this procedure X-ray quality crystals were obtained of the neutral, di-substituted, bis-NHC-

DNIC, $[(MeMes\text{-}NHC)_2Fe(NO)_2]$ (complex **4**), the molecular structure of which is shown in Table III-1. This complex may be directly prepared by reaction of 2 equiv. of the NHC with $Fe(CO)_2(NO)_2$. The IR spectrum of complex **4** is shown in Figure III-4a with bands at ν(NO): 1675 and 1634 cm^{-1}.

In complex **3**, isoelectronic replacement of CO by NO^+, by the addition of one equivalent of $[NO^+]BF_4$, led to the formation of the trinitrosyl iron complex (TNIC) **5** (Figure III-5). This can be characterized by $^1H/^{13}C$-NMR and IR spectroscopies. The latter shows 1914, 1814 cm^{-1} in the ν(NO) region with the typical two band (A + E) pattern indicating the C_{3v} symmetry typical for TNICs (Figure III-4b). X-ray quality crystals of **5** were obtained in THF/pentane at -35°C. The metrics of TNIC **5**, (Table III-1), are comparable to the known IMes (IMes = 1,3-dimesitylimidazol-2-ylidene) and I^iPr (I^iPr = 1,3-diisopropylimidazol-2-ylidene) analogues.[41,65]

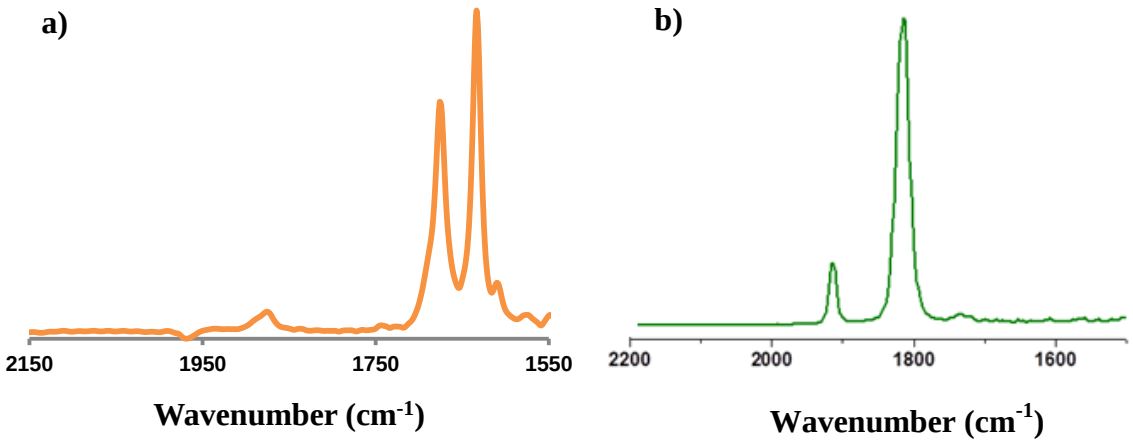

Figure III-4. IR spectra in THF of a) Complex **4** ν(NO): 1675, 1634 cm^{-1} and b) Complex **5** ν(NO): 1914, 1814 cm^{-1} with the typical two band (A + E) pattern indicating the C_{3v} symmetry typical for TNICs.

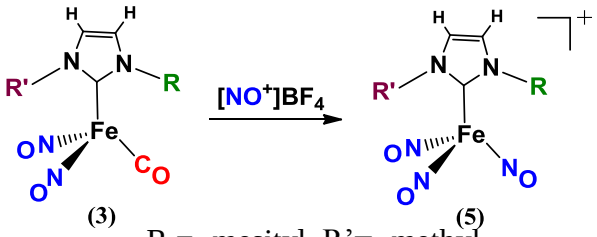

R = -mesityl, R'= -methyl

Figure III-5. Conversion of DNIC to TNIC.

The molecular structures of **3**, **4** and **5** are displayed and metric parameters given in Table III-1. All are tetrahedral complexes where the CN_2C_2 plane of the NHC bisects the N-Fe-N angle of the trigonal base of **5**. This plane is approximately aligned with one Fe-NO vector of **3**. The planes of the 'wing-tip' mesitylene in both **3** and **5** are roughly perpendicular to the CN_2C_2 plane and appear to umbrella the $Fe(NO)_2L$ motif on one side. In the bis-NHC complex **4**, the two CN_2C_2 planes are perpendicular to each other, each having a mesitylene perpendicular to the respective CN_2C_2 plane. Each CN_2C_2 plane in **4** is aligned with one Fe-NO vector and the phenyl rings of the two mesitylenes are also oriented perpendicular and 'trans' to each other. The average Fe-N-O angle of **3, 4** and **5** are similar (174.8°, 172.2° and 173.1° respectively). On comparing the metric data of two isoelectronic species **3** and **5**, we note that the $Fe\text{-}NO_{avg}$ distance of complex **3** is shorter by 0.035 Å and the $N\text{-}O_{avg}$ distance is longer by 0.031 Å than those of complex **5**. Furthermore, the ^{13}C NMR of complexes **3** and **5** show the carbene carbon chemical shifts at 190.7 and 142.3 ppm, respectively (Figure III-6). Baker and Huynh found that the ^{13}C NMR chemical shifts of the carbene carbon in Au and Pd complexes decrease with the increase in Lewis acidity of its metal center.[101,102] Although the

assignment of the oxidation state of Fe in these two isoelectronic species **3** and **5** cannot be based solely on the chemical shifts of the carbene carbon and the structurally linear NO ligands (i.e. linear NO is usually assigned as NO^+),[19,103] we can conclude that the electron density of the Fe center of neutral complex **3** is greater than that of cationic complex **5**. The changes of Fe-NO and N-O distances are as expected on the basis of back-bonding arguments.

In our previous work, the trinitrosyl $[\{Fe(NO)_3\}^{10}]^+$ complex was found to have greater NO lability upon the addition of nucleophiles when compared to the reduced dinitrosyl $[\{Fe(NO)_2\}^{10}]^0$, the latter needing one electron oxidation to trigger NO release in the presence of an NO trapping agent, e.g. metalloporphyrine.[65] It is noteworthy that TNICs are inherently thermally unstable species as seen in the complexes of the $XFe(NO)_3$ type by Beck *et al.*[104] and other TNICs of Hayton, Ledgzdins, *et al.*[78] and Berke *et al.*[79] Also, the trinitrosyl analogue cannot be obtained from direct reaction of $[(Imidazole)Fe(NO)_2(CO)]$ with $[NO^+]BF_4$.[41] Therefore, the ability of the NHC to stabilize otherwise unstable TNICs further validates the premise that NHCs have advantages over their imidazole counterparts on di/trinitrosyl iron platforms.

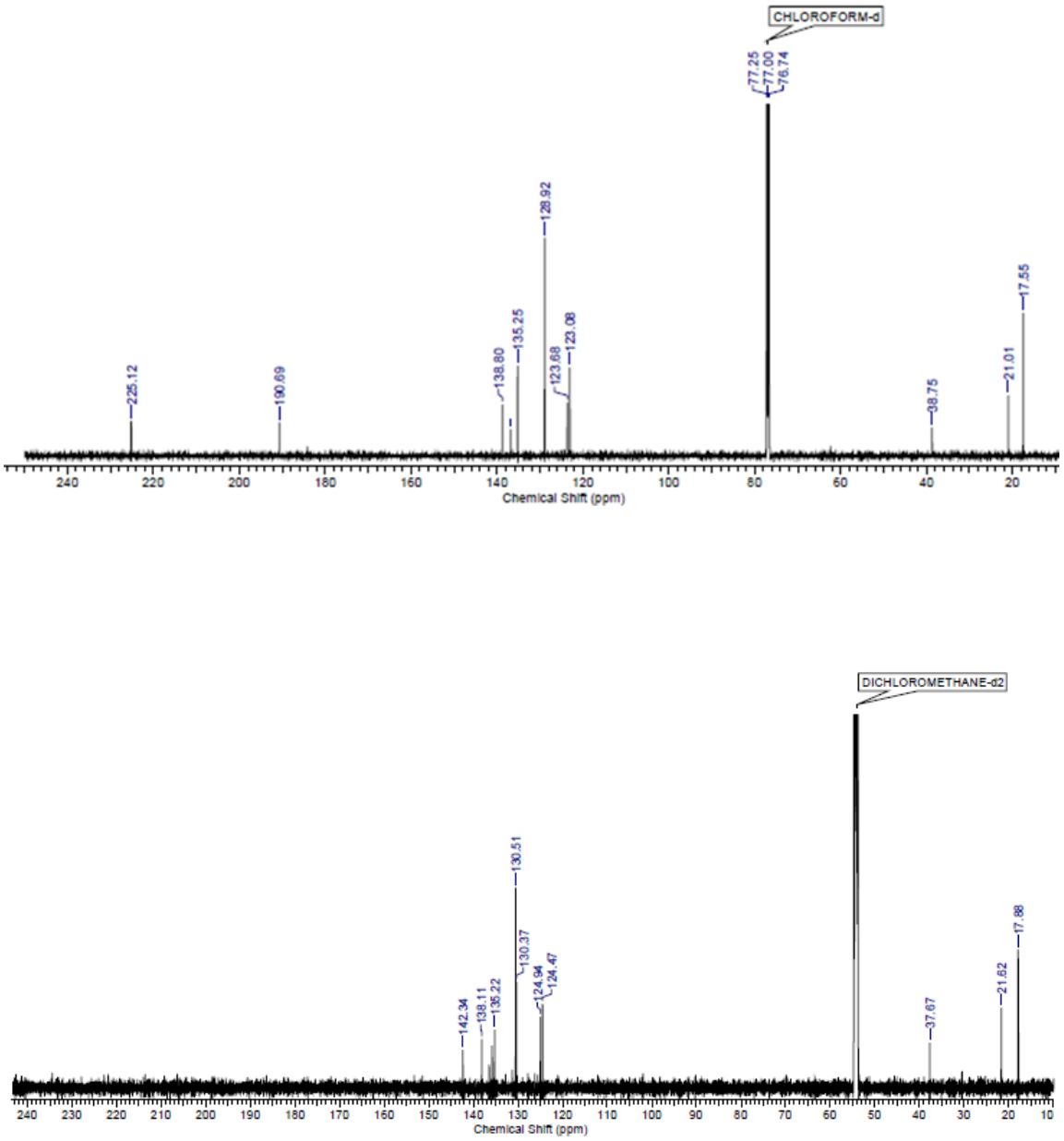

Figure III-6. ^{13}C-NMR spectrum of (Top) $[Fe(NO)_2(MeMes\text{-}NHC)(CO)]$ **(3)** in $CDCl_3$ and (Bottom) $[Fe(NO)_3(MeMes\text{-}NHC)][BF_4]$ **(5)** in CD_2Cl_2.

Additional reactivity of imidazole-DNICs

Attempts were made to characterize imidazole containing DNIC **1** (R = -mesityl) and its isopropyl substituted analogue by x-ray crystallography by growing crystals of the respective compounds in THF solutions layered by hexanes. However, over a period of several weeks, the isopropyl analogue yielded crystals of mononitrosyl-iron-nitrito species, complex **6**, $[Fe(NO_2)_2(NO)(MesIm)_3]$ (Figure III-7(a)), containing the iron atom in a six-coordinate environment. Over several weeks, DNIC **1** produced red-brown crystals, the preliminary x-ray crystallographic analysis of which showed an oxo-bridged dinuclear complex of the $[Fe_2O(NO_2)_4(MesIm)_4]$ form (A skeletal structure shown in Figure III-7(b)). However, the poor quality of the crystals in this case hindered complete crystallographic characterization. The formation of such species can be attributed to the presence of adventitious oxygen; further studies on these complexes were not carried out.

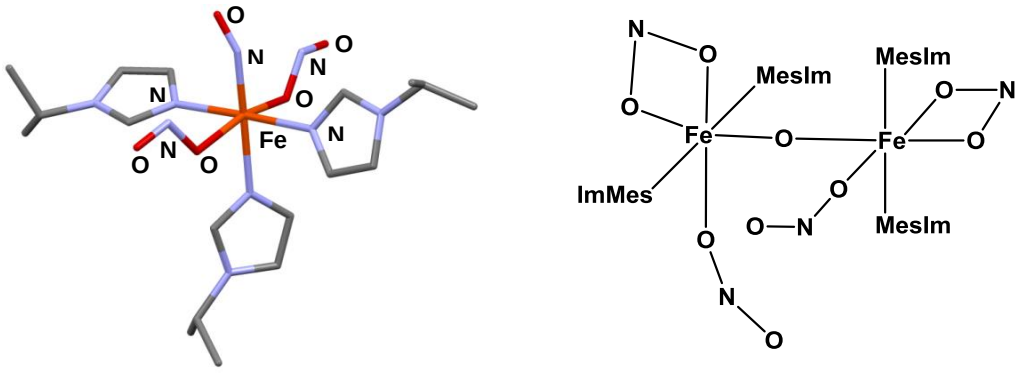

Figure III-7. (a) Capped stick rendition of the molecular structure of complex **6**. (b) Chem-draw depiction of the oxo-bridged dinuclear complex (MesIm = Mesityl imidazole).

Conclusions

In conclusion, the type of reactivity seen in this study may have implications on processes taking place in biological DNICs with histidine donors when exposed to alkaline media. We have provided evidence for the occurrence of a base-promoted conversion of an imidazole to an NHC on a dinitrosyl iron platform. The integrity of the dinitrosyl iron unit, a metallo-unit for which evidence of its biological significance accrues, is maintained throughout, thereby proving it to be stable under base treatment. Figure III-8 presents this possibility as well as the typical method for NHC synthesis via deprotonation of imidazolium salts. We maintain that either route A or B are potential pathways for the biosynthesis of $\{Fe(NO)_2\}$-NHC derivatives. Whether or not these are likely to be natural processes, the potential for labeling biomolecules at histidine to NHC converted sites is of significance.

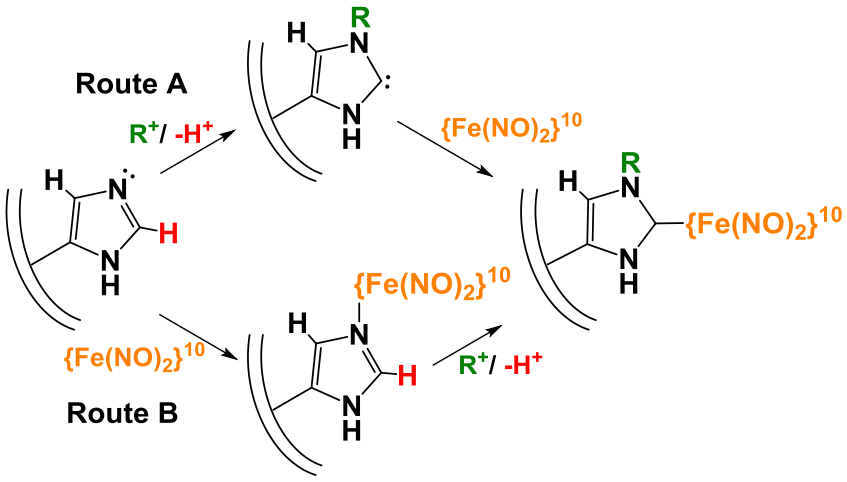

Figure III-8. Possible reaction routes for DNICs with histidine donors when exposed to alkaline media.

CHAPTER IV

CARBON MONOXIDE INDUCED REDUCTIVE ELIMINATION OF DISULFIDE IN AN N-HETEROCYCLIC CARBENE (NHC)/ THIOLATE DINITROSYL IRON COMPLEX (DNIC)*

Introduction

The remarkable $Fe(NO)_2$ unit, reputed to have an active role in controlling NO levels in biology[105-107] and commonly revealed as four-coordinate tetrahedral dinitrosyl iron complexes (DNICs),[32,46,50] harkens to the interphase of organometallic and classical coordination chemistry. For the former, neutral $L_2Fe(NO)_2$ complexes (L = CO, PR_3, imidazole or N-heterocyclic carbenes) yield the diamagnetic irondinitrosyl unit to be isoelectronic with $Fe^0(CO)_3$, for which myriad mononuclear $L_2Fe^0(CO)_3$ complexes are known.[41,53-55] A one-electron-oxidized form of $Fe(NO)_2$ is found in neutral $L(X)Fe(NO)_2$ and anionic $X_2Fe(NO)_2^-$ DNICs are paradigms for the latter. These are S = ½, paramagnetic species, typically identified in biology by a prominent EPR signal at 2.03, and ligated with X = cysteine or glutathione thiolate S-donors, and L = histidine N-donors.[105,108,109]

Monomeric oxidized $\{Fe(NO)_2\}^9$ DNIC species, $L(X)Fe(NO)_2$ or $L_2Fe(NO)_2^+$, typically display an electrochemically reversible one-electron reduction to the reduced $\{Fe(NO)_2\}^{10}$ form. A rare example of a neutral to anionic conversion, $(L\text{-}L)Fe(NO)_2$ to $(L\text{-}L)Fe(NO)_2^-$ has been successful in the case of L-L = the anionic chelating [(2,6-

*Reproduced in part with permission from Pulukkody, R.; Kyran, S. J.; Bethel, R. D.; Hsieh, C.-H.; Hall, M. B.; Darensbourg, D. J.; Darensbourg, M. Y. *J. Am. Chem. Soc.* **2013**, *135*, 8423-8430. Copyright **2013** American Chemical Society.

diisopropylphenyl)NC(Me)]$_2$CH (Ar-nacnac) ligand.[45] Bulk chemical synthesis of the reduced species usually requires the presence of a stabilizing ligand such as CO, PR_3 or NHCs. [41,53,54] In fact, transformations between the oxidized $\{Fe(NO)_2\}^9$ and the reduced $\{Fe(NO)_2\}^{10}$ forms in biology are considered to have implications on regulating the role of the DNIC for NO storage or as an NO-release agent.[44]

We have pursued fundamental properties of synthetic DNICs of $L(X)Fe(NO)_2$ composition making use of L = imidazoles and N-heterocyclic carbenes as surrogates for protein-bound histidine donor sites.[41] Such results find that N-heterocyclic carbene ligands are the "better" ligands. They readily displace imidazoles of $L(RS)Fe(NO)_2$, leaving the $Fe(NO)_2$ unit intact, and engender stability as compared to imidazoles or phosphine complexes, in the reduced $\{Fe(NO)_2\}^{10}$, oxidized $\{Fe(NO)_2\}^9$ and even the $\{Fe(NO)_3\}^{10}$ forms.[41,65]

As demonstrated in Figure IV-1, we have noted a $\{Fe(NO)_2\}^9/\{Fe(NO)_2\}^{10}$ reduction that proceeds under extremely mild conditions and uses a thiolate/disulfide oxidation as driving force. Mechanistic details of this reaction, from experiment and theory, and a unique role of CO as initiator for RS• for the disulfide elimination are reported herein.

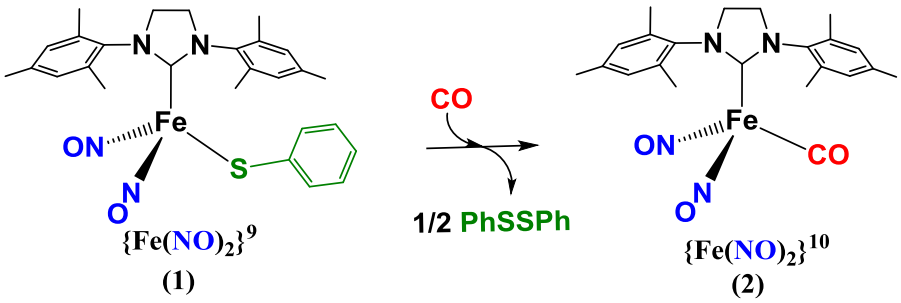

Figure IV-1. Conversion of oxidized $\{Fe(NO)_2\}^9$ species into reduced $\{Fe(NO)_2\}^{10}$ in the presence of CO.

Synthesis and characterization

Homolytic cleavage of $(\mu\text{-PhS})_2[Fe(NO)_2]_2$[64] by two equivalents of the sIMes ligand (freshly prepared by combining 1,3-bis(2,4,6-trimethylphenyl)imidazolinium chloride and NaO^tBu in a 1:1 stoichiometric ratio) leads to the formation of complex **1**, shown in Figure IV-1. This preparation is identical to that of the unsaturated NHC or IMes analogue reported earlier.[65] Reaction progress can be monitored *via* IR spectroscopy with notable shifts in the ν(NO) positions and pattern indicating the formation of complex **1** (ν(NO): 1763 (s), 1715(vs)) from the Roussin's Red Ester, $(\mu\text{-PhS})_2[Fe(NO)_2]_2$, precursor (ν(NO): 1783 (s), 1757(s)) (Figure IV-2). The room temperature EPR spectrum of complex **1** shows an isotropic signal at g = 2.03, the characteristic signature of the $\{Fe(NO)_2\}^9$ oxidized form of DNICs. Complex **1** is stable under inert atmosphere over several months in both solution and solid states.

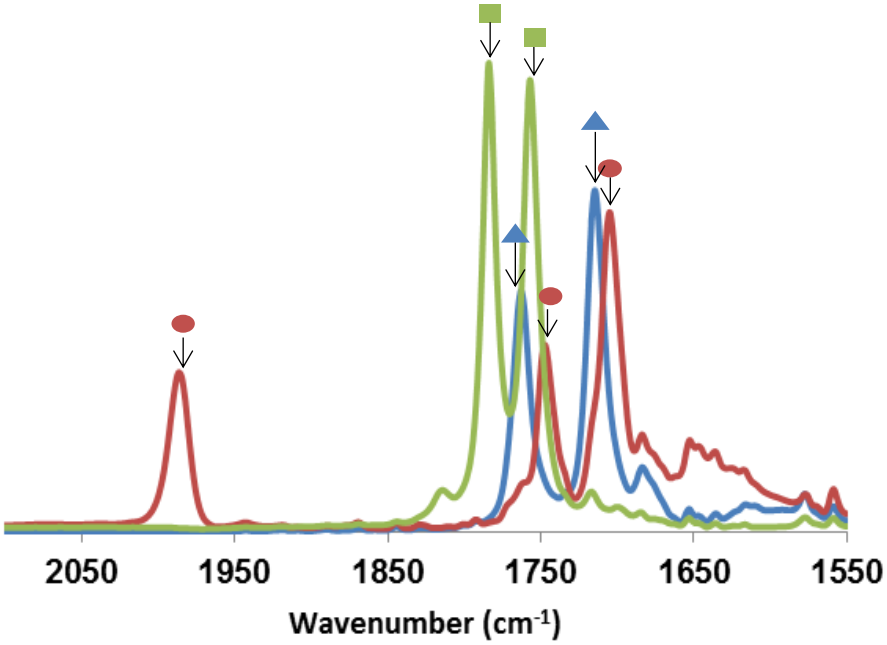

Figure IV-2. Overlaid IR Spectra of **RRE**, **1** and **2** in THF. [■, Olive: **RRE**: ν(NO) 1783(s), 1757(s) cm^{-1}], [▲, Blue: **1**: ν(NO) 1763(s), 1715(vs) cm^{-1}], [●, Red: **2**: ν(CO) 1986(s), ν(NO) 1747(s), 1705(vs) cm^{-1}].

In the presence of CO, the oxidized, paramagnetic $\{Fe(NO)_2\}^9$ complex **1** converts to the reduced, diamagnetic $\{Fe(NO)_2\}^{10}$ complex **2**, Figure IV-1. The spectral monitor indicated ν(NO) positions red shifted by ~15 cm^{-1} and the appearance of a new CO band at 1986 cm^{-1}, indicating the formation of the reduced DNIC **2** Figure IV-2. The by-product PhSSPh, confirmed by ^1H NMR (Figure IV-3) and mass spectrometry,[65] is generated by bimolecular reductive elimination from **1**. The DNIC **2** is fairly air-stable in the solid state, but slowly decomposes in THF solution in the presence of air at room temperature.

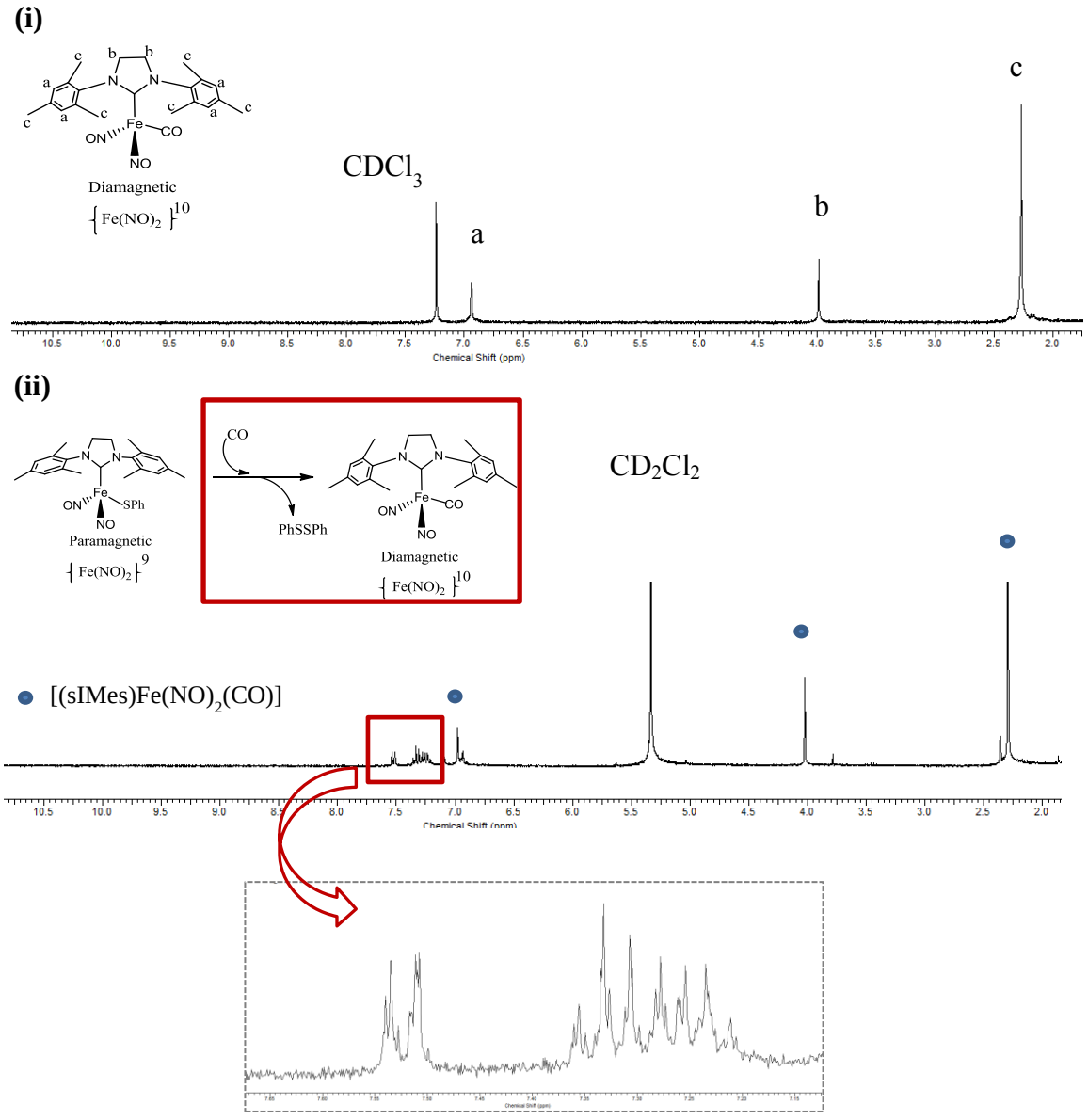

PhSSPh formation as observed in ^{1}H-NMR

Figure IV-3. (i) ^{1}H-NMR spectrum of pure [(sIMes)Fe(NO)$_2$(CO)] **(2)** in $CDCl_3$. (ii) ^{1}H-NMR spectrum of product mixture in CD_2Cl_2 showing formation of PhSSPh.

The DNICs **1** and **2** were obtained as dark purple and brown crystals, respectively, and their molecular structures are compared in Figure IV-4(a) and Figure IV-4(b). Both are tetrahedral complexes wherein the CN_2C_2 plane of the sIMes bisects the S-Fe-N angle of the trigonal base of **1**. This plane is aligned with one Fe-NO vector of **2**. The planes of the mesitylenes are roughly perpendicular to the CN_2C_2 plane and appear to umbrella the $Fe(NO)_2L$ motif. The average Fe-N-O angle of reduced **2** (172.7^o) is slightly more linear than oxidized **1** (168.5°). The two Fe-NO are oriented in towards each other in the "attracto" conformation.[75] With the exception of the saturated ethylene linkage C-C bond, all other metrics of **1** and **2** are similar to those of the IMes analogues.[65] Table IV-1 lists selected bond distances and angles for **1** and **2.**

Table IV-1. Selected bond distances and angles in complexes (sIMes)$Fe(NO)_2$(SPh), **1** and (sIMes)$Fe(NO)_2$(CO), **2.**

	1{$Fe(NO)_2$}[9]	**2**{$Fe(NO)_2$}[10]
Bond Distances (Å)		
Fe-C_{carb}	2.048(1)	1.998(2)
Fe-NO[a]	1.671(1)	1.682(2)
Fe-CO	-	1.771(2)
Fe-S	2.243(1)	-
N-O	1.174(5)	1.174(1)
	1.184(5)	1.164(1)
C-C[b]	1.523(1)	1.524(1)
Bond Angles (°)		
N-Fe-N	115.3(2)	116.6(1)
Fe-N-O[a]	168.4(1)	172.7(2)
C_{carb}-Fe-NO[a]	106.7(2)	109.5(1)
C_{carb}-Fe-S	109.1(1)	-
C_{carb}-Fe-CO	-	101.8(1)

[a] average distance or angles. [b] C-C distance in NHC.

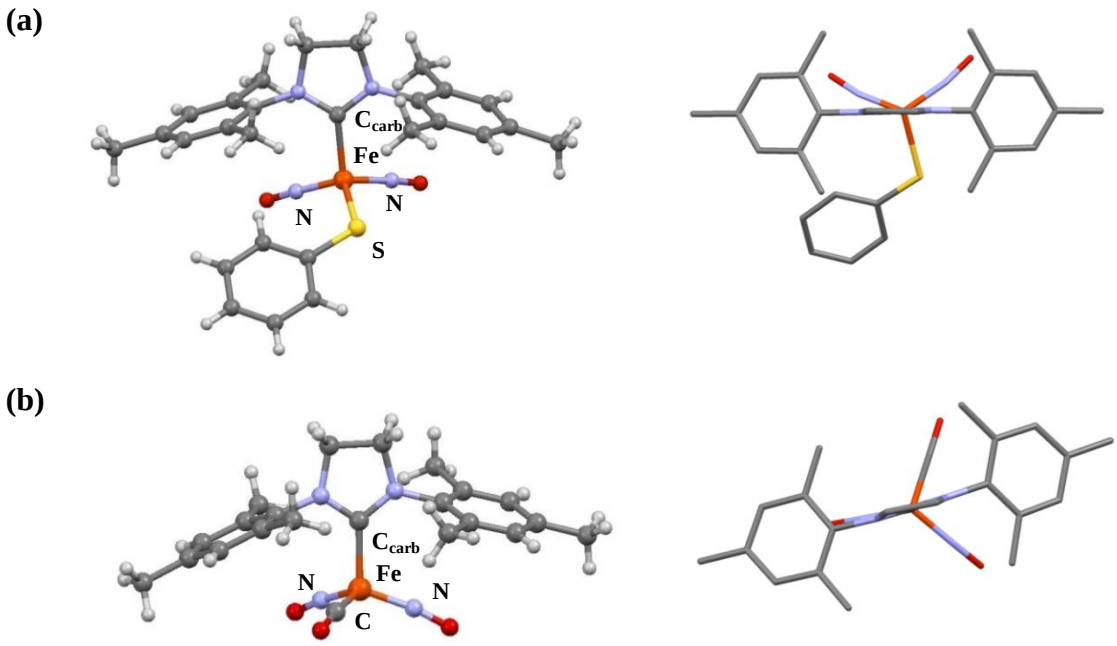

Figure IV-4. Molecular structures of complexes (a) **1** and (b) **2**: (left) in ball-and-stick view; (right) rotated stick views of the orientation of the NHC plane with respect to the trigonal base.

Kinetic studies

The conversion of **1** to **2** could be monitored by *in situ* IR spectroscopy in order to establish the rates of this process. These studies were carried out by Samuel Kyran under the supervision of Professor D. J. Darensbourg. Although the initial kinetic studies described in the previous section were carried out in THF, toluene was chosen as the preferred solvent to enable studies on temperature dependence. Solutions containing complex **1** were saturated with CO and maintained under a CO atmosphere during the *in situ* IR analysis, a three-dimensional stacked plot of which is shown in Figure IV-5. The decay of the reactant NO bands and the growth of new NO and CO bands corresponding

to product formation are clearly evident in the react-IR monitor and occur at the same rate as expected (Figure IV-6).

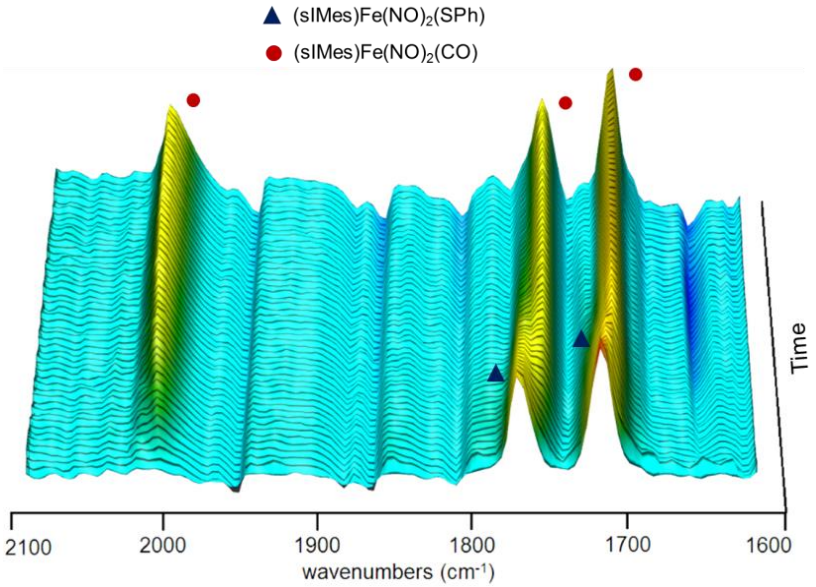

Figure IV-5. Three-dimensional stacked plot of the reaction of complex **1** with CO at 333 K in toluene.

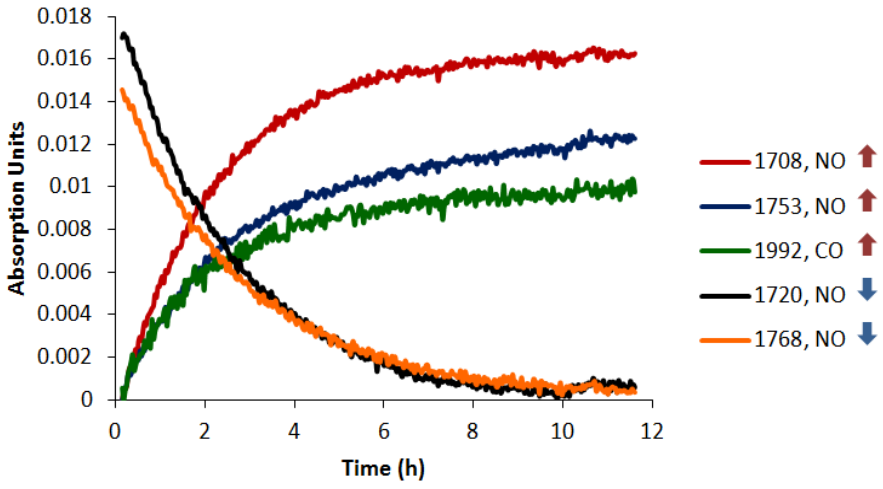

Figure IV-6. Reaction profiles of infrared bands for the conversion of **1** (ν(NO) 1708, 1753 cm^{-1}) to **2** (ν(CO) 1992, ν(NO) 1720, 1768 cm^{-1}) at 348 K in toluene.

The carbonyl band of the product complex **2** is in a region of the spectrum that is free of interference, and was therefore used to obtain the kinetic parameters. The natural log plot of the absorption data for the CO band of complex **2** over three half-lives at 323 K is shown in Figure IV-7. Its linear form suggests first order dependence of the rate on the concentration of the iron complex (eq IV-1).

$$\text{Rate} = k_{obs}\,[\text{Fe}]^1 \quad \text{where, } k_{obs} = k\,[\text{CO}]^n \qquad \textbf{(eq IV-1)}$$

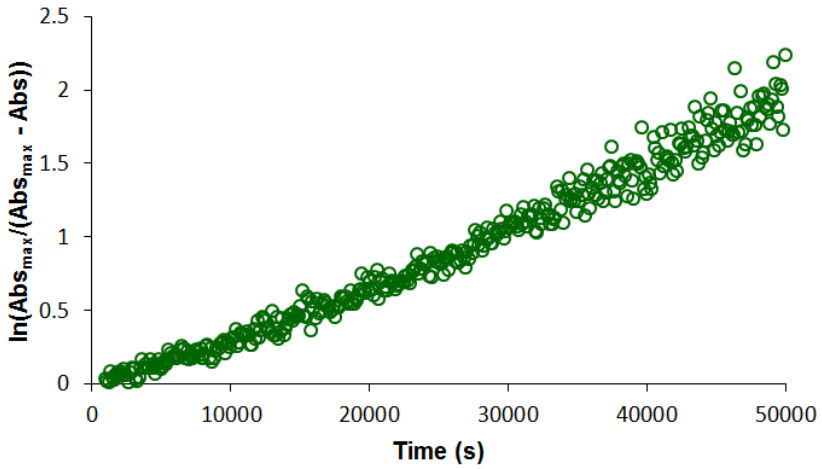

Figure IV-7. Natural log plot of absorption data versus time of the ν(CO) band of complex **2** at 323 K. A linear trend consistent with first-order in **2** gives a k_{obs} value of 4.03×10^{-5} s^{-1} calculated from the slope.

In order to determine the order with respect to CO in the rate expression in equation 1, pressure dependence studies were conducted, where the CO pressure was varied to 3.1 atm and 6.1 atm at 323 K. A plot of k_{obs} vs [CO] at these pressures is linear with a zero *y*-intercept, in accordance with first-order behavior with respect to the

concentration of CO (Figure IV-8). The overall rate expression could therefore be established as bimolecular, first-order in each reactant; complex **1** and CO (eq IV-2).

$$\text{Rate} = k\,[\text{Fe}]^1\,[\text{CO}]^1 \qquad \textbf{(eq IV-2)}$$

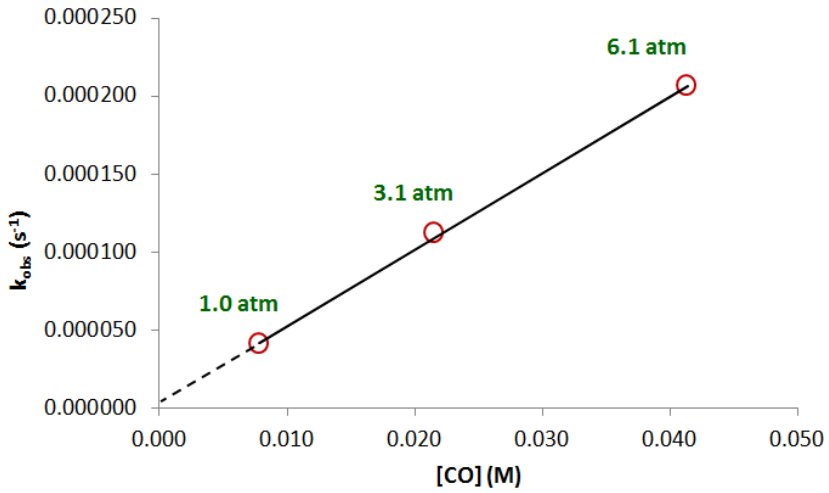

Figure IV-8. Plot of k_{obs} vs [CO] for the formation of complex **2** at 323 K. The R^2 value of 0.9996.

The temperature dependence of the rate constant *k* for the conversion of complex **1** to **2** was determined in order to establish the activation parameters for this process. Solutions of complex **1** were exposed to 1 atm of CO in a similar manner as described previously over a temperature range of 25 K. The natural log plots maintain linearity over the entire temperature range studied (Figure IV-9), and the *k* values, as derived from eq 2 are shown in Table IV-2.

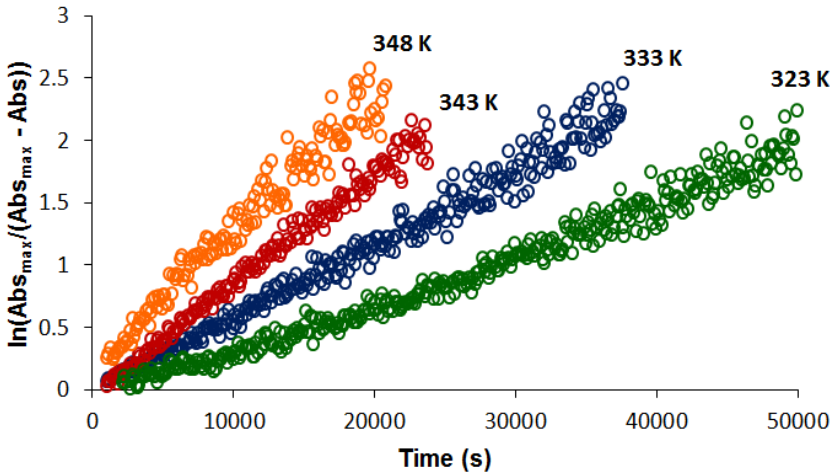

Figure IV-9. Natural log plots of absorption data versus time of the ν(CO) of complex **2** at various temperatures.

Table IV-2. Kinetic parameters obtained from a linear fit of the natural log plots. CO concentrations in toluene at 1 atm were derived from literature.[88]

T (K)	k_{obs} (s^{-1})	[CO] (M)	k (M^{-1} s^{-1})
323.15	4.03 x 10^{-5}	0.00785	5.13 x 10^{-3}
333.15	6.03 x 10^{-5}	0.00798	7.56 x 10^{-3}
343.15	8.81 x 10^{-5}	0.00810	1.09 x 10^{-2}
348.15	1.09 x 10^{-4}	0.00816	1.34 x 10^{-2}

An Eyring analysis afforded the activation parameters for the formation of complex **2** as $\Delta H^{\ddagger}$ of 7.80 ± 0.16 kcal/mol and a $\Delta S^{\ddagger}$ of -45.0 ± 0.5 e.u. (Figure IV-10). The $\Delta G^{\ddagger}$ at 298.15 K can be calculated as 21.2 ± 0.2 kcal/mol. The small $\Delta H^{\ddagger}$ value and

large negative $\Delta S^{\ddagger}$ value are indicative of an associative mechanism, consistent with the second order rate expression.

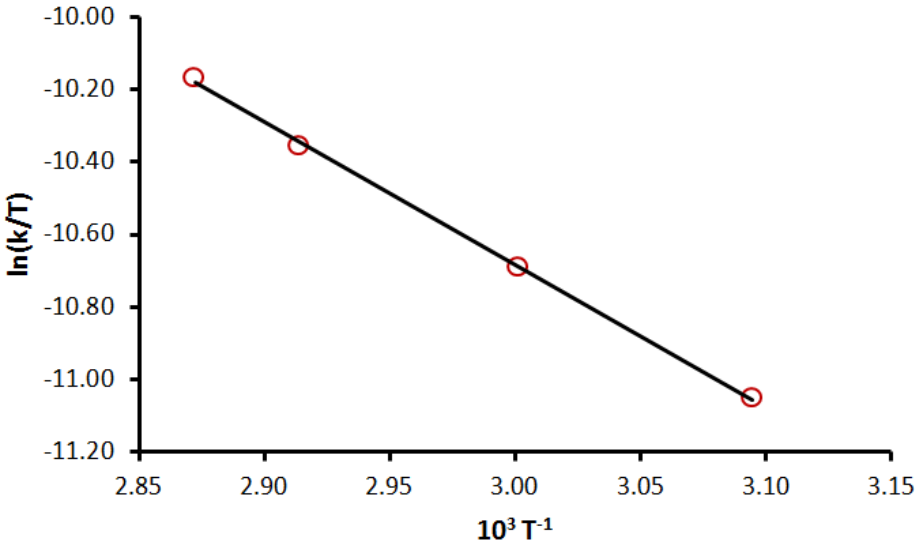

Figure IV-10. Eyring plot obtained from the temperature dependence of *k*. The R^2 value is 0.999.

Computational investigations

Computational studies were conducted, seeking to define a reasonable mechanistic pathway consistent with a bimolecular experimental rate law. Computations were carried out by Ryan Bethel under the supervision of Dr. M. B. Hall. Figure IV-11 shows structures that were explored as intermediates that might result by the addition of CO to **1**.

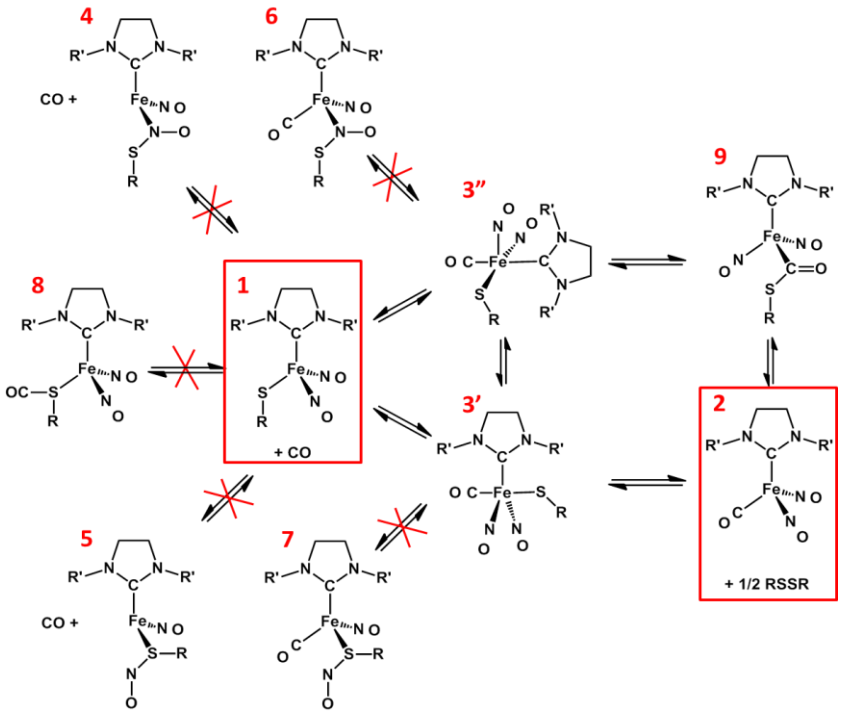

Figure IV-11. Structures explored as intermediates in CO addition to complex **1.** In the DFT study, R = R' = Me. In kinetics study R = Ph, R- = Mes.

Putative intermediates **4** and **5** are RSNO containing three-coordinate iron species, where the formation of an open site is assumed as necessary to initiate interaction with CO, due to the poor nucleophilicity of CO. Nitrosyl insertion into the Fe−SR bond leads to **4**, an N-bound RSNO, and NO migration to the sulfur of Fe−SR, results in **5**, which maintains S-binding of the RSNO. Intermediate **8** is a thiolate S/CO adduct, expected to be followed by CO insertion between S and Fe. However, DFT computations showed all three intermediates (**4, 5** and **8**) to be unlikely. Intermediates **4** and **5** were not stable structures, reverting back to **1** upon geometry optimization, and introduction of CO at the sulfur of the Fe-SR did not produce S-CO or Fe-C(=O)SR

interactions, thereby eliminating these choices. Intermediates **3′** and **3″** in Figure IV-11 are five coordinate species and were calculated by Ryan Bethel to be the most stable isomers of this type with very close energies (only 0.2 kcal/mol difference in free energy). Computations further showed that these intermediates also do not tend towards iron-bound RSNO complexes **6** and **7.** Therefore, the five coordinate species **3′** and **3″** were considered as likely intermediates in the conversion of **1** to **2**.

Transition states [**1**−**3′**]‡ and [**1**−**3″**]‡ were seen to have similar activation barriers, at +19.2 and +19.6 kcal/mol respectively, consistent with the experimental value of 21.2 kcal/mol for $\Delta G^{\ddagger}$ at 298.15 K. Computations presented two possible mechanistic pathways for the conversion to **2**, involving intermediates **3′** and **3″**, respectively. The first (Figure IV-12 (A)) includes direct loss of a thiyl radical from **3′**, with an activation barrier of +19.2 kcal/mol, matching the experimental activation barrier value, i.e., the 21.2 kcal/mol. The second possibility involves the insertion of CO into the Fe-SR bond of **3″**, to form a thioester type intermediate **9** (Figure IV-12), followed by the loss of a thiyl radical. Although the free energy for the formation of the product **2** and a thiyl radical is +9.4 kcal/mol, the pairing of the radicals to form disulfide is the driving force for this reaction with ΔG = -12.8 kcal/mol.

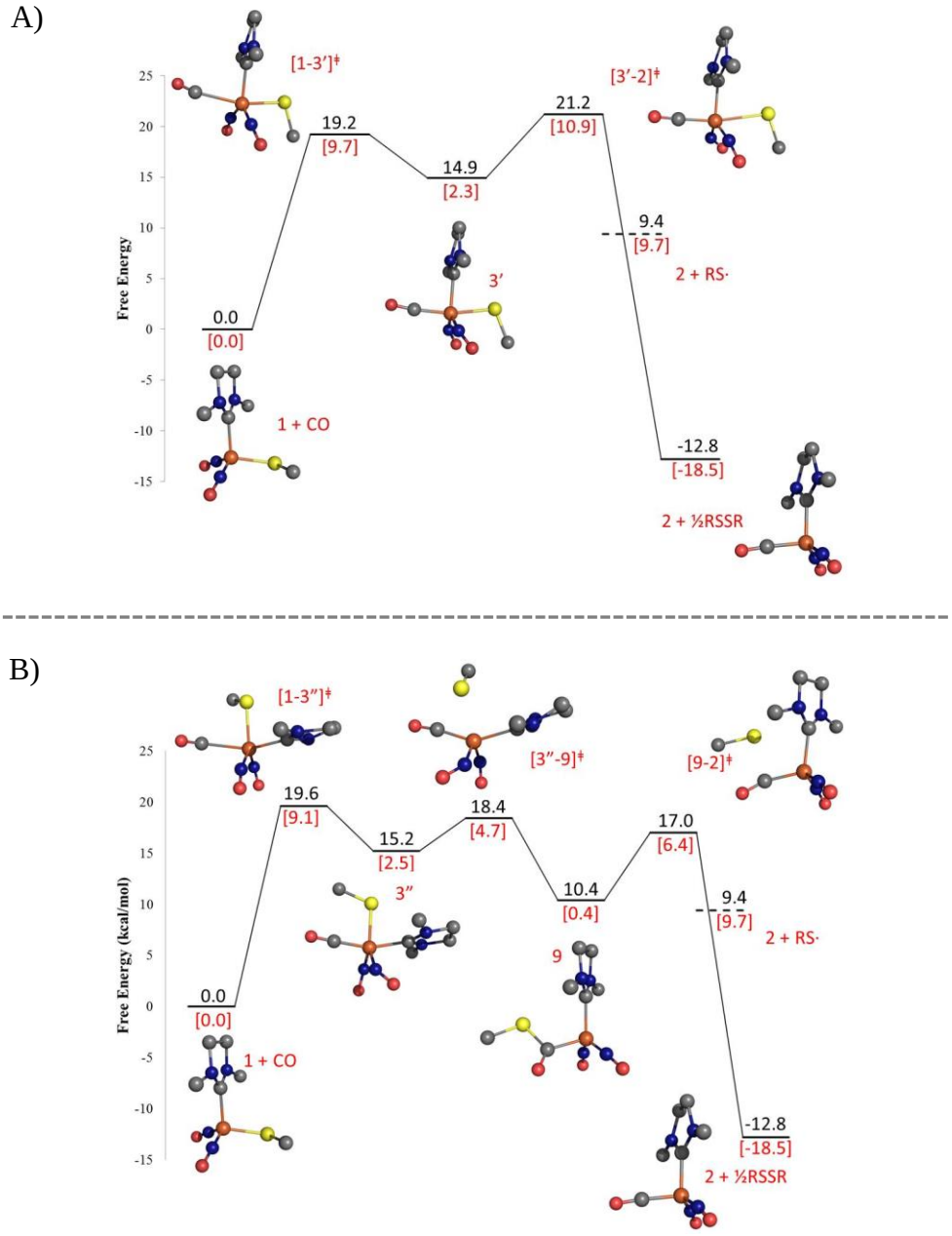

Figure IV-12. Computed reaction pathways for the formation of **2.** A) Direct loss of RS$^{\bullet}$ from **3′**. B) Insertion of CO into the Fe-SR bond of **3″**, to form a thioester type intermediate. Numbers in black are free energy; numbers in red with brackets are enthalpy.

The calculated activation energies are not significantly different in both proposed mechanisms, and are consistent with the experimentally observed activation energy. These predictions are also in agreement with an associative rate law. While the mechanism involving thioester formation is limited to CO as an incoming ligand, the mechanism involving direct loss of the thiyl radical from **3′** is applicable to other incoming ligands as well. Such a mechanism was therefore useful as further studies involved a series of phosphines as incoming ligands, as discussed later in this chapter.

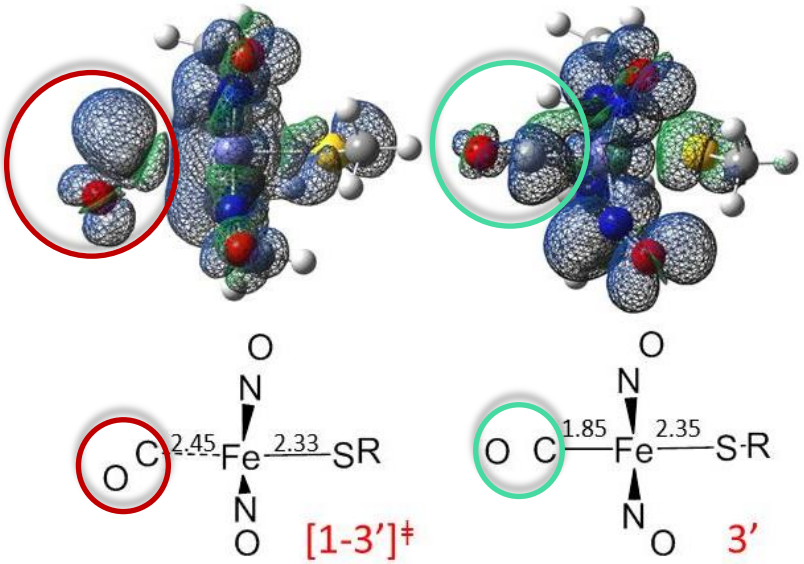

∠Fe-N-O **164.0°** **152.1°**

Figure IV-13. Spin density plots for **[1−3′]‡** and **3′** in the mechanism involving the homolytic cleavage of the Fe-S bond resulting in the direct loss of the thiyl radical, with distances in structures below. Relevant changes in the ∠Fe-N-O are shown underneath each structure. Note that the NHC ligand is behind the Fe in the five-coordinate species.

The formation of a five-coordinate intermediate as predicted by computations was unexpected, especially given that CO is a poor nucleophile. Interestingly, the orbital interaction during the "attack" of the incoming CO with 17-electron complex **1** is proposed to involve a side-on approaching CO leading to transition state [**1**−**3′**]‡ (Figure IV-13). Hence, according to computations, the reaction is initiated with nucleophilic attack by the electron density of the $Fe(NO)_2$ unit on the empty π* orbitals of the CO, and once the CO draws closer to the Fe, it reverts to the classical σ-donor/ π-acceptor type bonding, as seen in intermediate **3′**. Intermediate **3′** is therefore a 19-electron intermediate, where the NO ligands bend to accommodate the excess charge. Subsequent loss of a RS• results in a stable, 18-electron complex.

Further ligand dependence

As discussed above, calculations suggest that $Fe(NO)_2$ transiently serves as a nucleophile towards the empty π* orbitals of CO. This would suggest that ligands without available electrophilic sites might react with a different mechanism. Inspired by the computational results, a preliminary study of such ligand effects was carried out using PPh_3, PMe_3 and $P(OMe)_3$ ligands. In fact, under the same solvent and monitoring conditions as was determined for CO (whose second-order rate constant is 2.4×10^{-3} $M^{-1} \bullet s^{-1}$ at 30°C), PPh_3 was unreactive with complex **1**. In order to rule out possible steric impedence, the smaller PMe_3 and $P(OMe)_3$ ligands were exposed to **1**, maintaining pseudo first order conditions through 20-fold excesses of the ligands.

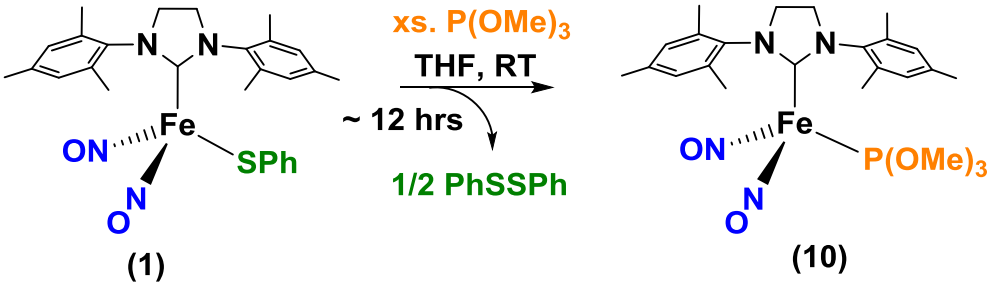

Figure IV-14. Reaction of oxidized $\{Fe(NO)_2\}^9$ complex **1** with $P(OMe)_3$ to form reduced $\{Fe(NO)_2\}^{10}$, $(NHC)((MeO)_3P)Fe(NO)_2$.

In the presence of $P(OMe)_3$, the oxidized $\{Fe(NO)_2\}^9$ complex **1** converts to the reduced, $\{Fe(NO)_2\}^{10}$ complex $(NHC)((MeO)_3P)Fe(NO)_2$, complex **10** over the course of 12 hours. The *in situ* IR spectral monitor indicated ν(NO) positions shifting from 1768, 1720 cm^{-1}(toluene) to 1720, 1672 cm^{-1} (toluene) (Figure IV-15), and **10** was isolated as red crystals and identified by x-ray crystallography (Figure IV-16). The elimination of PhSSPh in this process was confirmed by ^{1}H-NMR spectroscopy as described earlier in the reaction of **1** with CO. The rate constant as calculated (preliminary kinetic studies done by Sam Kyran) for this reaction is 10.2 x 10^{-4} $M^{-1}•s^{-1}$ at 30°C.

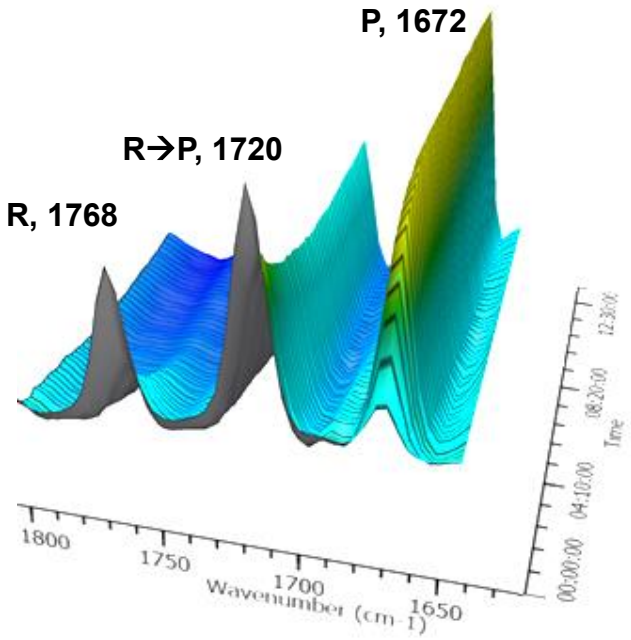

Figure IV-15. Three-dimensional stacked plot of the reaction of complex **1** with $P(OMe)_3$ at 303 K in toluene. R = reactant bands, P = product bands.

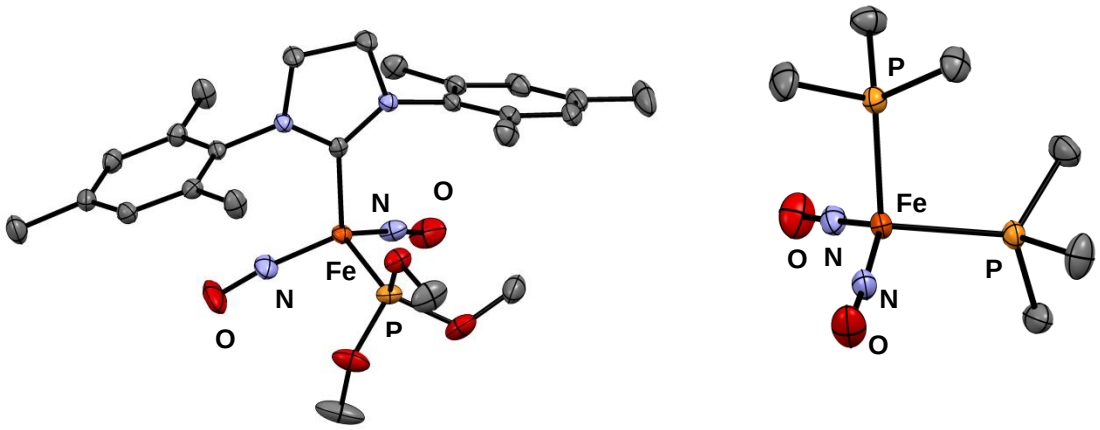

Figure IV-16. Molecular structures of complex **10** (left) and complex **11** (right). ORTEP with thermal ellipsoids drawn at 50% probability (H atoms omitted).

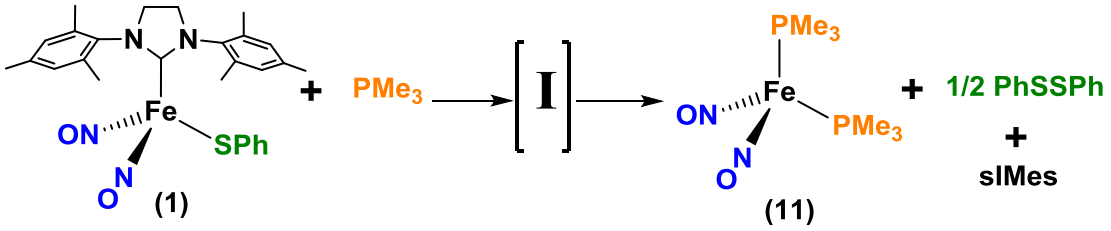

Figure IV-17. Reaction of oxidized $\{Fe(NO)_2\}^9$ complex **1** with $P(Me)_3$ to form reduced $\{Fe(NO)_2\}^{10}$, $(Me_3P)_2Fe(NO)_2$.

The PMe_3 reaction is however complicated as both NHC and •SPh are displaced by the phosphine (Figure IV-17). From this reaction the reduced $(Me_3P)_2Fe(NO)_2$ product (complex **11**) was identified by x-ray crystallography (Figure IV-16). Complex **11** was also synthesized *via* an alternate route to confirm characterization. In this route, $Fe(CO)_2(NO)_2$ was reacted with excess PMe_3 at 50 °C for 5 days. Infrared spectral monitor showed that disubstitution to form $(Me_3P)_2Fe(NO)_2$ proceeded through initial complete conversion of $Fe(CO)_2(NO)_2$ into the monosubstituted product, $Fe(CO)(PMe_3)(NO)_2$ (Figure IV-18), prior to the second CO/ PMe_3 exchange.

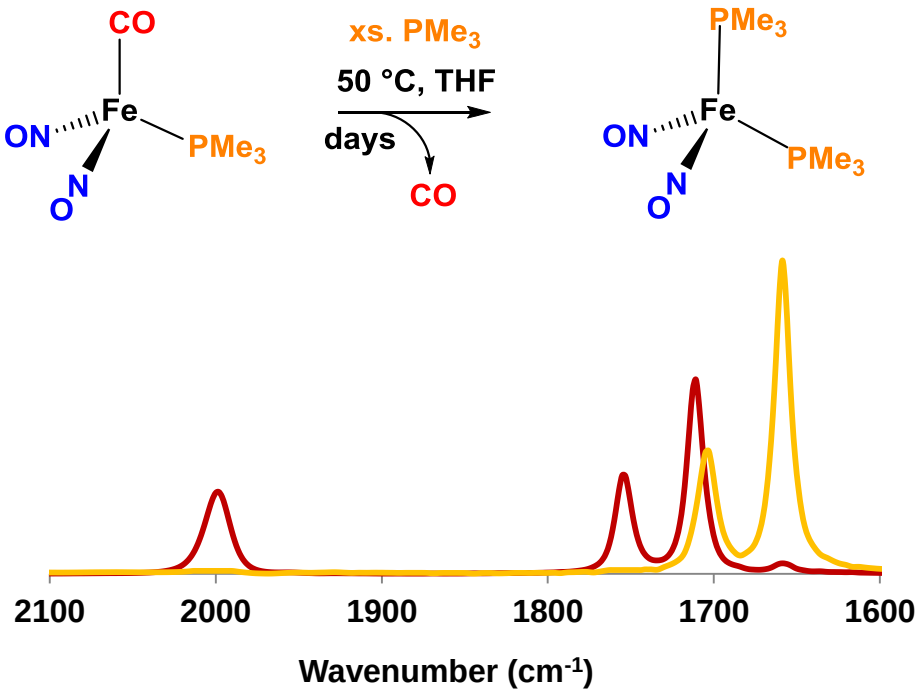

Figure IV-18. Top: Alternate route for the synthesis of complex **11.** Bottom: Overlay of corresponding IR spectra in THF. [Red: $Fe(CO)(PMe_3)(NO)_2$: ν(CO) 1998(s), ν(NO) 1754(s), 1709(vs) cm^{-1}], [Orange: **11**: ν(NO) 1705(s), 1659(vs) cm^{-1}].

The *in situ* IR monitor of the reaction of **1** with PMe_3 showed IR ν(NO) positions shifting to lower wavenumbers (preliminary kinetic studies done by Sam Kyran). The formation and fast decay of an intermediate (ν(NO) 1753, 1708 cm^{-1}(toluene)) simultaneous with product (complex **11**, (ν(NO) 1708, 1664 cm^{-1}(toluene)) formation was observed (Figure IV-19). The rate constant calculated based on the disappearance of the reactant NO bands is 7.2 x 10^{-4} $M^{-1}•s^{-1}$ at 30°C. We have thus far been unable to identify the aforementioned intermediate; but speculate a five-coordinate species is involved, *vide infra*. Attempts to identify this intermediate are as follows.

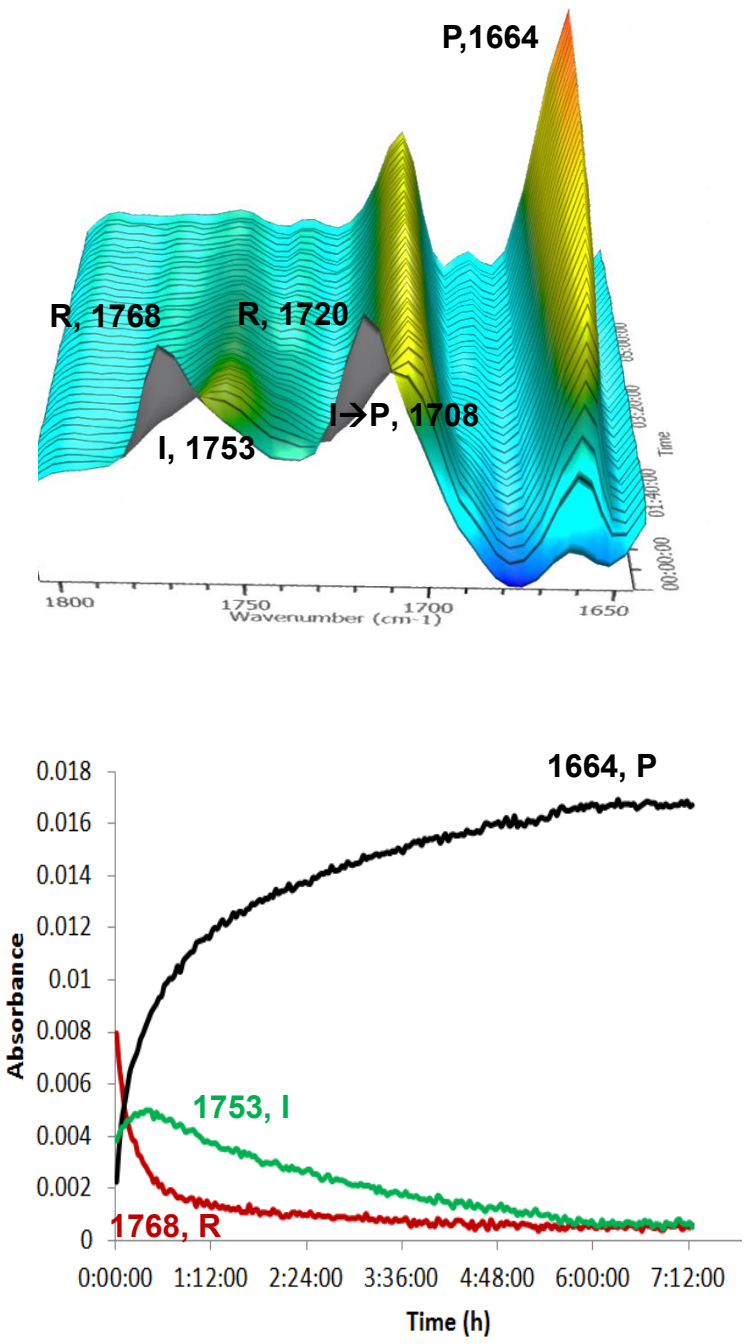

Figure IV-19. (Top) Three-dimensional stacked plot (Bottom): Reaction profiles, of the reaction of complex **1** with $P(Me)_3$ at 303 K in toluene. R = reactant bands, P = product bands, I = intermediate bands.

A mixed NHC/ PMe_3 DNIC, complex **12**, was synthesized to test the possibility of it being the unknown intermediate. Complex **2**, $Fe(CO)(sIMes)(NO)_2$ (synthesized directly according to literature procedure for the corresponding IMes analogue)[65] was photolyzed using a regular sun lamp, in the presence of 1 eq. PMe_3 over 12 hours, yielding complex **12** (Figure IV-20), which was purified by washing with hexanes to produce red crystals of x-ray quality (Figure IV-21). The IR ν(NO) positions for complex **12** in THF were found at 1697, 1653 cm^{-1}, lower than the bis-PMe_3 DNIC **11** by ca. 7 cm^{-1}. However, these IR ν(NO) positions are clearly much lower than those observed for the aforementioned intermediate, thereby eliminating it from being a possible candidate.

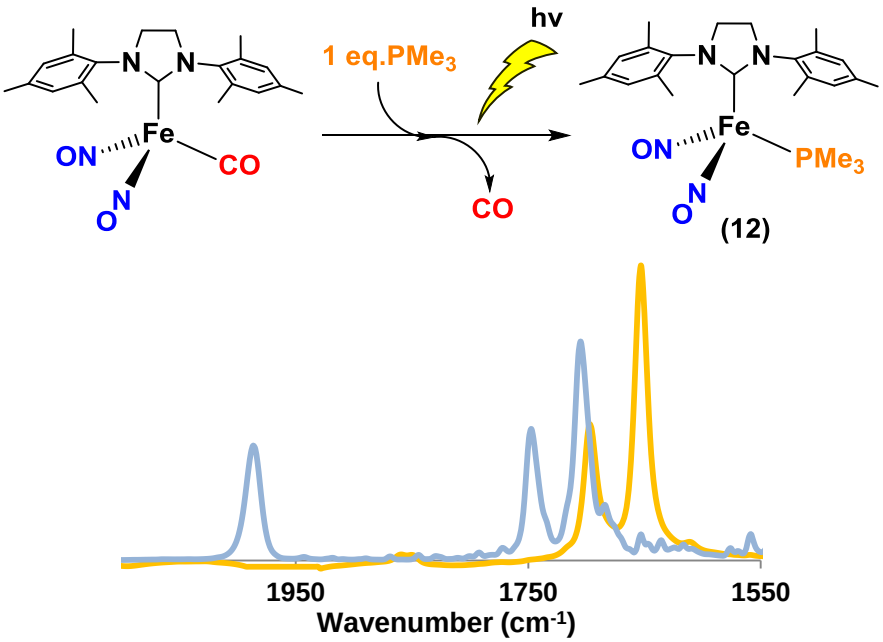

Figure IV-20. Top: Reaction scheme for the synthesis of complex **12.** Bottom: Overlay of corresponding IR spectra in THF. [Blue: **2**: ν(CO) 1986(s), ν(NO) 1747(s), 1705(vs) cm^{-1}], [Orange: **12**: ν(NO) 1697(s), 1653(vs) cm^{-1}].

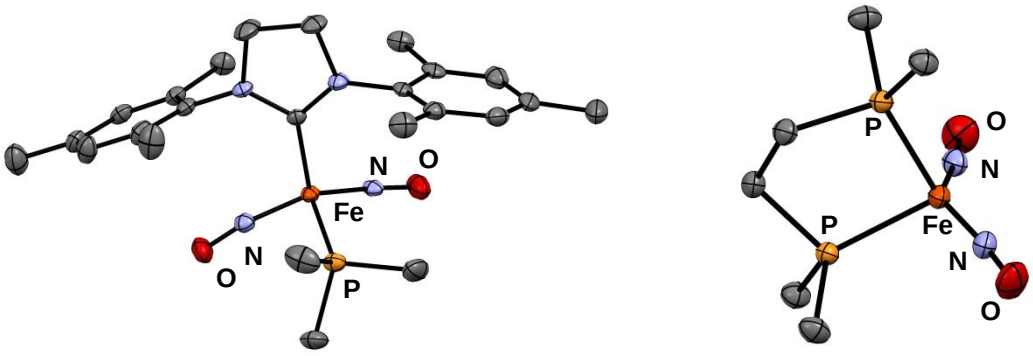

Figure IV-21. Molecular structures of complex **12** (left) and complex **13** (right). ORTEP with thermal ellipsoids drawn at 50% probability (H atoms omitted).

Preliminary reactions of complex **1** with 1,2-Bis(dimethylphosphino)ethane (DMPE) were conducted to test the possibility of the formation of the κ^1- coordinated product. If such a product could be isolated, it would confirm which of the NHC or •SPh displacement took place first, and whether the mono-substituted product was the observed intermediate. This reaction also proceeded with the ν(NO) positions shifting to lower wavenumbers. However in this case, the IR spectra indicated a mixture of products, from which, bands at 1703 cm^{-1} and 1658 cm^{-1} could be assigned to $Fe(NO)_2$(DMPE) as confirmed by the synthesis of this compound *via* an alternate route (i.e. reaction of $Fe(CO)_2(NO)_2$ with 1 eq. DMPE) (Figure IV-22). Furthermore, x-ray quality crystals of this DMPE-DNIC (complex **13**) were isolated from the product mixture from concentrated solutions of diethyl ether (Figure IV-21). The second pair of IR bands at 1740 cm^{-1} and 1692 cm^{-1} are of the expected pattern and $\Delta\nu_{NO}$ ($\Delta\nu_{NO}$ = the difference between the ν(NO) band positions) for a DNIC.[46] However, whether this is in fact the κ^1- coordinated product needs further study.

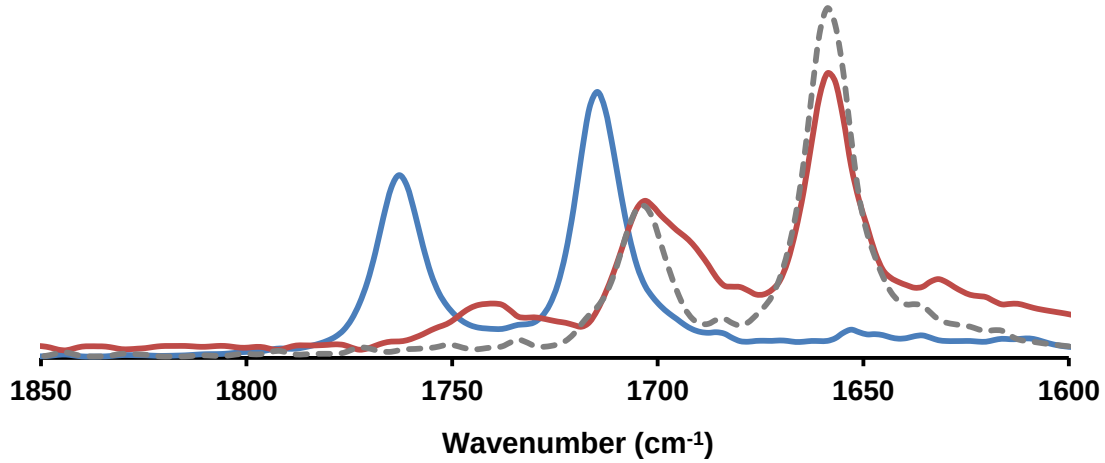

Figure IV-22. Overlaid IR spectra in THF for the reaction of **1** with DMPE. [Blue: **1**: ν(NO) 1763(s), 1715(vs) cm^{-1}], [Red: Product mixture: ν(NO) 1703(s), 1658(vs) cm^{-1}, 1740(w), 1692(sh) cm^{-1}]. [Dashed line inset: **13**: ν(NO) 1703(s), 1658(vs) cm^{-1}].

The observation of an intermediate in the case of the reaction of **1** with PMe_3 is not completely understood. The IR $\Delta\nu_{NO}$ value has been suggested in the literature as a parameter for the characterization of four coordinate vs. five coordinate DNICs.[46] Accordingly, the IR $\Delta\nu_{NO}$ for four coordinate DNICs is 40-60 cm^{-1}, while that for the rare five coordinate species is reported as ~ 80 cm^{-1}.[46] The IR $\Delta\nu_{NO}$ of the intermediate observed in the reaction of **1** with PMe_3 is 45 cm^{-1}, falling into the range of the four coordinate DNICs. However, in the event that synthesis by alternate routes could rule out a four coordinate intermediate, we speculate a five coordinate intermediate is possible with a weakly interacting phosphine.

Despite the complexities of the PR_3 substitution process, preliminary data presented above indicate slower reaction rates for such incoming ligands when compared

to CO. This observation is inconsistent with typical nucleophilic substitution processes, but is consistent with our interpretation of the importance of the $\pi - \pi^*$ interaction available to the $Fe(NO)_2$ unit in the case of CO. A more extensive study of this unusual ligand effect would benefit in understanding this process.

Structural studies of phosphine-DNICs

Only a handful of DNICs containing phosphine ligands have been crystallographically characterized.[40] These preliminary studies with phosphine ligands have therefore contributed several structures to the available collection of phosphine-bound DNICs. Table IV-3 lists selected metric parameters of the new reduced, $\{Fe(NO)_2\}^{10}$ phosphine-bound DNICs together with their IR ν(NO) values. The trend in the IR ν(NO) values is bisNHC-DNIC < (NHC)(PMe_3)-DNIC < bisPMe_3-DNIC, indicating that at least within this series, NHCs are better donors to the $\{Fe(NO)_2\}$ unit compared to phosphines.

Table IV-3. IR ν(NO) values and important metric parameters and selected for selected NHC and phosphine containing DNICs. Crystallographic data/ refinement parameters for the newly synthesized compounds are shown.

	ν(NO) (cm^{-1})	**∠Fe-N-O[a] (°)**	**Fe-N(O)[a] (Å)**	**N-O[a] (Å)**
$Fe(NO)_2(IMe)_2$[41]	1667, 1624	174.0 (5)	1.659 (6)	1.202 (6)
$Fe(NO)_2(sIMes)(PMe_3)$ **(12)**	1697, 1653	173.9 (3)	1.656(3)	1.189 (4)
$Fe(NO)_2(PMe_3)_2$ **(11)**	1705, 1659	178.3 (1)	1.657 (3)	1.196 (4)
$Fe(NO)_2$(DMPE) **(13)**	1703, 1658	174.4 (1)	1.654 (1)	1.200 (1)
$Fe(NO)_2(sIMes)(P(OMe)_3)$ **(10)**	1716, 1669	173.6 (1)	1.652 (1)	1.193 (2)
$Fe(NO)_2(PPh_3)_2$[110]	1724, 1678	178.2 (7)	1.650 (7)	1.190 (0)

	Empirical formula	**Space group**	**Z**	**R**
(10)	C24 H35 Fe N4 O5 P	P21/c	4	0.03
(11)	C6 H18 Fe N2 O2 P2	P-1	4	0.04
(12)	C24 H35 Fe N4 O2 P	P -1	2	0.06
(13)	C6 H16 Fe N2 O2 P2	C 1 2/c 1	4	0.03

[a]Average values

All complexes are pseudotetrahedral; the average Fe-N(O) and N-O distances compare well with previously reported $Fe(NO)_2(IMe)_2$ and $Fe(NO)_2(PPh_3)_2$complexes as shown in Table IV-3.[41,110] The average Fe-N-O angles for the new complexes is ~174°, that can be considered linear and compare well with previously reported neutral $\{Fe(NO)_2\}^{10}$ DNICs with strongly donating NHC and phosphine ligands. As seen in Figure IV-23, in complexes **11** and **13**, the methyl groups of the phosphines have a staggered arrangement, with a twist in the backbone of the DMPE ligand in **13**. Figure IV-23 also compares the ∠N-Fe-N and ∠O-Fe-O of the newly characterized phosphine-DNICs. While complexes **10** and **11** show the previously discussed "attracto" conformation[75] where the NO ligands bend in towards each other (larger ∠N-Fe-N than ∠O-Fe-O), the bis-PMe_3 complex **11** has near linear average Fe-N-O angles (178.3°), closely matching Fe-N-O angles of the previously reported bis-PPh_3 complex (178.2°).[110] Of particular interest is complex **13** bearing the DMPE ligand, which shows the rare "repulso" conformation where the NO ligands bend away from each other (Figure IV-23). This is characterized by the smaller N-Fe-N angle (139.17° (8)) compared to the O-Fe-O angle (143.76° (5)). To our knowledge, only two other DNICs with the "repulso" conformation exist in the literature.[76]

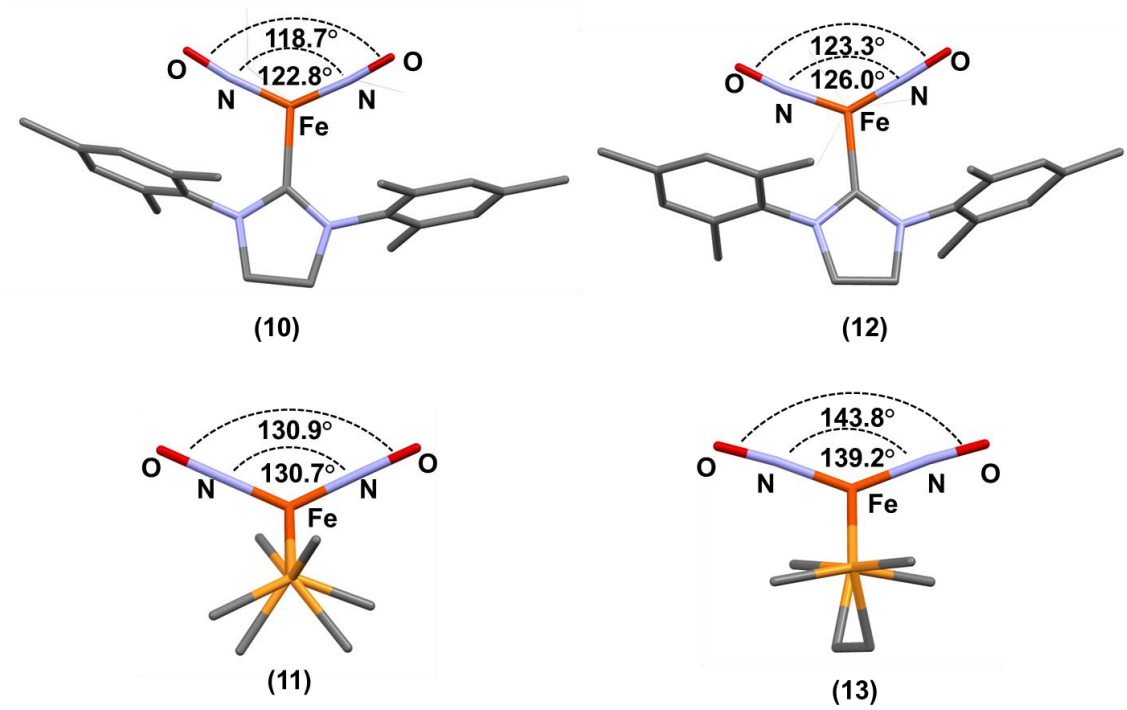

Figure IV-23. Rotated capped stick renditions of molecular structures of complexes **10-12**, showing ∠N-Fe-N (as inner angles) and ∠O-Fe-O (as outer angles). Complexes **10** and **12** are viewed along the Fe-P bond vector, and the PMe_3 and $P(OMe)_3$ groups are at the back in wireframe form for clarity. Complexes **11** and **13** are viewed along the P-P bond vector and show the staggered arrangement of methyl groups.

Conclusions

This study is centered on the relationship of thiolate-disulfide redox activity and its facilitation of the one-electron reduction of an oxidized dinitrosyl iron moiety. While stringent reductive conditions are required for the reduction of $\{Fe(NO)_2\}^9$ to $\{Fe(NO)_2\}^{10}$ in anionic $[X_2Fe(NO)_2]^-$ species,[44] in the case of neutral $L(RS)Fe(NO)_2$ (of which there are few well characterized) as explored in this study, exceedingly mild conditions effect the reduction, needing only the presence of the neutral π acceptor

ligand carbon monoxide. Kinetic studies carried out on this system establish an overall second order experimental rate expression, and the activation parameters calculated thereby point towards an associative mechanism of CO substitution. Computational studies indicate a unique role for the delocalized frontier molecular orbitals of the $Fe(NO)_2$ unit whereby the entering CO ligand is initially engaged through its vacant π^* orbital. The integrity of the $Fe(NO)_2$ unit is verified throughout, permitting ligand exchange of thiolate and CO through a 5-coordinate, 19-electron intermediate with the NO ligands accommodating the excess charge. The rarely isolated 5-coordinate DNICs are known to have significantly bent Fe-N-O on the order of 155-165°,[111,112,48] similar to those calculated for the intermediate **3'**, 146° and 158°.

Major questions exist regarding the roles of NO and CO as diatomic ligands in biology and physiology. In fact, even the possibility that these ligands might appear together in biological milieu has received some notice.[113] Carbon monoxide, derived from heme oxygenase 1 or 2 is reported to stimulate the nitric oxide synthase-NO pathway, reinforcing NO production.[113] Hence, on two levels of chemical features of biological significance, our study of CO-induced disulfide elimination from a dinitrosyl iron thiolate might be taken as a potential model for intracellular, thiol-complexed DNICs, exposed to intracellular CO, inducing redox level changes at iron, and attendant spectroscopic and reactivity properties.

CHAPTER V

HAMMETT CORRELATIONS AS TEST OF MECHANISM OF CO-INDUCED DISULFIDE ELIMINATION FROM DINITROSYL IRON COMPLEXES*

Introduction

That diatomic molecules in combination with metals play vital roles in a variety of physiological functions is well established. While physiologically beneficial carbon monoxide and nitric oxide concentrations are in picomolar to nanomolar range, increasing concentrations result in cytotoxic effects.[18,27,114] Under physiological control CO and NO function as important regulatory and signaling molecules, and are members of a class of endogenously-produced gaseotransmitters.[11-13,115] Much current research is directed at the fundamental biochemistry especially significant in the cardiovascular system, as well as development of compounds as pro-drugs, capable of controlled delivery and release of NO and CO to biological targets—the most important in vasodilation activity being iron in porphyrin environments.[116] As an extensive literature exists for transition metal complexes containing CO and NO, much attention has been directed towards appropriate combinations of ligands and metals designed for specific pharmacological properties.[117] Indeed, explorations of one class of complexes, dinitrosyl iron complexes (DNICs), are inspired by their natural occurrence,[105] and by the intriguing proposal that they might be the "most abundant nitric oxide-derived cellular

*Reproduced in part by permission of The Royal Society of Chemistry. Pulukkody, R.; Kyran, S. J.; Drummond, M. J.; Hsieh, C. H.; Darensbourg, D. J.; Darensbourg, M. Y. *Chem. Sci*. **2014**, *5*, 3795-3802.

adduct", i.e., superceding the S-nitrosothiols (RSNOs).[22] Others have posited that synthetic versions may be developed as NO-release agents.[38]

The chemical properties of CO and NO as ligands to metals are substantially different; the former is viewed as an innocent ligand with weak σ-donor/strong π-acceptor properties in its M-CO bond formation.[118] In contrast, the radical character of NO imparts reactivity that surpasses that of CO, in that its ability to readily switch between the NO^+, •NO, and NO^- forms depends on the redox levels accessible by the metal to which it binds, thereby defining non-innocent ligand binding.[119]

As a poor nucleophile, CO exchange reactions with a metal-bound CO or L typically take place by dissociative mechanisms allowing external CO to be trapped by an open site as in eq V-1.[120] Chapter IV describes an example of CO displacement of $RS^\bullet$ in a dinitrosyliron complex, the kinetics of which followed a second-order rate expression with activation parameters consistent with an associative mechanism, eq V-2. This process entailed a change in the redox state of the reactant DNIC as the oxidized state, $\{Fe(NO)_2\}^9$, converted into the reduced analogue, $\{Fe(NO)_2\}^{10}$. Proceeding under mild conditions, the thermodynamics of the reaction is driven by the formation of RSSR as a result of the release of $RS^\bullet$.

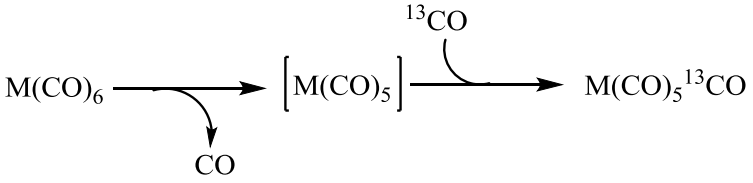

(eq V-1)

$M = Cr^0, Mo^0, W^0$

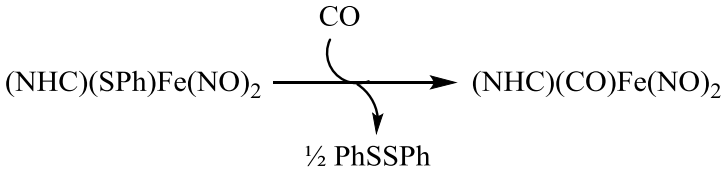

(eq V-2)

$$\text{Rate} = k_2 [CO]^1 [(NHC)(SPh)Fe(NO)_2]^1$$

$$\Delta H^{\ddagger} = 7.80 \pm 0.16 \text{ kcal/mol and } \Delta S^{\ddagger} = -45.0 \pm 0.5 \text{ e.u.}$$

As further described in Chapter IV, computational studies were carried out in pursuit of a reasonable mechanistic proposal for the observed reactivity, resulting in the suggestion that the π-density of the $\{Fe(NO)_2\}$ unit was involved in nucleophilic attack on CO, the latter acting as an electrophile, Figure V-1. Theory suggested a side-on approach of CO leading to a 5-coordinate intermediate, species **I** of Figure V-1, with the NO ligands accommodating the excess charge. Such nucleophilicity of the iron in $\{Fe(NO)_2\}$, especially in the oxidized $\{Fe(NO)_2\}^9$, was unexpected.

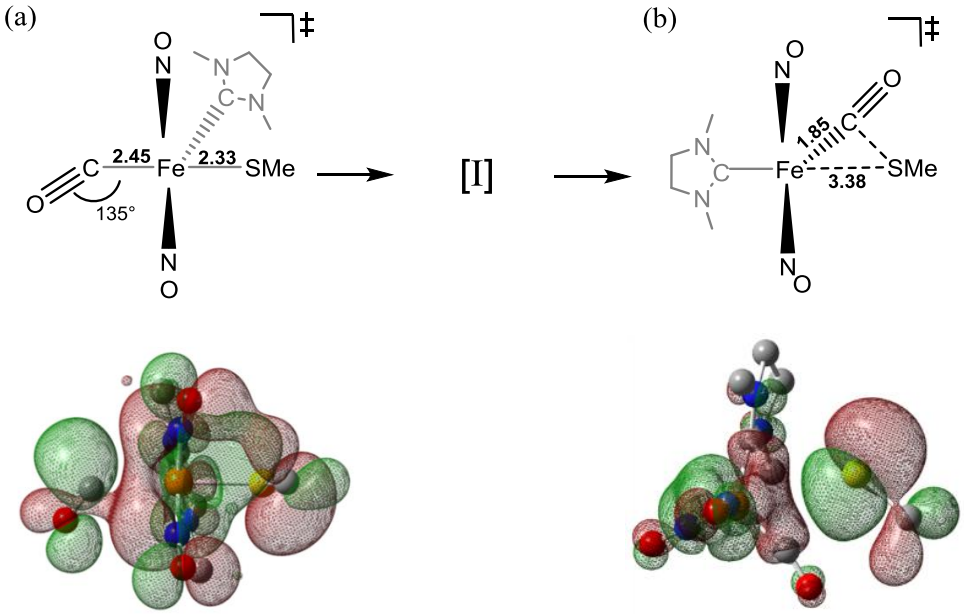

Figure V-1. (Top) (a) A sketch of the calculated collision complex, involved in the rate determining step for CO and (NHC)(RS)Fe(NO)$_2$, proceeding through a 5-coordinate intermediate **I**. Theory finds that as the Fe-CO bond becomes linear as in (b), the Fe-SR bond lengthens, and releases a thiyl radical, either by direct homolytic Fe-S bond cleavage or *via* homolytic C-S cleavage from a transient metallothioester group. (Bottom) Corresponding plots of the transition state SOMOs: (a) the unpaired electron on the {Fe(NO)$_2$} donates into the π* orbital of the side-on entering CO; and (b) the shift of the unpaired electron releases thiyl radical.

This chapter describes experiments designed to test the mechanistic proposal that had suggested such a unique role of the {Fe(NO)$_2$} unit in the CO - induced disulfide elimination. We have prepared a series of analogous {Fe(NO)$_2$}[9] [(NHC)(*p*-S-C$_6$H$_4$X)Fe(NO)$_2$] complexes, where the *para*- substituents X were systematically varied from electron donor to electron withdrawing groups that might be used in a Hammett analysis of their effects on electron density at the Fe(NO)$_2$ unit. Data from ν(NO) IR

spectroscopy and cyclic voltammetry was used to track the differences of the electron density at the {$Fe(NO)_2$} unit in response to the aryl substituent. Systematic changes were observed in the rates of reaction when each derivative was exposed to $CO_{(g)}$, consistent with the electronic changes at the $Fe(NO)_2$ unit.

Synthesis and isolation

A series of dinitrosyliron complexes containing *para*-substituted aryl thiolates, (sIMes)(S-C_6H_4X)$Fe(NO)_2$ (compounds **1a-1e**) was synthesized by homolytic cleavage of the corresponding Roussin's Red Ester (RRE),[64] (μ-(S-C_6H_4X))$_2$[$Fe(NO)_2$]$_2$ by two equivalents of the sIMes ligand (freshly prepared by combining 1,3-bis(2,4,6-trimethylphenyl)imidazolinium chloride and NaO^tBu in a 1:1 stoichiometric ratio). Figure V-2 shows the synthetic protocol along with Hammett parameters[121] for the substituents of the *p*-SC_6H_4X series. The brown RRE solution changed to blue/purple, from which purple solids were isolated upon recrystallization with cold hexane.

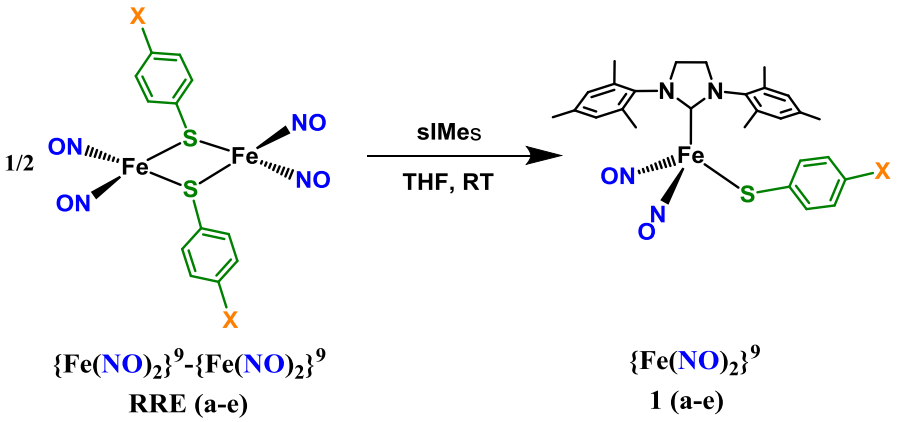

$\{Fe(NO)_2\}^9$-$\{Fe(NO)_2\}^9$
RRE (a-e)

$\{Fe(NO)_2\}^9$
1 (a-e)

	a	**b**	**RRE/1**	**c**	**d**	**e**
X	OCH_3	CH_3	H	Cl	CF_3	NO_2
σ_p[121]	-0.268	-0.170	0.000	0.230	0.540	0.778

Figure V-2. Synthesis of substituted aryl thiolates, $(sIMes)(S\text{-}C_6H_4X)Fe(NO)_2$.

The DNICs **1a-1e** were stable under inert atmosphere for several months in the solid state. In solution, under inert atmosphere, stability was diminished to 2-3 weeks. Four members of the series (**1a, 1b, 1c** and **1e)** were characterized by X-ray crystallography and their molecular structures are compared in Figure V-3. X-ray quality crystals of **1b** and **1c** were obtained by slow evaporation of concentrated ether solutions, while those of **1a** and **1e** were obtained from solutions of THF/ Hexane.

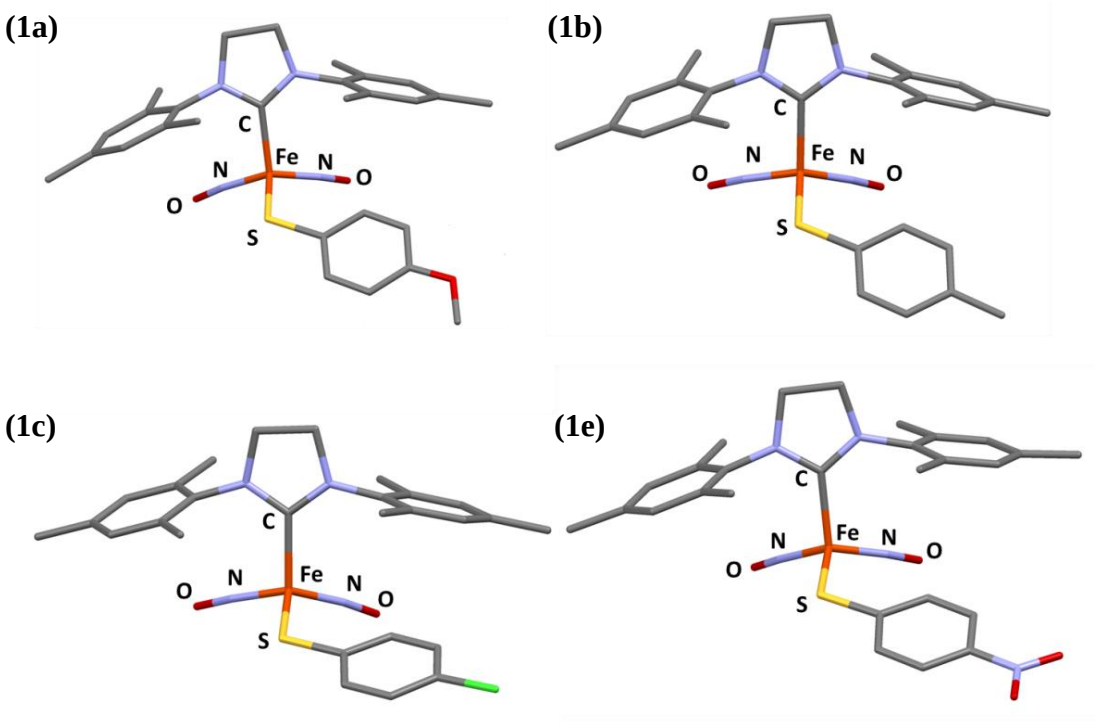

Figure V-3. Molecular structures of **1a**, **1b** (cyclohexane packing solvent omitted for clarity), **1c** and **1e**, from X-ray diffraction analysis.

The complexes in Figure V-3 are tetrahedral wherein the CN_2C_2 plane of the sIMes bisects the S-Fe-N angles of the trigonal base; that is, the NHC plane does not eclipse the Fe-N or Fe-S bond vectors. The planes of the mesitylenes are roughly perpendicular to the CN_2C_2 plane and appear to umbrella the $Fe(NO)_2SR$ motif. All structures maintain the previously described "attracto" conformation[55] where the two Fe-N-O with slight deviations from linearity, are oriented towards each other. The Fe-N-O angles and all other metric parameters of structures **1a, 1b, 1c** and **1e** are comparable to each other and to those of the $[(sIMes)(SPh)Fe(NO)_2]$ analogue (Chapter IV). Although barely within significant limits, there appears to be a gradual decrease of Fe-C_{NHC} bond

lengths with the electron withdrawing ability of the *para* substituent on the S-C_6H_4, concomitant with an increase in the Fe-S bond distance. This correlation is further reflected in the ν(NO) vibrational spectra. Table V-1 lists selected bond distances and angles for **1a, 1b, 1c** and **1e**. Crystals of the complex **1d** have thus far eluded crystallization.

Table V-1. Selected bond distances and angles in [(sIMes)(S-C_6H_4X)Fe$(NO)_2$] complexes **1a, 1b, 1c** and **1e.**

	1a **X = OCH_3**	**1b** **X = CH_3**	**1c** **X = Cl**	**1e** **X = NO_2**
		Bond Distances (Å)		
Fe-C	2.052(2)	2.049(2)	2.048(2)	2.044(2)
Fe-NO[a]	1.672(2)	1.674(1)	1.675(2)	1.673(2)
Fe-S	2.243(1)	2.239(1)	2.248(1)	2.259(1)
N-O	1.177(2)	1.172(2)	1.176(2)	1.172(2)
	1.178(2)	1.175(2)	1.168(2)	1.172(3)
		Bond Angles (deg)		
N-Fe-N	115.5(1)	115.4(1)	116.8(1)	110.9(1)
Fe-N-O	167.4(1)	168.6(1)	169.5(1)	165.7(1)
	169.0(1)	167.8(1)	169.7(2)	163.7(2)
C-Fe-NO[a]	106.0(1)	106.3(1)	106.0(1)	106.0(1)
C-Fe-S	112.0(1)	109.5(1)	109.1(1)	107.5(1)

[a] average distance or angles. The maximum deviations from the average distances and angles are shown in the table.

Infrared spectroscopy

Noticeable shifts in the positions and pattern of the ν(NO) bands in the solution IR spectra allowed monitoring of the complete conversion of the RRE precursor to the corresponding dinitrosyl iron monomers. The ν(NO) position of both the **RRE(a-e)** series and the DNIC series **(1a-1e)**, showed small but systematic shifts to lower wavenumber over an overall range of *ca.* 12 cm^{-1} when the *para* substituent was varied from electron-withdrawing groups (EWGs) to electron-donating groups (EDGs), in agreement with arguments of π-back bonding (Figure V-4). Analysis of the ν(NO) positions and their correspondence to the *para* substituent on the $–SC_6H_4X$ using the Hammett parameter[121] σ_p is given in Figure V-4. The unsubstituted analogues (where X = H), the **RRE** $[(\mu\text{-}(S\text{-}C_6H_5))_2[Fe(NO)_2]_2]$, and complex **1** $[(sIMes)(SPh)Fe(NO)_2]$, are also included in the above analysis.

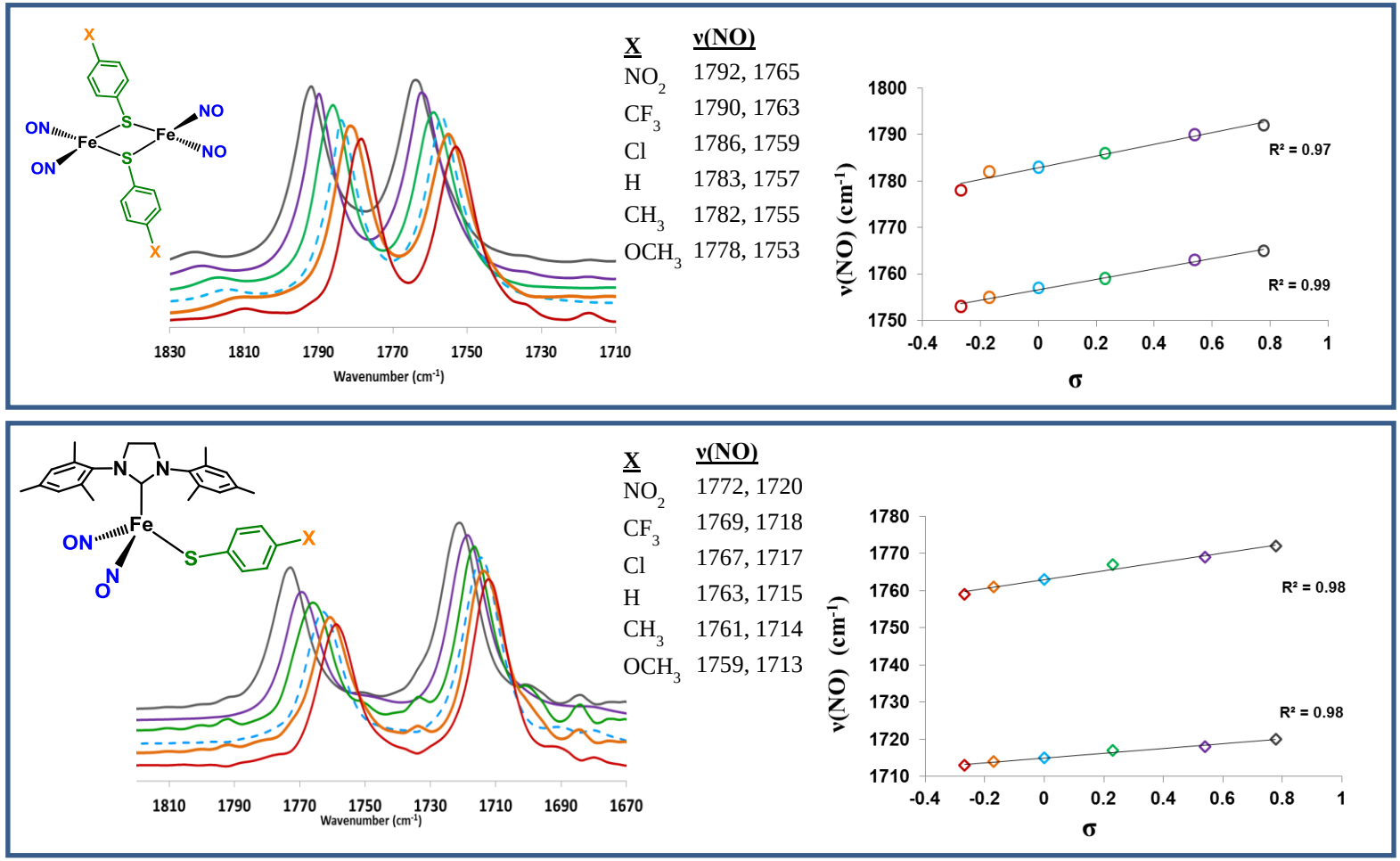

Figure V-4. Top panel (left) overlaid IR spectra for **RRE**, **RRE(a-e)**; (right) plots of the two ν(NO) bands for **RRE, RRE(a-e)** vs. the Hammett substituent parameter σ_p. Bottom panel (left) overlaid IR spectra for **1**, **1a-1e**; (right) plots of the two ν(NO) bands for **1**, **1a-1e** vs. the Hammett substituent parameter σ_p. **a** (red), **b** (brown), **1/RRE** (blue; dashed line), **c** (green), **d** (purple), **e** (grey).

Assuming idealized C_{2v} symmetry, the ν(NO) values were used to calculate the relevant NO force constants using an analogous process to that developed by Cotton-Kraihanzel for CO stretching force constants (eqs V-3 and V-4),[122,123] where k_1 is the NO stretching force constant and k_c is the interaction constant, Table V-2. Figure V-5 shows a plot of the calculated force constants (k_1) and the Hammett parameter σ_p. Thus, although remote from the metal, the X substituent on the aryl group has a subtle but systematic effect on the electron density at the metal center, as reported by the ν(NO) values.

$$\lambda_1 = \mu (k_1 + k_c) \qquad \textbf{(eq V-3)}$$

$$\lambda_2 = \mu (k_1 - k_c) \qquad \textbf{(eq V-4)}$$

where

$$\lambda = (5.8890 \times 10^{-2}) \nu^2$$

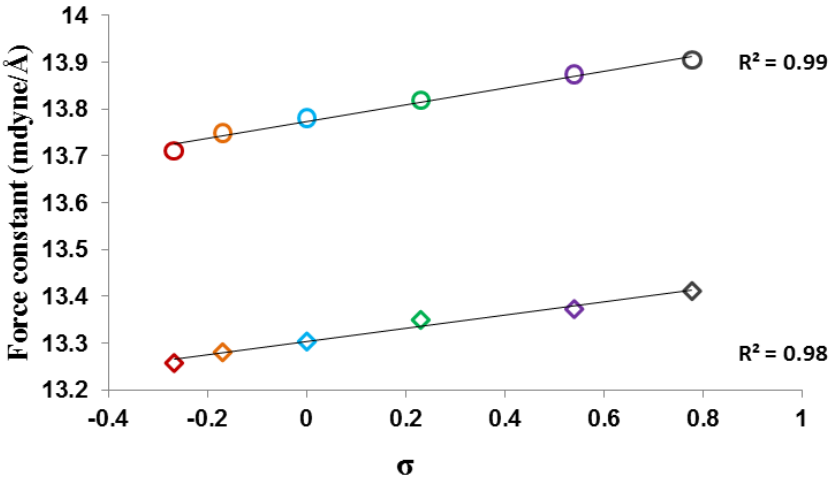

Figure V-5. Plots of force constant (k_1) for (top, circles) **RRE, RRE(a-e)** and (bottom, diamonds) **1**, **1a-1e** vs. the Hammett substituent parameter σ_p.

Table V-2. Summary of characterization data used to obtain Hammett correlations of complexes **1a-1e.**

Complex	*p*-X substituent	ν(NO) cm^{-1} (THF)		Force constant (k_1) (mdyne $Å^{-1}$)	$E_{1/2}$ [a] (mV)
		Sym	Asym		
1a	OCH_3	1759	1713	13.26	-1.44
1b	CH_3	1761	1714	13.28	-1.41
1	H	1763[b]	1715[b]	13.30	-1.40
1c	Cl	1767	1717	13.35	-1.33
1d	CF_3	1769	1718	13.37	-1.30
1e	NO_2	1772	1720	13.41	-1.19

[a] $E_{1/2}$ values are referenced to Cp_2Fe/Cp_2Fe^+. [b] Previous work (Chapter IV)

EPR spectroscopy

The EPR spectra of complexes **1a-1e** were recorded in THF solution at 295 K. All complexes display broad rhombicity in the EPR signal, with observed *g* values: g_1 = 2.027, g_2 = 2.024, g_3 = 2.020 (Figure V-6 is a representative EPR spectrum). Varying the substituent at the *para* position does not appear to affect the EPR derived g value of these complexes.

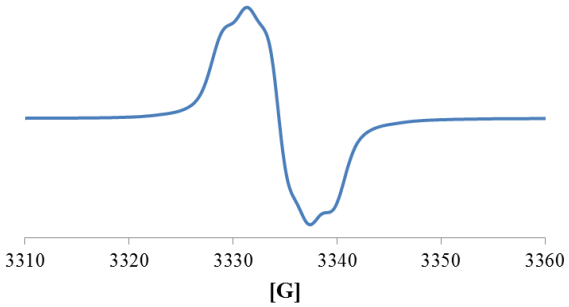

Figure V-6. X-band EPR spectrum of complex **1a** in THF solution at 295 K.

Electrochemistry

The electronic effect of the X-substituent of the $–SC_6H_4X$ series as interpreted from the ν(NO) IR values is also reflected in the electrochemistry. The unsubstituted analogue, complex **1** [(sIMes)(SPh)Fe$(NO)_2$], shows a reversible redox event at -1.39 V (in THF solution), which is assigned to the $\{Fe(NO)_2\}^{9/10}$ couple, similar to the previously reported IMes analogue.[41] Reversibility is indicated by an i_{pa}/i_{pc} ratio of 0.997 (at a scan rate of 100 mV/s), and is scan-rate-independent in the range 75 to 250 mV/s, figure V-7. For **1**, the ΔE_p value is ~226 mV. However, under these conditions, the Fc/Fc^+ standard also shows similar separation (Table V-3), again indicating good reversibility.

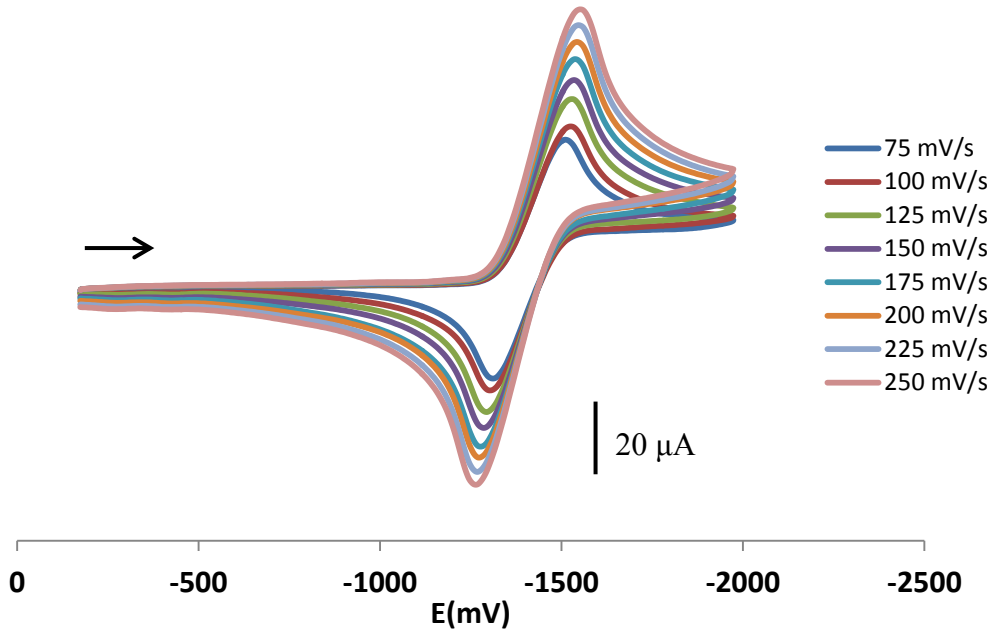

Figure V-7. Scan rate – independent reversibility of **1b** (THF solution, scan rates 75-250 mV/s) as representative of DNICs **1, 1a-1e.** Referenced to Cp_2Fe/Cp_2Fe^+.

Table V-3. Cyclic voltammetric parameter values at a scan rate of 100 mV/s for **1a-1e** in THF solution. $E_{1/2}$ values are referenced to Cp_2Fe/Cp_2Fe^+.

DNICs 1, **1a-1e**	**Scan rate = 100 mV/s**			
X	$\mathbf{i_{pc}/i_{pa}}$	$\mathbf{E_{1/2}}$ **(V)**	**ΔE (mV)**	**ΔE for Fc/Fc^+ standard(mV)**
NO_2	0.96	-1.19	-239	-261
CF_3	0.92	-1.30	-254	-261
Cl	0.98	-1.33	-255	-246
H	1.0	-1.40	-226	-246
CH_3	1.1	-1.41	-261	-246
OCH_3	1.0	-1.44	-256	-261

All other derivatives in the series show similar reversible redox events, also assigned to the $\{Fe(NO)_2\}^{9/10}$ redox couple. These events range from -1.19 V to -1.44 V for the $–NO_2$, $-CF_3$, -Cl, $-CH_3$ and $–OCH_3$ derivatives respectively. The trend in the $E_{1/2}$ is as expected, shifting to higher negative potentials when moving from electron withdrawing groups to electron donating groups (Figure V-8) . There is good correlation between $E_{1/2}$ and the Hammett parameter σ_p as shown in Figure V-9. Also correlating with the ν(NO) values and force constants, these $E_{1/2}$ values are therefore indicative of the changes in electron density occurring at the $Fe(NO)_2$ unit upon changes in the substituent at a remote position. Table V-2 summarizes the characterization data used to obtain Hammett correlations of complexes **1a-1e**.

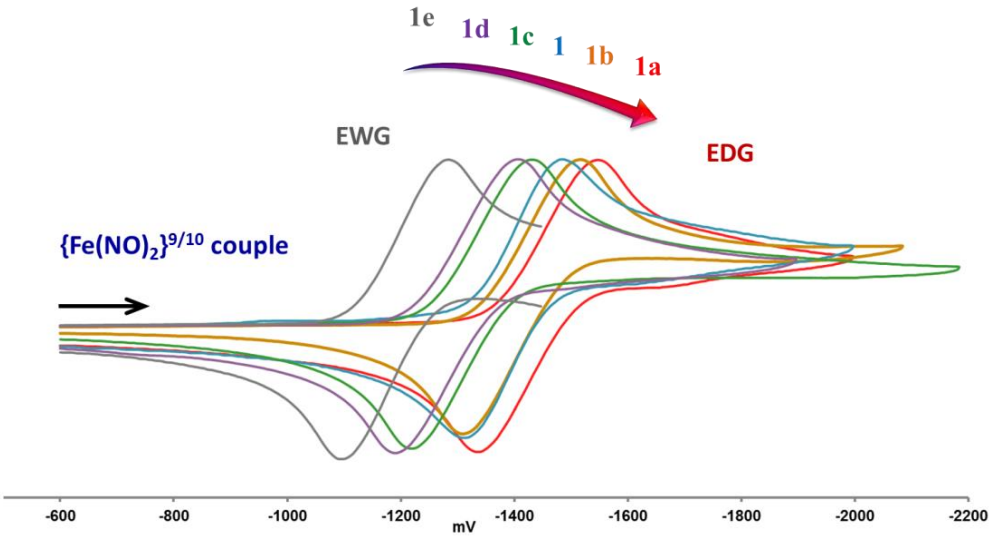

Figure V-8. Overlaid cyclic voltammograms (THF solution, scan rate 100 mV/s, 100 mM [*n*-Bu_4N][BF_4] as supporting electrolyte) of **1a** (red), **1b** (brown), **1** (blue), **1c** (green), **1d** (purple), **1e** (grey; full voltammogram shown in Figure V-10(ii)). All are referenced to Cp_2Fe/Cp_2Fe^+.

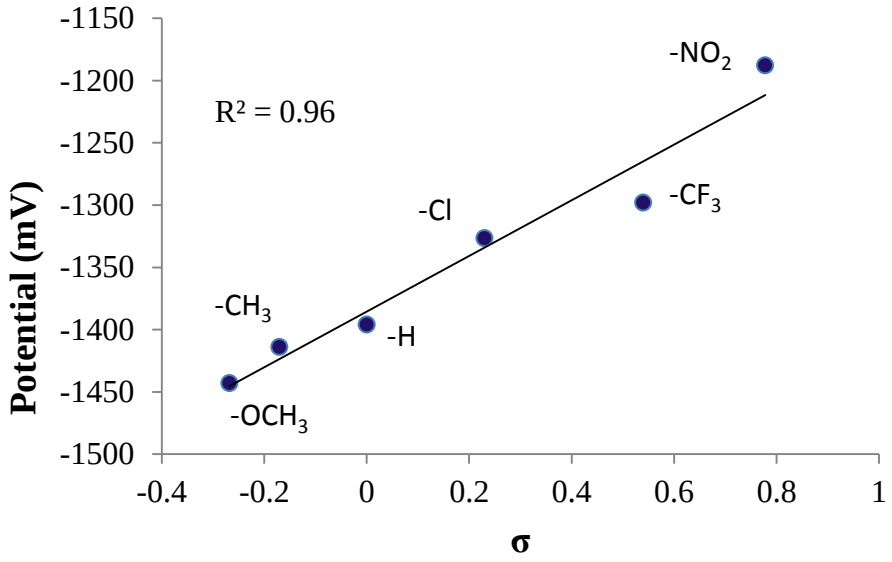

Figure V-9. Plot of $E_{1/2}$ for **1a-1e** vs. the Hammett substituent parameter σ_p. All are referenced to Cp_2Fe/Cp_2Fe^+.

Figure V-10 compares the single reversible redox event for **1c** (Figure V-10(i)) as representative of all members of the series as opposed to the *p*-NO_2 derivative, **1e** (Figure V-10(ii)). For the latter, the reversible redox event centered at -1.19 V is assigned to the $\{Fe(NO)_2\}^{9/10}$ redox couple in accordance with the occurrence of the same redox event for other derivatives in this range of potentials (Figure V-10(i), **1c**). A second reversible event appears at -2.10 V. The latter is assigned to a redox event involving the nitro group of the $S(C_6H_4\text{-}NO_2)$ ligand. Support for this assignment is as follows: Figure V-10(iii) displays the cyclic voltammogram of an authentic sample of bis(4-nitrophenyl) disulfide. The unusual shape is typical of aromatic disulfides in the -500 to -1500 mV range and it is fully reproducible.[124-127] Considering the above, the nearly reversible feature centered around -2.10 V for both bis(4-nitrophenyl) disulfide and **1e** is assigned to a reduction involving the $–NO_2$ group. The small features between the two major redox events in the voltammogram of **1e** are present regardless of the scan direction and still appear when reverse scans are initiated. We have thus far been unable to assign these features to specific redox events.

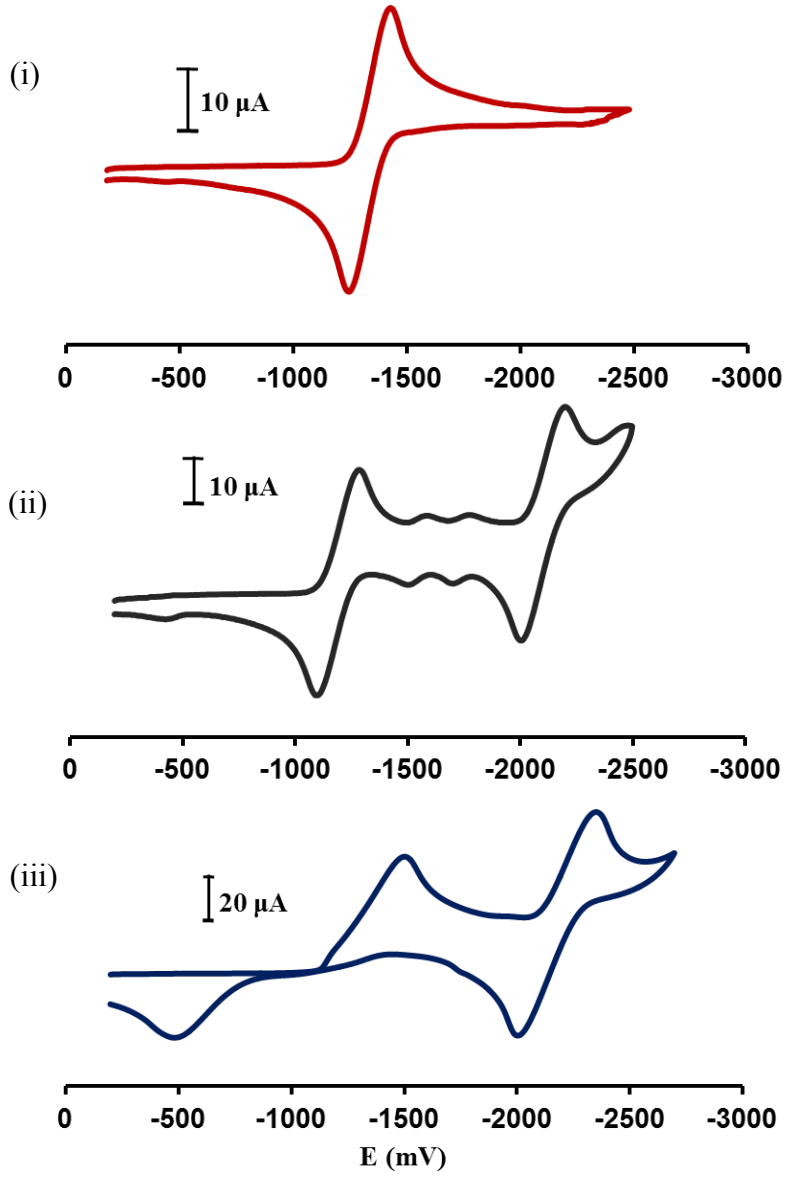

Figure V-10. Cyclic voltammograms of (i) **1c** (ii) **1e** and (iii) bis(4-nitrophenyl) disulfide at scan rates of 100 mV/s in THF (100 mM [*n*-Bu_4N][BF_4] as supporting electrolyte). All are referenced to Cp_2Fe/Cp_2Fe^+.

Kinetic measurements

The rates of conversion of complexes **1a-1e** to **2,** were examined using *in situ* IR spectroscopy (Figure V-11). These studies were conducted by Samuel Kyran under the supervision of Professor D. J. Darensbourg. All iron complexes were maintained under an excess of CO, thereby ensuring pseudo-first-order reaction conditions. Figure V-12 shows the reaction monitor and its respective natural log plot for the reaction between **1b** and CO as representative of all members of the series. Kinetic studies of the closely related unsubstituted analogue as mentioned in chapter IV had established an overall bimolecular process for its reaction with CO. It is reasonable to assume that the reaction of each derivative (**1a-1e)** with CO also followed a second order rate expression, first order in each reagent, (eq V-5) since the kinetic profiles of each were similar to that of the aforementioned unsubstituted analogue. Therefore, the rate constants, *k*, of each reaction were derived from the respective linear natural log plots (eq V-5).

$$\text{rate} = k_{obs}\,[\text{Fe}], \text{ where } k_{obs} = k\,[\text{CO}] \qquad \textbf{(eq V-5)}$$

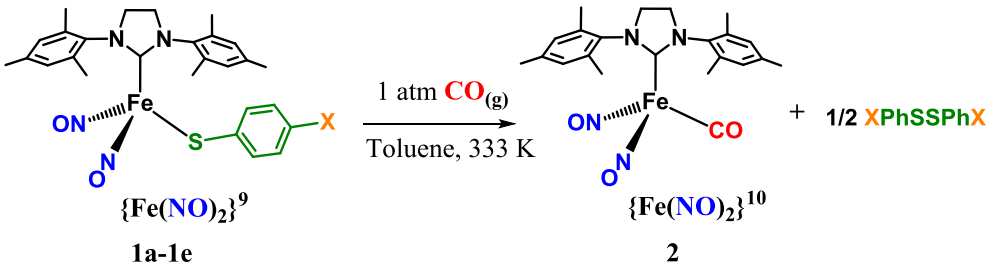

Figure V-11. Reaction of complexes **1a-1e** with CO.

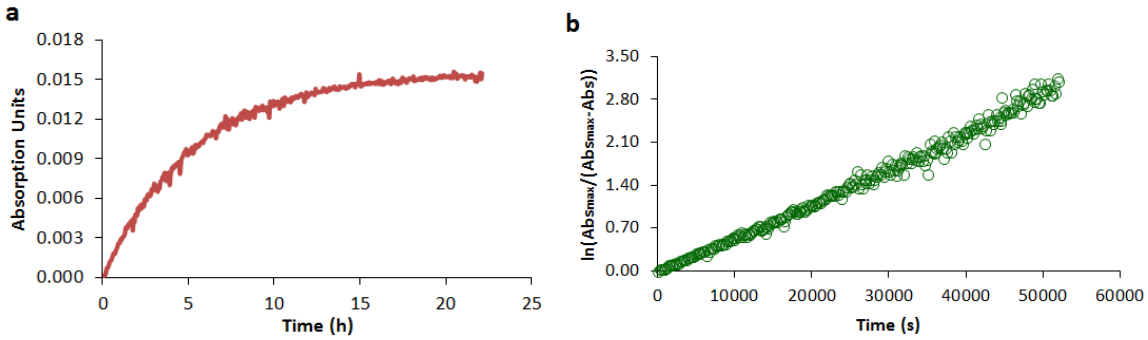

Figure V-12. a) Infrared reaction profile of **2**, monitored at ν(CO) = 1992 cm^{-1}, formed by the reaction of [(sIMes)(S-C_6H_4-CH_3)Fe$(NO)_2$], **1b**, and CO at 333 K in toluene solution. b) Natural log plot of absorption data versus time showing linear trend over three half-lives. The R^2 value is 0.991.

Table V-4 lists the rate constants (*k*) and $t_{1/2}$ values obtained through the kinetic analysis. Rate retardation is observed when the para substituent on the aryl thiolate is changed from electron donating groups to electron withdrawing groups. It must be noted that the nitro species (compound **1e**); containing the most electron withdrawing substituent of the series, shows reaction times that appear to be longer than the solution lifetime of the compound. This is apparent in the significant decomposition that is observed with progression of the reaction. Therefore, in the calculation of the rate parameters, only the first 10% of the reaction data was used, which proved to be linear upon logarithmic treatment. While the inclusion of complete rate data could have resulted in a higher error in the rate measurement, we can conclusively state that the rate of reaction of **1e** with CO is slower than the other complexes. The CF_3 analogue, complex **1d**, containing the next strongest electron withdrawing group, also showed decomposition over its reaction time, but to a lesser extent. The only other point of

notice is the slight deviation seen with the methyl derivative, **1b** where its rate is comparable with the previously described unsubstituted species, compound **1**.

Table V-4. Kinetic parameters for reactions of **1a-1e** with CO obtained from linear fits of natural log plots.

Complex	Substituent	k_{obs} x 10^3 (s^{-1})	k x 10^3 ($M^{-1}s^{-1}$)	$t_{½}$ (h)
1a[i]	OCH_3	0.103 ± 0.012	12.9 ± 1.5	1.9
1b[i]	CH_3	0.0555 ± 0.0030	6.95 ± 0.38	3.5
1[40]	H	0.0603	7.56	3.2
1c	Cl	0.0424	5.31	4.5
1d[ii]	CF_3	0.0172	2.16	11.2
1e[ii]	NO_2	0.00270	0.338	71.4

i) Average of 3 trials. ii) Rates based on first 10% of data due to decomposition of reaction mixture over time.

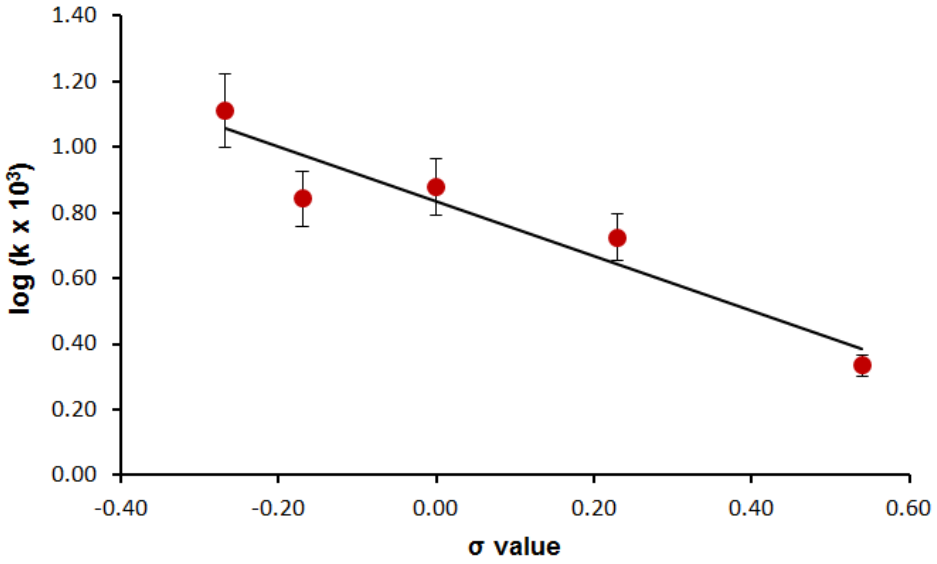

Figure V-13. Hammett plot of rate constants from reactions of DNICs **(1a-1d, 1)** with CO. Error bars are 10% of original value. Slope of trend line is -0.831 with an R^2 of 0.901.

Figure V-13 shows the classical Hammett plot where the rate constants have been plotted against the Hammett parameter $\sigma_{p.}$ The linear trend as evident in the Hammett plot, with a negative slope and a ρ value of -0.831 with an R^2 of 0.901 confirm rate retardation with increasing electron-withdrawing nature of the substituents. The plot in figure V-13 does not include the nitro species, for stability reasons mentioned above, but figure V-14 shows that its inclusion still gives good correlation between the rate data and the Hammett parameter (R^2 of 0.869) with a ρ value of -1.293. The negative ρ value is indicative of the loss of negative charge at the reaction center in the rate determining step. These results are therefore in agreement with our previous computational proposal (Chapter IV) for the mechanism involved, where there is loss of negative charge at the $Fe(NO)_2$ unit as a result of its initial nucleophilic attack on an incoming CO molecule.

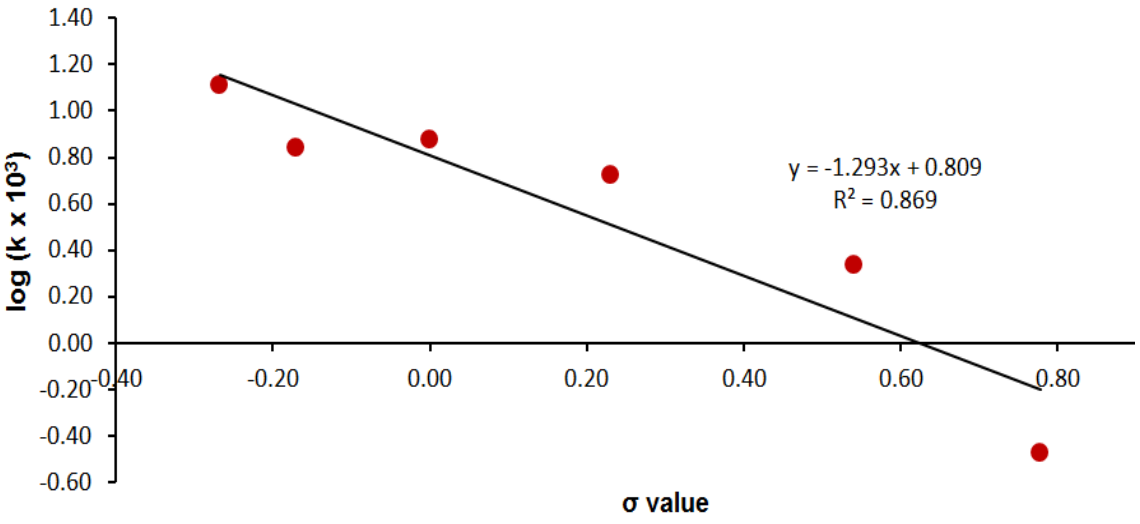

Figure V-14. Complete Hammett plot of rate constants from reactions of DNICs **(1a-1e, 1)** with CO.

Conclusions

For visualizing relationships between structure and reactivity, Hammett correlations are a hallmark of physical organic and physical organometallic chemistry. Such correlations in a series of *para* substituted [(sIMes)(S-C_6H_4X)$Fe(NO)_2$] DNICs (compounds **1a-1e**) with variations in the donor characteristics of the aryl thiolate were used to provide a firmer experimental foundation for the unusual theoretical proposal that an oxidized $\{Fe(NO)_2\}$ moiety, i.e. $\{Fe(NO)_2\}^9$, served as a nucleophile towards CO in a process that releases RSSR. Significant electronic rearrangement leads to a reduced $\{Fe(NO)_2\}$ product in the form of $[Fe(CO)(NO)_2(NHC)]$.

Although variation of the substituent at the *para* position of the phenyl thiolate takes place remote from the metal center of the $\{Fe(NO)_2\}^9$ core, plots of infrared ν(NO) values, calculated NO force constants and voltammetric $E_{1/2}$ values with the Hammett parameter σ_p show good correlations, verifying the presence of systematic changes in electron density as experienced by the $\{Fe(NO)_2\}^9$ core through changes in the S-donor. Having thus established the presence of electronic changes at the metal center between the members of the series of DNICs **1a-1e**, rates of their reaction with CO(g), resulting in the formation of the reduced $\{Fe(NO)_2\}^{10}$ DNIC, $[(sIMes)(CO)Fe(NO)_2]$ were examined as monitored by *in situ* IR spectroscopy. A plot of the second-order rate constants and the Hammett parameter σ_p is linear and has a negative slope, indicative of rate retardation with increasing electron-withdrawing nature of the substituents. Together, these results find that subtle, systematic alterations of the electronic character

of the $\{Fe(NO)_2\}$ unit moderate the conversion of the $\{Fe(NO)_2\}^9$ into the reduced analogue $\{Fe(NO)_2\}^{10}$ under mild conditions.

As reported in the earlier prototypical study reported in Chapter IV, the calculated free energy of the transition state is close to that of the intermediate, suggesting a late transition state.[128] Experimental results obtained in our current study show that this reaction is sensitive to the nucleophilicity at the metal center, thereby indicating the importance of the CO interaction in the transition state. This study therefore supports the previous computationally derived mechanistic hypothesis of the unique role of the delocalized frontier molecular orbitals of the $Fe(NO)_2$ unit, whereby the reaction is initiated by the overlap of such filled orbitals with the vacant π^* orbitals of the entering CO ligand.

As "cross-talk" between small endogenous gaseotransmitters: CO, NO and H_2S gains rapid interest in the scientific community,[115] the interplay between these molecules and bio-organometallic entities such as DNICs is intriguing. Efforts to understand these processes in the complex biological environment continue to be a challenge, highlighting the importance of the mechanistic understanding obtained in biomimetic studies.

CHAPTER VI

SUGAR APPENDED N-HETEROCYLIC CARBENE DINITROSYL IRON COMPLEXES

Introduction

The discovery of the therapeutic potential of nitric oxide, and the existence of dinitrosyl iron complexes (DNICs) in the biological system, have led to biomimetic work in synthetic inorganic chemistry in presenting DNICs as a potential new class of NO-releasing agents. Inspired by the thiol-containing biological DNICs, Vannin *et al.* have synthesized DNICs with natural thiol ligands (cysteine or glutathione) and investigated their therapeutic potential.[37,105] A stable preparation of glutathione containing DNIC that resulted from these studies is currently in clinical trials, and has displayed a variety of therapeutic responses including prolonged hypotension, attenuated platelet and erythrocyte aggregation and promotion of skin wound healing.[38]

The NO release ability and other chemical properties, including the redox level, of synthetic DNICs can be modulated by altering the electronic and steric properties of the ancillary ligands, which thereby provide control over the DNIC's NO storage, transport and targeting abilities. Apart from Vannin's thiol-DNICs, few literature reports focus on the development of synthetic DNICs as NO release agents. Among these, Liaw *et al.* reported the biological activity of dimeric Roussin's Red Ester (RRE), $[Fe(\mu\text{-}SC_2H_4COOH)(NO)_2]_2$ and a monomeric DNIC, $[(PPh_2(Ph\text{-}3\text{-}SO_3Na))_2Fe(NO)_2]$, bearing –COOH and $–SO_3$ functionalities for improved water solubility.[35] The photochemical

NO release of RRE and derivatized RREs has been investigated by Ford *et al.*, see Chapter 1.[33,34] More recently, Kim *et al.* showed NO release from a (TMEDA)Fe$(NO)_2$ complex, both within and outside a cellular environment.[39] Our work on NO release by N-Heterocylic carbene (NHC)-stabilized DNICs in organic solutions has shown the potential of these compounds to release NO to biologically relevant NO trapping agents such as iron or cobalt porphyrins.[41] However, the limitation to the use of the library of synthetic DNICs in biological studies has been the lack of compatibility of many of these compounds with biological media. Therefore, there is a need for strategies of improving biocompatibility of these compounds. In this regard, NHC stabilized DNICs possess a basic architecture with several tuning sites, that can be utilized in incorporating functional groups that would improve biocompatibility (Figure VI-I). Using pre-synthesized NHC ligands that contain biocompatible 'wingtip' groups and varying the ancillary ligand are straightforward and plausible techniques for attaining this goal.

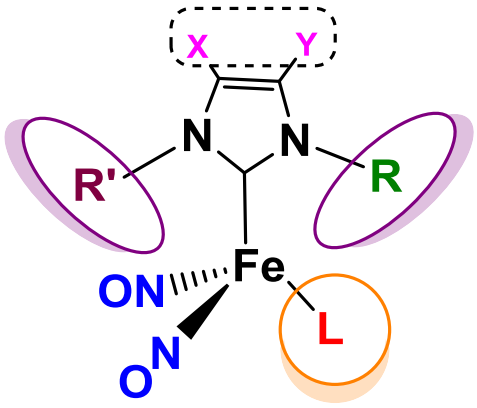

Figure VI-1. Schematic of the common architecture of NHC-DNICs with several tuning sites; the N-C-C-N backbone, the 'Wingtip' groups and the ancillary ligand.

There is ample precedence in the literature for sugar-bound metal complexes in biomedical applications, ranging from contrast agents to therapeutics.[129,130] Saccharides and their derivatives are naturally involved in many intracellular processes, acting as energy sources and involved in recognition processes.[131,132] The use of sugars and their derivatives as ligands conjugated to metal complexes therefore presents many advantages including improved targeting properties that make use of the natural mechanisms within the cell for sugar uptake. For example, literature reports exist on studies of cellular internalization through lipophilic diffusion or *via* the membrane-bound glucose transporter, GLUT 1, of imaging agents containing ^{99m}Tc(I), ^{55}Co(II) and Ga(III) bound to glucose-based ligands.[130] In addition, the tunability of saccharide ligands themselves provides essential control over the lipophilicity and stability of metal based drugs. Several carbohydrate-metal complexes, including platinum derivatives, have been studied for anticancer properties.[129]

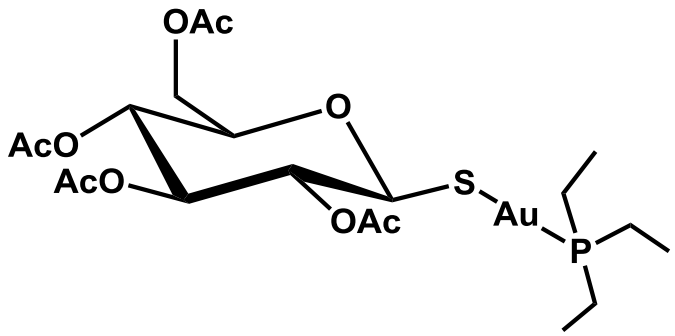

Figure VI-2. Chemical structure of the antiarthritis metallodrug, Auranofin.

The sugar-based gold containing drug, Auranofin [(2,3,4,6-tetra-*O*-acetyl-1-thio-β-D-glucopyranosato-*S*)(triethylphosphine)]-gold(I) (Figure VI-2), is currently used in modern clinical protocols in the treatment of rheumatoid arthritis.[133] It is a monomeric, neutral gold compound; therefore it is lipophilic and administered orally.[134] A number of Auranofin derivatives have also been synthesized, and current work is directed towards testing these compounds for anticancer properties.[135,136] Inspired by Auranofin, we synthesized and characterized the first examples of 'sugar appended' monomeric and dimeric DNICs. We have conducted preliminary NO release studies of these complexes in the presence of NO trapping agents. These compounds could combine the therapeutic properties of NO with the cell-attracting properties of a glucose moiety, and are amongst the few examples of DNICs with bio-functionalized ligands.

Results and discussion

The NHC stabilized IMes-TNIC, $[(IMes)Fe(NO)_3]^+$, synthesized according to a literature procedure,[65] was used as a precursor for the synthesis of the oxidized, $\{Fe(NO)_2\}^9$ complex **1** as shown in Figure VI-3 (route a). Reaction of $[(IMes)Fe(NO)_3]^+$ with 1-thio-β-D-glucosetetraacetate in 1:1 stoichiometric ratio results in a color change from green to brown within time of mixing. The change in the positions and pattern of the IR bands accompanying this color change in THF solutions, indicates the conversion of the TNIC (υ(NO) 1932 (s), 1831 (s), 1804 (vs)) to complex **1** (υ(Me-C(O)O): 1759, 1749 (sh) cm^{-1} υ(NO): 1768 (sh), 1718 cm^{-1}) (Figure VI-4). Complex **1** when exposed to air, in the solid state was stable for ca. 2 hours, it was stable over several weeks in the

solid state when stored under inert atmosphere. In solution, it was stable for about 36 hours under inert atmosphere (including solutions of DMSO) and about 1 hour exposed to air. X-ray quality red colored crystals of **1** were obtained by recrystallization from THF/ hexane solutions. These were submitted to the x-ray diffraction laboratory at Texas A&M University, and were analyzed by Dr. N. Bhuvanesh.

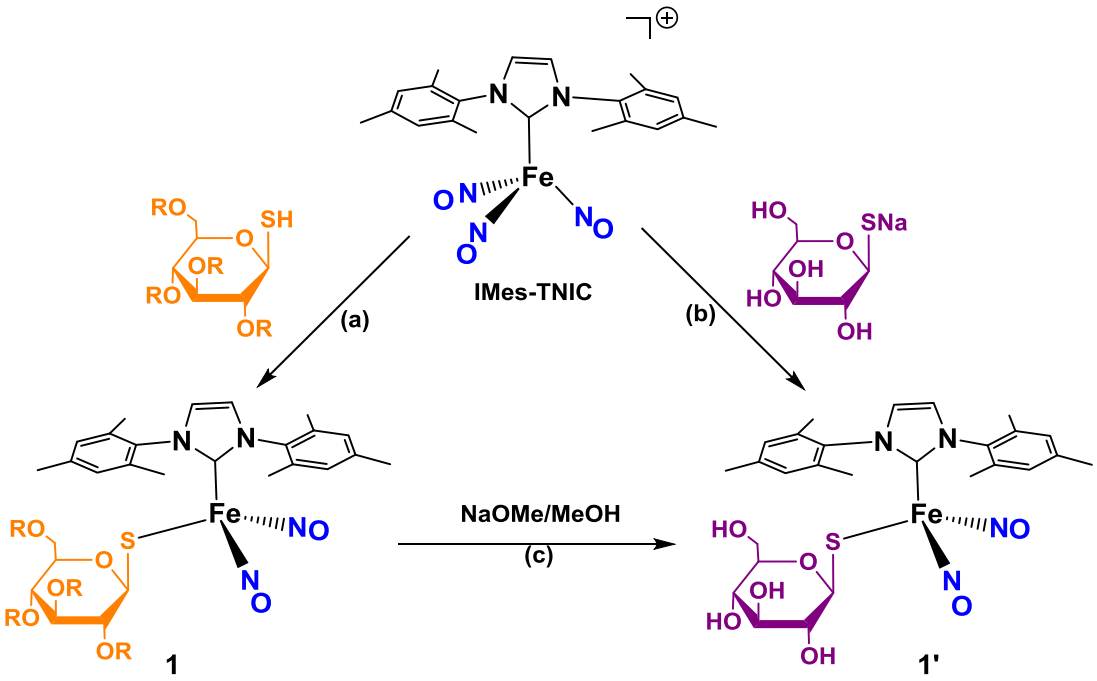

Figure VI-3. Synthetic routes to sugar-appended DNICs from the starting precursor $[(IMes)Fe(NO)_3]^+$. R = $(C=O)CH_3$.

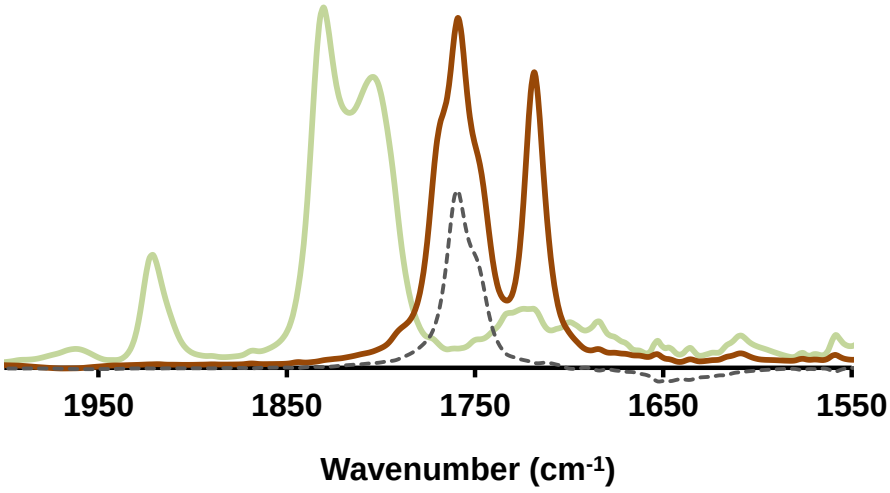

Figure VI-4. Overlaid IR Spectra of IMes-TNIC and **1** in THF [Olive: IMes-TNIC : ν(NO) 1932 (s), 1831 (s), 1804 (vs) cm^{-1}], [Brown: **1**: ν(NO) 1768 (sh), 1718 cm^{-1}(s); ν(Me-C(O)O): 1759 (s), 1749 (sh) cm^{-1}], [Dashed-line inset: pure 1-thio-β-D-glucosetetraacetate: ν(Me-C(O)O): 1760 (s), 1749 (sh) cm^{-1}].

The molecular structure of **1** is shown in Figure VI-5, and important crystallographic data and metric parameters are summarized in Table VI-1. The molecule maintains the pseudotetrahedral geometry seen in all previously reported NHC-DNICs, and the planes of the mesitylenes are roughly perpendicular to the CN_2C_2 plane, providing an 'umbrella' to the $Fe(NO)_2SR$ base. The NO ligands are slightly bent with average ∠Fe-N-O of 170.8° and maintain the "attracto" conformation,[55] bending in towards each other as defined by smaller ∠O-Fe-O compared to ∠N-Fe-N, in the planar FeN_2O_2 unit. All other metric parameters are similar to the prototypic analogue of this compound, $Fe(NO)_2$(IMes)(SPh).[65] Complex **1** also showed the classic isotropic EPR signal for DNICs, at g = 2.03 at room temperature (Figure VI-6).

Table VI- 1. Selected crystal data/ refinement parameters, bond distances and angles in complex **1**.

Empirical formula	C35 H43 Fe N4 O11 S
Space group	P 21 21 21
Z	4
R	0.04
Bond Distances (Å)	
Fe-NO[a]	1.662(1)
Fe-S	2.274(1)
N-O	1.154(15)
	1.174(2)
Bond Angles (°)	
N-Fe-N	112.3(7)
O-Fe-O	105.0(3)
Fe-N-O[a]	170.8(2)
C_{carb}-Fe-NO[a]	107.1(3)
C_{carb}-Fe-S	110.9(1)

[a]average distances or angles.

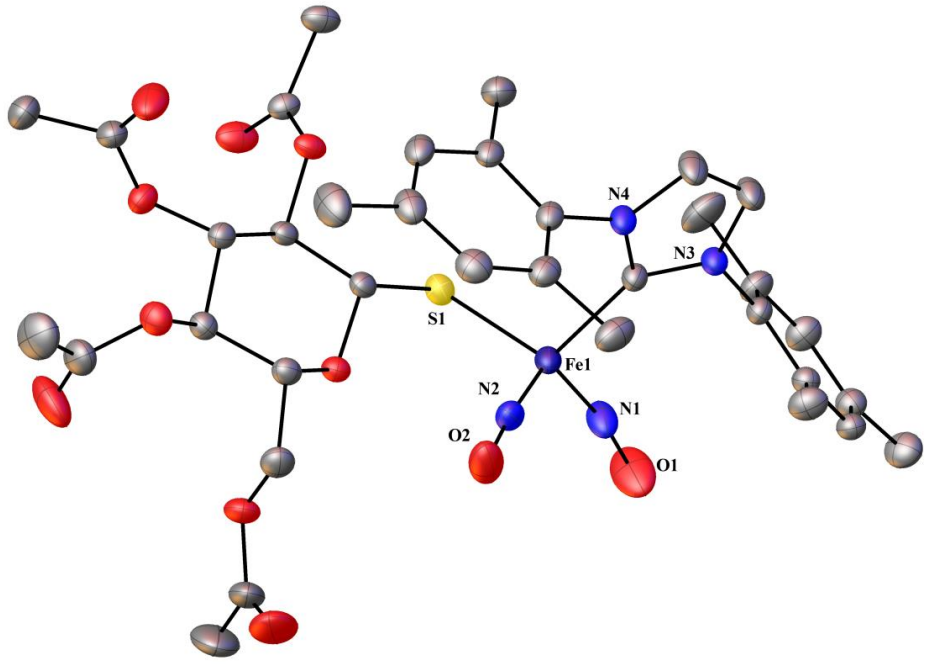

Figure VI-5. Molecular structure of complex **1**. ORTEP with thermal ellipsoids drawn at 50% probability (H atoms omitted).

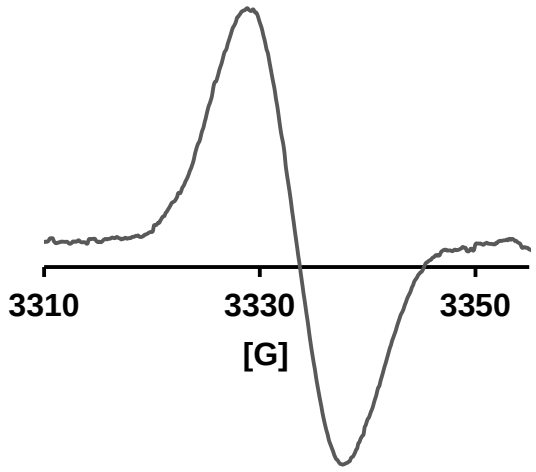

Figure VI-6. X-band EPR spectrum of complex **1** in THF solution at 295 K.

Deprotection of compound **1** was achieved by reacting it with excess NaOMe in MeOH (Figure VI-3 (route c)). The identity of the deprotected product (complex **1′**) was verified by directly synthesizing it *via* an alternate route. In this alternate route, $[(IMes)Fe(NO)_3]^+$ was reacted with the sodium salt of 1-thio-β-D-glucose in 1:1 stoichiometric ratio, yielding a color change from green to brown, together with completion of reaction in ca. 2 hours as confirmed by IR spectroscopy (Figure VI-3 (route b)). The resulting IR spectrum showed the absence of the (Me-C(O)O) stretch of the acetyl group in **1**, and clear NO bands at ν(NO) 1768 and 1716 cm^{-1} in THF as shown in Figure VI-7, indicating successful deprotection of the acetyl groups. However, we have thus far been unable to crystallize the deprotected complex **1′**. This also appeared less stable than the protected analogue, with solution lifetime of only several hours even under inert atmosphere. This instability of complex **1′** hindered good elemental analysis.

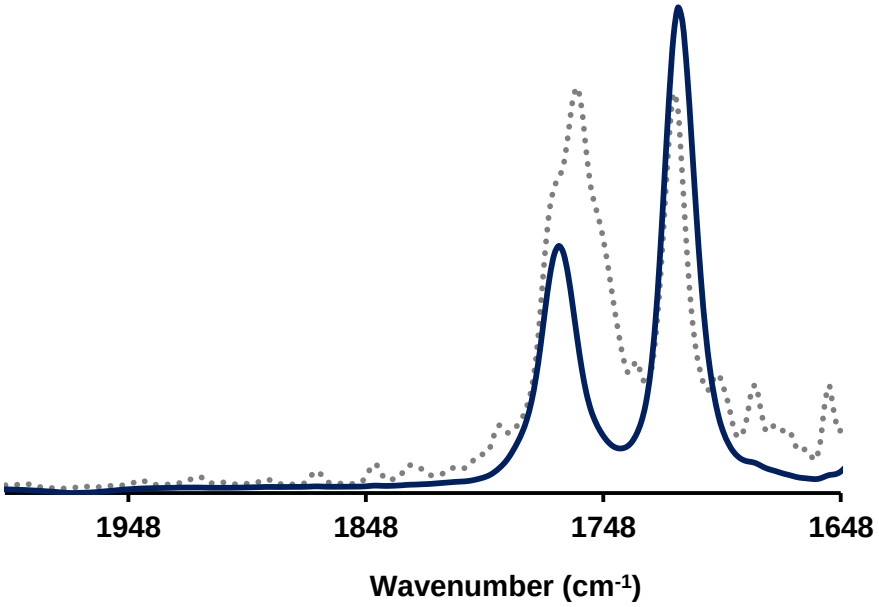

Figure VI-7. IR spectrum of complex **1′** in THF: ν(NO) 1768 (sh), 1716 cm^{-1}. Dotted-line inset: IR spectrum of complex **1** (THF).

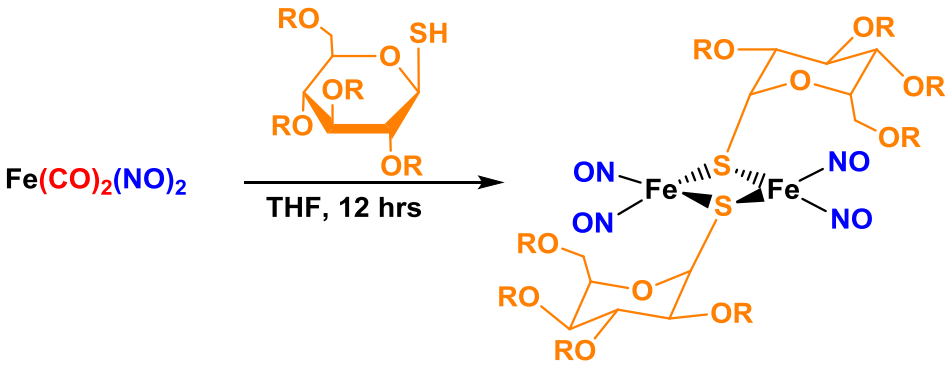

Figure VI-8. Synthesis of sugar-appended RRE, complex **2.**

The dimeric $(\mu\text{-RS})_2[Fe(NO)_2]_2$ form of the monomeric complex **1** was synthesized by the known method for other RRE analogues[64] (Figure VI-8); i.e., reaction of 1-thio-β-D-glucosetetraacetate with freshly prepared $Fe(CO)_2(NO)_2$ (in THF) in stoichiometric ratio. The reaction was complete in about 12 hours, and the synthesis of $(\mu\text{-RS})_2[Fe(NO)_2]_2$ complex **2**, bearing acetylated thio glucose units could be verified by the corresponding IR pattern shown in Figure VI-9. A brown solid was obtained upon recrystallization of THF solutions of complex **2** with hexanes. As expected for an EPR-silent dinuclear $[\{Fe(NO)_2\}^9-\{Fe\text{-}(NO)_2\}^9]$ DNIC, this compound was EPR silent and was further characterized by ESI mass spectrum signals at m/z = 959 $[M + H]^+$ and 980 $[M + Na]^+$. In contrast to complex **1**, complex **2** showed notably improved stability in air. It was stable in air for 2 days even in solution, and stability was increased to several months under inert atmosphere in the solid state. Attempts to crystallize this compound have thus far been unsuccessful. Similar to complex **1**, complex **2** was also completely soluble in DMSO, a commonly used solvent in cell studies for administering pro-drugs.

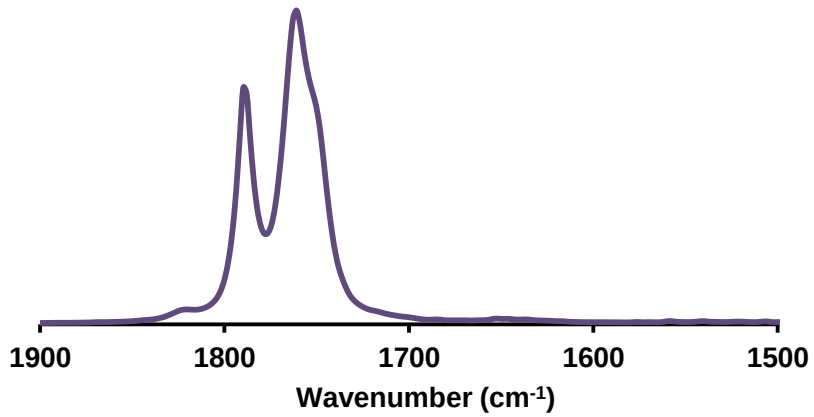

Figure VI-9. IR spectrum of complex **2** in THF: ν(NO) 1787, 1750 cm^{-1}; ν(Me-C(O)O): 1759, 1749 cm^{-1}.

Previous studies by Hess *et al.* on NO release ability of the prototypic NHC-DNICs suggested that oxidized, $\{Fe(NO)_2\}^9$ DNICs are better sources of NO in the presence of NO trapping agents when compared to the reduced $\{Fe(NO)_2\}^{10}$ analogues.[41] However, these oxidized NHC-DNICs ($[Fe(NO)_2(NHC)_2]^+$) were seen to release NO very fast to the porphyrin derived NO trapping agent used. To qualitatively probe the ability of the sugar-derivatized DNICs to release or transfer NO, complex **1** was combined with 2 equivalents of the NO-trapping reagent Co(TPP) (Co(TPP) = 5,10,15,20-tetraphenyl-21H,23H-porphine cobalt(II)) in THF solution at room temperature. Over ca. 48 hours, a slow decrease in intensity of the IR NO bands of complex **1** was observed. The poor resolution in this spectrum necessitated product separation. According to previous reports, the expected NO bound product, (TPP)Co(NO) is poorly soluble in THF and its isolation by MeOH precipitation was

used for definite characterization.[137,68] The product mixture produced a purple residue on addition of MeOH; an IR band at 1683 cm^{-1} in DCM solutions, indicated the formation of (TPP)Co(NO). In agreement with the reports by Chiang *et al.*[68] and Richter-Addo *et al.*,[137] the isolated Co nitrosyl complex shows UV-Vis absorbance bands at 410 and 534 nm; an ESI mass spectrum signal of m/z = 671 was assigned to $[(TPP)Co]^{+}$. This suggests oxidative nitrosylation of Co(II)TPP by released NO radical.[68] However, poor resolution in the IR spectra suggested the use of alternate NO trapping agents for further verification of NO release.

A host of transition metal- N_2S_2 complexes have been well studied, utilizing a variety of metal ions such as Fe^{II}, Ni^{II}, Pd^{II}, Co^{II}, Cu^{II}, and Zn^{II} with various N_2S_2 ligands.[58] Iron and cobalt N_2S_2 complexes where N_2S_2 = bme-daco (*N*,*N*′-bis(2-mercaptoethyl)-1,4-diazacycloheptane), or bme-dach (*N*,*N*′-bis(2-mercaptoethyl)-1,4-diazacyclooctane), are known to form penta-coordinate, dimeric N_2S_2M units or the corresponding NO-cleaved product, $N_2S_2M(NO)$.[90,138] Therefore, such metal-N_2S_2 dimers are attractive NO trapping agents. The N_2S_2M dimer, $[(bme\text{-}dach)Fe]_2$ was successfully used as an NO-trapping agent by Hsieh *et al.* in "double-tube" experiments, where an NHC-TNIC released NO as free NO radical/gas.[65]

Based on such precedence, complexes **1** and **2** were reacted with excess $[(bme\text{-}dach)Co]_2$ in THF solutions to test for possible release of NO, which would subsequently be trapped in the form of the monomeric (bme-dach)Co(NO). In the reaction of complex **1**, the loss of the IR NO bands was observed after about 24 hours, indicating loss of NO from **1**. Similar reactivity was seen when complex **2** was reacted with excess [(bme-

dach)Co]$_2$ in THF, with loss of NO bands in about 12 hours. On solvent removal and washing of the brown residue with diethyl ether in which it is insoluble, the resulting IR spectrum of the residue taken up in dichloromethane showed a strong, broad signal at ν(NO) 1601 cm^{-1}, assigned to the (bme-dach)Co(NO).[138] A second IR band at 1754 cm^{-1} (1747 (sh)) can be assigned to the (Me-C(O)O) stretch that belonged to the acetylated thio-sugar unit. The exact identity of this species is unclear. Nevertheless, these results provide conclusive evidence for the release of NO from complex **1** and **2** in the presence of NO trapping agents.

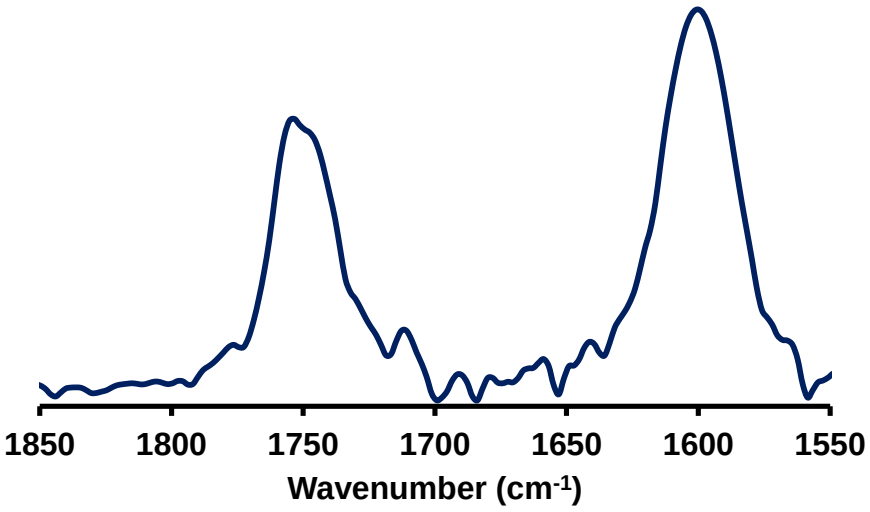

Figure VI-10. IR spectrum resulting from completer reaction of complex **1**/ **2** with [(bme-dach)Co]$_2$ in THF: ν(NO) 1601 cm^{-1} indicates the formation of (bme-dach)Co(NO).

Summary

This study reports the synthesis and characterization of the first examples of sugar-appended iron dinitrosyl complexes. The synthetic protocol developed here shows that the strategy of glycoconjugation of DNICs holds potential for extension to the attachment of other carbohydrate units already in use as targeting ligands in drug delivery. The use of saccharide ligands on metal complexes is both proven and attractive as they impart hydrophilicity and improved targeting properties *via* cellular recognition in the resulting transition metal complex.[130]

The sugar-containing ligand radioactive-labelled with ^{18}F, 2-^{18}F-2-deoxy-D-glucose (FDG) is a popular sugar-based tracer for PET and for imaging.[130,139] Several studies have also reported the use of peracetylated [^{18}F]FDG (1,3,4,6-tetra-*O*-acetyl-2-^{18}F-2-deoxyglucose) as building blocks for the radiosynthesis of ^{18}F-labeled compounds.[140] The attachment of such a unit onto a DNIC using synthetic strategies based on the work reported here should prove to be very valuable in tracking the *in vivo* distribution of such DNICs.

Qualitative NO release studies in the presence of NO-trapping agents derived from porphyrins or Co(N_2S_2) complexes developed in our laboratory displayed the ability of these compounds to release NO to such traps. Ongoing collaborative efforts are focused on testing the NO release properties of these compounds in cellular environments, of which preliminary results have been positive.

CHAPTER VII

CONCLUSIONS AND FUTURE DIRECTIONS*

In the past decade, extensive synthetic and biomimetic progress has been made in the DNIC (Dinitrosyl iron compounds) area, including detailed investigations of electronic properties "beyond the E−F notation",[9,103] the establishment of requirements for NO release from DNICs,[44] discovery of DNICs of higher coordination number,[48,111,112] assessment of potential for phototherapeutic applications,[34] etc. Intrigued by the integrity of the unique dinitrosyl iron unit, and the possibility of roles for it in human physiology or medicinal applications, the work reported in this dissertation has focused on the understanding of fundamental properties of mixed ligand environments and mechanisms of ligand exchange processes that might regulate switches in redox levels.

Building on the premise that NHC's are favored by DNICs over imidazole,[41] and inspired by a DFT study which suggested a metal dependent preference for C- vs. N-binding of imidazoles,[94] Chapter III describes an investigation into the possibility of isomerization of an imidazole to an NHC on a dinitrosyl iron scaffold. This model study demonstrated the impressive stability of the dinitrosyliron unit under base treatment, while supporting the isomerization of metal-bound imidazole to an NHC ligand. To our knowledge, other examples of such inter-conversions exist only in the organometallic literature.[95,96] Also alluded to in Chapter III are two molecular structures obtained from

*Reproduced in part with permission from Pulukkody, R.; Kyran, S. J.; Bethel, R. D.; Hsieh, C.-H.; Hall, M. B.; Darensbourg, D. J.; Darensbourg, M. Y. *J. Am. Chem. Soc.* **2013**, *135*, 8423-8430. Copyright **2013** American Chemical Society.

the imidazole-DNICs, presumably exposed to adventitious oxygen. An oxo bridged structure very similar to the incompletely characterized mesityl imidazole bound compound mentioned in Chapter III was reported by Kim *et al.* in the form of a dinuclear iron(III)–nitrato complex, $[Fe_2O(NO_3)_4(dmp)_2]$ (Figure VII-1).[52] This was reported as a product of O_2 reactivity with $[(dmp)Fe(NO)_2]$, which proceeded *via* a putative iron–peroxynitrite intermediate, capable of nitrating phenols. In a biological context, this study proposed a new role for endogenous DNICs, as the nitration of phenols in protein tyrosine nitration (PTN) is considered to be an important posttranslational modification.[52] Such posttranslational modifications are associated with various pathological conditions including inflammatory, neurodegenerative, and cardiovascular diseases.[141] Based on such precedence, further studies involving the O_2 reactivity of imidazole DNICs should prove interesting, which might also be expected to proceed through peroxynitrite intermediates ([Fe(Im)-(NO)(ONOO)]). These results could also signal their possible use as oxygenation catalysts.

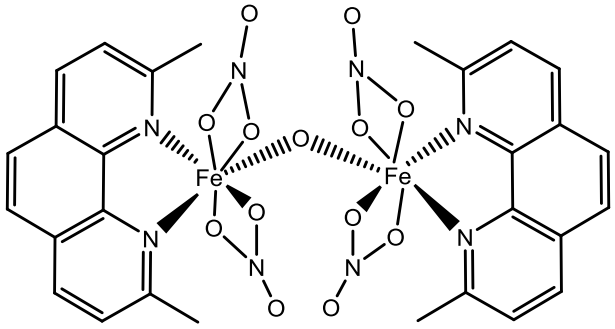

Figure VII-1. Dinuclear iron(III)–nitrato complex, $[Fe_2O(NO_3)_4(dmp)_2]$ reported by Kim *et al.*[52]

Spectroscopic and DFT computational data indicate extensive delocalization of the electron density of iron via π back-bonding in NHC-DNICs. Such π delocalization presents an unusual reaction path for the one electron process of RS^{-}/RSSR inter-conversion as described in Chapters IV and V. In these studies, the reaction of an NHC-stabilized $\{Fe(NO)_2\}^9$ DNIC, $(sIMes)(SPh)Fe(NO)_2$ with CO, involving a $\{Fe(NO)_2\}^9$ /$\{Fe(NO)_2\}^{10}$ redox conversion was proposed to proceed through an unprecedented initial side-on approach of CO. The involvement of thiol-disulfide conversion as triggered by CO was intriguing as it could be viewed as a potential model for intracellular, thiol-complexed DNICs, exposed to intracellular CO.

Thiolate-disulfide redox processes are of extensive chemical and biological relevance. Limited reports of thiolate-disulfide reactivity in an inorganic context include a kinetic study by McAuley, *et al.*,[142] that concentrates on the oxidation of 2-mercaptosuccinic acid by Cu^{II} ions, ultimately yielding the disulfide and a Cu^{I} dimer. Formation of the disulfide is said to be facilitated by the dimer template. Similarly, Henkel *et al.*, reported on chloride ion induced thiolate-disulfide conversion concomitant with Cu^{II}/Cu^{I} redox activity, again taking place on a dithiolate ligand scaffold bound to copper.[143] Copper(II) is known to be a potent oxidant for disulfide formation in proteins. Amongst many reports is that of a suggested role for such Cu-facilitated disulfide formation in the maturation process of the superoxide dismutase 1, SOD1. A copper chaperone superoxide dismutase, CCS, is proposed to assemble cysteinyl thiolates resulting in disulfides between the CCS and the apo-Cu-SOD1, ultimately leading to the translocation of copper into the SOD1.[144]

There is an obvious correlation between the two redox levels of the DNICs, $\{Fe(NO)_2\}^9$ /$\{Fe(NO)_2\}^{10}$ and the two redox levels of copper (Cu^{II}: d^9/ Cu^{I}: d^{10}). Given this, the occurrence of analogous reactivity patterns involving thiolate/disulfide reactivity between the $\{Fe(NO)_2\}^9$ /$\{Fe(NO)_2\}^{10}$ and Cu^{II}/ Cu^{I} systems could be viewed as probable. Even structural studies have shown similarities. For example, as described in Chapter I, we and others have observed the formation of tetrameric, imidazolate-bridged DNIC, $\{Fe(NO)_2\}^9$ structures,[73,145] that are analogous to imidazolate-bridged tetracopper, Cu^{II}, d^9, molecular squares.[74,146] Therefore, further studies on investigating similarities between the $\{Fe(NO)_2\}^9$ /$\{Fe(NO)_2\}^{10}$ and Cu^{II}/ Cu^{I} systems will be intriguing.

Chapter VI describes glyco-conjugation as a strategy to synthesize DNICs with improved biocompatibility. The tuning sites provided by the common architecture of NHC-DNICs appear attractive choices for the derivatization of such complexes. The results reported in Chapter VI place particular emphasis on the successful manipulation of the ancilliary ligand in the attachment of a glucose-based ligand. Reported in the literature is the synthesis of an imidazolium salt, with wing-tip groups derivatized with an acetylated glucose unit (Figure VII-2 (a)).[147] In contrast to the oxidized DNIC reported in Chapter VI, I have carried out preliminary studies on the synthesis of a reduced $Fe(NO)_2(CO)$(NHC) type DNIC (Figure VII-2 (b)) using the above ligand, which was confirmed with IR spectroscopic evidence (Figure VII-3). The low stability of this complex hindered further characterization.

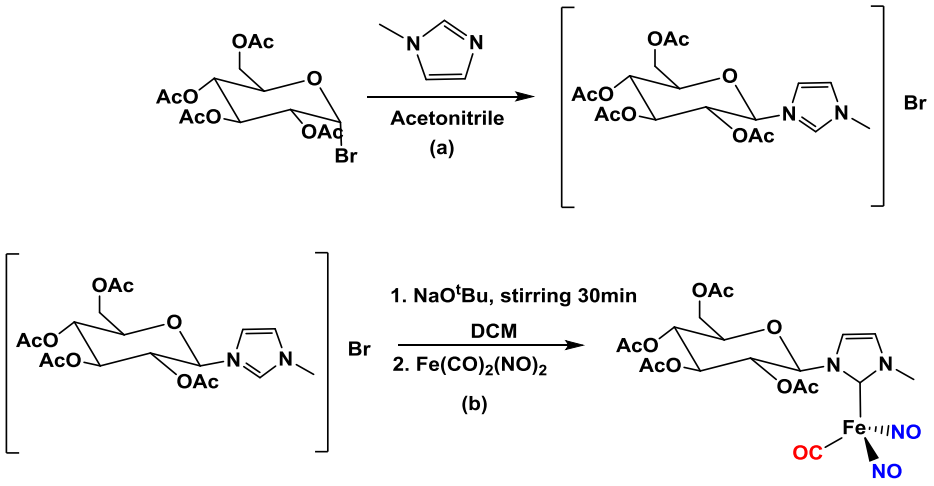

Figure VII-2. (a) Synthesis of 1-methyl-3-(2,3,4,6-tetra-*O*-acetyl-*β*-D-glucopyranosyl) imidazolium bromide.[147] (b) Synthesis of $\{Fe(NO)_2\}^{10}$ DNIC containing sugar-bound NHC.

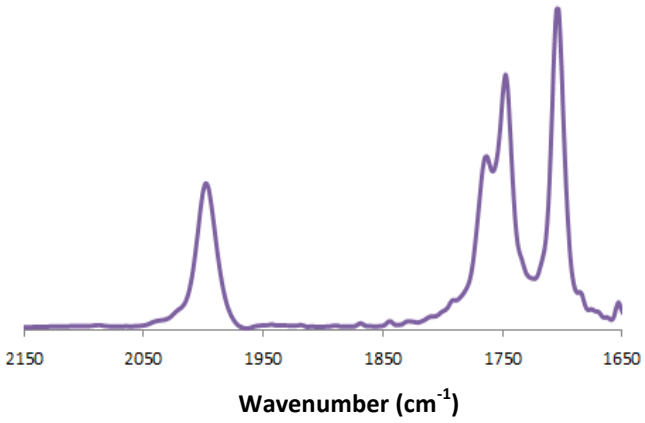

Figure VII-3. IR spectra in THF for the $Fe(NO)_2(CO)(NHC)$ type $\{Fe(NO)_2\}^{10}$ DNIC containing sugar-bound NHC. ν(CO) 1998; ν(NO) 1762(sh), 1703(vs) cm^{-1}, ν(Me-C(O)O): 1747 (s) cm^{-1}.

Further studies could focus on strategies that can use the same synthetic protocol to synthesize DNICs of greater stability. As seen in the case of the prototypic NHC-DNICs, one strategy might be the synthesis of the di-substituted, bis-NHC analogue of the aforementioned $\{Fe(NO)_2\}^{10}$ DNIC, which might have greater stability. Sugar-bound NHCs with bulky substituents have been reported in the literature and might be another successful strategy in this regard. For example, Glorius *et al.*[148] used mesityl imidazole in place of the methyl substituent described in the above preliminary test, for the synthesis of an analogous imidazolium salt (Figure VII-4(a)). They have crystallographically characterized Pd(II) complexes containing such NHC ligands.[148] In another example, Jia *et al.* report the synthesis of an imidazolium salt with bulky, symmetric carbohydrate units (Figure VII-4(b)), and the synthesis of a Rh(I) complex *via* the in situ generation of the corresponding NHC.[149]

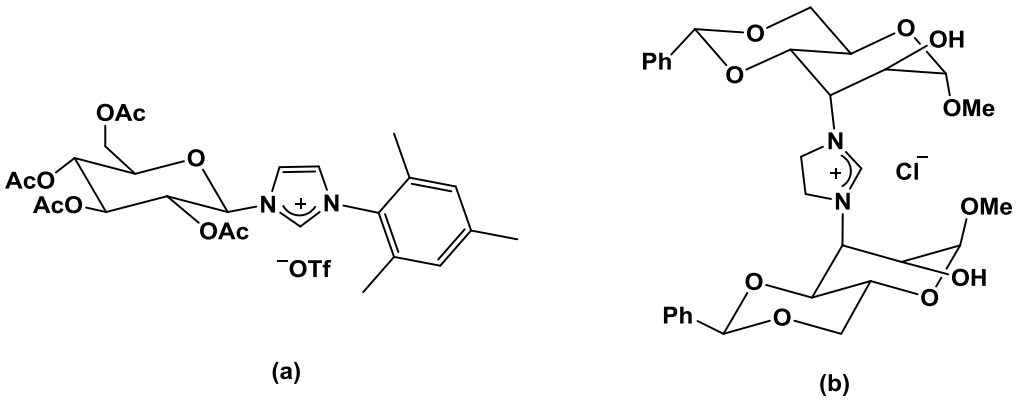

Figure VII-4. Examples of previously reported sugar-derived imidazolium salts with improved steric bulk.[148,149]

The ability to utilize any generic imidazolium moiety in synthesizing NHC-DNICs opens up a wide variety of options in terms of derivatization of DNICs with desired properties. For example, caffeine (Figure VII-5), a xanthine derivative, contains a methylimidazole moiety, making it a valuable candidate for the synthesis of an NHC.[150] The minimal *in vivo* toxicity and the well-known role of caffeine as a central nervous system stimulant are factors that favor its use as a derivatization unit on metal complexes.[150] The caffeine derived imidazolium salt precursor known as methylated caffeine, 1,3,7,9-tetramethylxanthinium (Figure VII-5) has been successfully used in the synthesis of several metal carbene complexes including Ag, Rh and Pt.[150-152] The water soluble silver complexes have been tested for and were seen to display antimicrobial properties.[150] Speculated caffeine-bound DNICs as shown in Figure VII-6 could be readily made and used in biological studies.

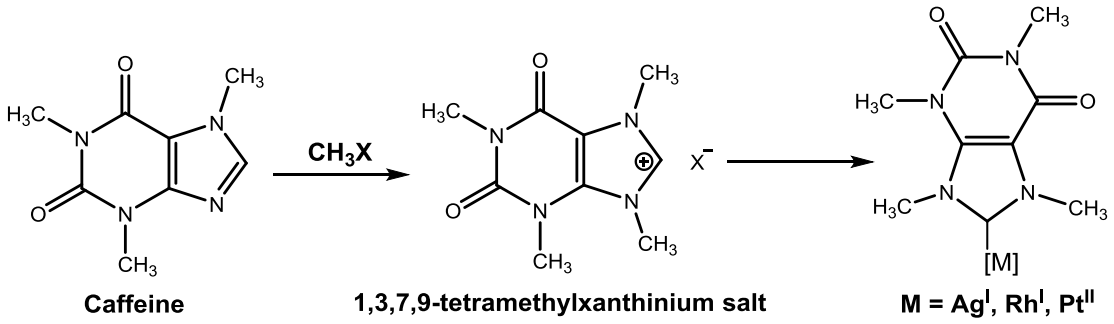

Figure VII-5. Synthetic route for caffeine-derived metal complexes *via* an imidazolium salt precursor.[151,152]

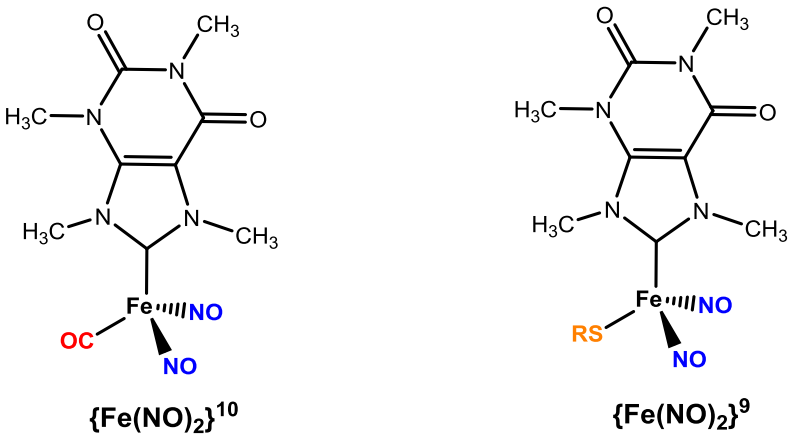

Figure VII-6. Speculated caffeine-bound DNICs of different redox levels.

Several studies have attempted to better understand the NO release properties of DNICs. A previous study by the Darensbourg group on the reaction of a model dithiolate-DNIC with Fe(II) and Co(II) porphyrin ((P)M(II)), indicated oxidative nitrosylation of the porphyrin by the transfer of $NO^{\bullet}$ to form (P)M(NO).[68] Extending this work, another study showed similar reactivity of NHC-DNICs, and found that DNICs in the oxidized $\{Fe(NO)_2\}^9$ state appeared better sources of NO compared to the reduced analogue.[41] Thiolate-induced $NO^{\bullet}$ release in the absence of direct contact with a trapping agent was also shown from "double-tube" experiments using the cationic IMes-TNIC (trinitrosyl iron compound), where the released NO gas diffused into a solution containing a NO-trapping agent.[65]

Although such previous studies have shown NHC-DNICs to release NO to biologically relevant NO trapping agents such as metallo porphyrins, major questions still exist in understanding the mechanisms involved in the release of NO from DNICs *in*

vivo. A systematic approach to understanding the role of a synthetic DNIC as a physiologically relevant NO release agent would require understanding a) the process of entry into the cell; b) the triggers (interacting molecules or agents) that might cause NO release; c) protocols for quantification of the NO released; and d) possible correlations between the quantity of NO released from such compounds and corresponding physiological responses. Such a systematic approach needs attention to appropriate systems that might model cell permeation.

The first report on the analysis of the cellular uptake mechanism of an RRE type dimeric DNIC by Liaw *et al.* is based on EPR spectroscopic evidence. EPR signals of $\{Fe(NO)_2\}^9$ DNICs were observed in cells treated with the RRE. Through elaborate control experiments, this study shows that the RRE either directly permeated into cells or was transported into the cells in the form of low molecular weight (LMW)-DNIC species.[35] As such, the use of EPR spectroscopy can be used in the determination of the cell permeation of the oxidized, paramagnetic NHC-DNICs as well, due to their well-known EPR signal at g = 2.03.

The determination of possible triggers for *in vivo* NO release, which would thereby shed light on the mechanism involved, appears a more intricate problem, considering the highly complex nature of the interior of the cell. However, as mentioned in Chapter I, Kim *et al.* hypothesize that the low concentration of chloride ions inside the cell compared to outside causes dissociation of the halide from $Fe(TMEDA)(NO)_2I$ (TMEDA = *N,N,N',N'*-tetramethylethylenediamine), which causes spontaneous NO release from the resulting cationic DNIC species.[39] Also of interest in this regard is the

mechanism of NO release for the well-known NO donor, sodium nitroprusside (SNP). It has been proposed that interaction of SNP with cellular thiols such as glutathione and electron transfer between these entities causes NO release.[31] Based on such precedence, benchtop studies could be designed to test the effects of physiologically relevant factors such as halide ion concentration, the presence of thiols/ thiolates and changes in pH on triggering NO release from NHC-DNICs, in order to obtain an idea of the mechanism *in vivo*.

The fact that the physiological effects of NO are concentration dependent calls for the quantification of the NO released from an exogenous NO donor. The three most common techniques used for this purpose are the Griess assay, chemiluminescence based NO analyzers and NO sensitive electrodes.[153] While the use of the Griess assay that detects NO indirectly as NO_2^- has limitations in terms of detection of NO in the presence of nitrites/ nitrates, analyzers that directly measure free NO through chemiluminescence are gaining more widespread use.[153] Therefore, if NHC-DNICs are administered into cells, such detection/ quantification methods can be used to measure their NO release ability *in vivo*. Ultimately, such NO release measurements could be correlated to parameters indicating relevant physiological responses. For instance, Vannin has reported testing such compounds for hypotensive effects using measurements of mean arterial pressure (MAP) as an indicator.[105] Similarly, Kim *et al.*, in a study mentioned earlier in this chapter, report the measurement of the levels of pro-inflammatory and anti-inflammatory cytokines in macrophages upon treatment with

exogenous DNIC in order to establish anti-inflammatory responses induced by the compound.[39]

Overall, the amazing scope of the dinitrosyl iron unit in terms of its compatibility with natural ligands as well as ligands common to coordination chemistry, together with its reactivity that spans over redox chemistry, catalysis and medicinal applications point towards an almost inexhaustible array of ideas that could be explored. Current work should therefore focus on the design of studies that may lead to progress in this area in a structured and productive manner.

REFERENCES

1. Bagley, K. A.; Vangarderen, C. J.; Chen, M.; Duin, E. C.; Albracht, S. P. J.; Woodruff, W. H. *Biochemistry* **1994**, *33*, 9229-9236.
2. Nicolet, Y.; Lemon, B. J.; Fontecilla-Camps, J. C.; Peters, J. W. *Trends Biochem. Sci.* **2000**, *25*, 138-143.
3. Volbeda, A.; Garcin, E.; Piras, C.; deLacey, A. L.; Fernandez, V. M.; Hatchikian, E. C.; Frey, M.; FontecillaCamps, J. C. *J. Am. Chem. Soc.* **1996**, *118*, 12989-12996.
4. Hsieh, C. H.; Ding, S. D.; Erdem, O. F.; Crouthers, D. J.; Liu, T. B.; McCrory, C. C. L.; Lubitz, W.; Popescu, C. V.; Reibenspies, J. H.; Hall, M. B.; Darensbourg, M. Y. *Nat. Commun.* **2014**, *5*.
5. Harmjanz, M.; Saak, W.; Haase, D.; Pohl, S. *Chem. Commun.* **1997**, 951-952.
6. Lubitz, W.; Ogata, H.; Rudiger, O.; Reijerse, E. *Chem. Rev.* **2014**, *114*, 4081-4148.
7. Liaw, W. F.; Chiang, C. Y.; Lee, G. H.; Peng, S. M.; Lai, C. H.; Darensbourg, M. Y. *Inorg. Chem.* **2000**, *39*, 480-484.
8. Enemark, J. H.; Feltham, R. D. *Coord. Chem. Rev.* **1974**, *13*, 339-406.
9. Ye, S. F.; Neese, F. *J. Am. Chem. Soc.* **2010**, *132*, 3646-3647.
10. Culotta, E.; Koshland, D. E. *Science* **1992**, *258*, 1862-1865.
11. Furchgott, R. F. *Biosci. Rep.* **1999**, *19*, 235-251.
12. Ignarro, L. J. *Biosci. Rep.* **1999**, *19*, 51-71.
13. Murad, F. *Biosci. Rep.* **1999**, *19*, 133-154.

14. Szacilowski, K.; Chmura, A.; Stasicka, Z. *Coord. Chem. Rev.* **2005**, *249*, 2408-2436.

15. Calabrese, V.; Mancuso, C.; Calvani, M.; Rizzarelli, E.; Butterfield, D. A.; Stella, A. M. G. *Nat. Rev. Neurosci.* **2007**, *8*, 766-775.

16. Santolini, J. *J. Inorg. Biochem.* **2011**, *105*, 127-141.

17. Tennyson, A. G.; Lippard, S. J. *Chem. Biol.* **2011**, *18*, 1211-1220.

18. Toledo, J. C.; Augusto, O. *Chem. Res. Toxicol.* **2012**, *25*, 975-989.

19. Mingos, D. M. P., *Struct. Bond.* **2014**, *153*, 1-232.

20. Eldik, R. v.; Olabe, J. A., *Adv. Inorg. Chem.* **2015**, *67*, 2-375.

21. Vanin, A. F. In *Bioorganometallic Chemistry*; Wiley-VCH Verlag GmbH & Co. KGaA: **2014**, 203-238.

22. Hickok, J. R.; Sahni, S.; Shen, H.; Arvind, A.; Antoniou, C.; Fung, L. W. M.; Thomas, D. D. *Free Radical Biol. Med.* **2011**, *51*, 1558-1566.

23. Lewandowska, H.; Kalinowska, M.; Brzoska, K.; Wojciuk, K.; Wojciuk, G.; Kruszewski, M. *Dalton Trans.* **2011**, *40*, 8273-8289.

24. Mulsch, A.; Mordvintcev, P.; Vanin, A. F.; Busse, R. *FEBS Lett.* **1991**, *294*, 252-256.

25. Lok, H. C.; Sahni, S.; Richardson, V.; Kalinowski, D. S.; Kovacevic, Z.; Lane, D. J. R.; Richardson, D. R. *Free Radical Biol. Med.* **2014**, *75*, 14-29.

26. Cesareo, E.; Parker, L. J.; Pedersen, J. Z.; Nuccetelli, M.; Mazzetti, A. P.; Pastore, A.; Federici, G.; Caccuri, A. M.; Ricci, G.; Adams, J. J.; Parker, M. W.; Lo Bello, M. *J. Biol. Chem.* **2005**, *280*, 42172-42180.

27. Miller, M. R.; Megson, I. L. *Brit. J. Pharmacol.* **2007**, *151*, 305-321.

28. Wang, P. G.; Xian, M.; Tang, X. P.; Wu, X. J.; Wen, Z.; Cai, T. W.; Janczuk, A. J. *Chem. Rev.* **2002**, *102*, 1091-1134.

29. Burgaud, J. L.; Ongini, E.; Del Soldato, P. *Ann. NY. Acad. Sci.* **2002**, *962*, 360-371.

30. Yamamoto, T.; Bing, R. J. *P. Soc. Exp. Biol. Med.* **2000**, *225*, 200-206.

31. *Nitric Oxide Donors: for Pharmaceutical and Biological Applications*; Wang, P. G., Cai, T. B., Taniguchi, N., Eds.; Wiley-VCH: Weinheim, **2005**.

32. Butler, A. R.; Megson, I. L. *Chem. Rev.* **2002**, *102*, 1155-1166.

33. Conrado, C. L.; Bourassa, J. L.; Egler, C.; Wecksler, S.; Ford, P. C. *Inorg. Chem.* **2003**, *42*, 2288-2293.

34. Ford, P. C. *Acc. Chem. Res.* **2008**, *41*, 190-200.

35. Chen, Y. J.; Ku, W. C.; Feng, L. T.; Tsai, M. L.; Hsieh, C. H.; Hsu, W. H.; Liaw, W. F.; Hung, C. H. *J. Am. Chem. Soc.* **2008**, *130*, 10929-10938.

36. Vanin, A. F.; Burbaev, D. S. *J. Biophys.* **2011**, *2011*, 1-14.

37. Chazov, E. I.; Rodnenkov, O. V.; Zorin, A. V.; Lakomkin, V. L.; Gramovich, V. V.; Vyborov, O. N.; Dragnev, A. G.; Timoshin, A. A.; Buryachkovskaya, L. I.; Abramov, A. A.; Massenko, V. P.; Arzamastsev, E. V.; Kapelko, V. I.; Vanin, A. F. *Nitric Oxide-Biol. Chem.* **2012**, *26*, 148-156.

38. Vanin, A. F.; Chazov, E. I. *Biophysics* **2011**, *56*, 268-275.

39. Skodje, K. M.; Kwon, M. Y.; Chung, S. W.; Kim, E. *Chem. Sci.* **2014**, *5*, 2374-2378.

40. Tran, C. T.; Skodje, K. M.; Kim, E. In *Progress in Inorganic Chemistry: Volume 59*; John Wiley & Sons, Inc.: 2014, 339-380.

41. Hess, J. L.; Hsieh, C. H.; Reibenspies, J. H.; Darensbourg, M. Y. *Inorg. Chem.* **2011**, *50*, 8541-8552.

42. Huang, H. W.; Tsou, C. C.; Kuo, T. S.; Liaw, W. F. *Inorg. Chem.* **2008**, *47*, 2196-2204.

43. Lu, T. T.; Tsou, C. C.; Huang, H. W.; Hsu, I. J.; Chen, J. M.; Kuo, T. S.; Wang, Y.; Liaw, W. F. *Inorg. Chem.* **2008**, *47*, 6040-6050.

44. Tsai, F. T.; Chiou, S. J.; Tsai, M. C.; Huang, H. W.; Chiang, M. H.; Liaw, W. F. *Inorg. Chem.* **2005**, *44*, 5872-5881.

45. Tonzetich, Z. J.; Do, L. H.; Lippard, S. J. *J. Am. Chem. Soc.* **2009**, *131*, 7964-7965.

46. Tsai, M.-L.; Tsou, C.-C.; Liaw, W.-F. *Acc. Chem. Res.* **2015**, *48*, 1184-1193.

47. Tsai, M.-L.; Chen, C.-C.; Hsu, I. J.; Ke, S.-C.; Hsieh, C.-H.; Chiang, K.-A.; Lee, G.-H.; Wang, Y.; Chen, J.-M.; Lee, J.-F.; Liaw, W.-F. *Inorg. Chem.* **2004**, *43*, 5159-5167.

48. Shih, W.-C.; Lu, T.-T.; Yang, L.-B.; Tsai, F.-T.; Chiang, M.-H.; Lee, J.-F.; Chiang, Y.-W.; Liaw, W.-F. *J. Inorg. Biochem.* **2012**, *113*, 83-93.

49. Fitzpatrick, J.; Kalyvas, H.; Shearer, J.; Kim, E. *Chem. Commun.* **2013**, *49*, 5550-5552.

50. Tonzetich, Z. J.; Héroguel, F.; Do, L. H.; Lippard, S. J. *Inorg. Chem.* **2011**, *50*, 1570-1579.

51. Nhut, G. T.; Kalyvas, H.; Skodje, K. M.; Hayashi, T.; Moenne-Loccoz, P.; Callan, P. E.; Shearer, J.; Kirschenbaum, L. J.; Kim, E. *J. Am. Chem. Soc.* **2011**, *133*, 1184-1187.

52. Skodje, K. M.; Williard, P. G.; Kim, E. *Dalton Trans.* **2012**, *41*, 7849-7851.

53. McBride, D. W.; Stafford, S. L.; Stone, F. G. A. *Inorg. Chem.* **1962**, *1*, 386-388.

54. Atkinson, F. L.; Blackwell, H. E.; Brown, N. C.; Connelly, N. G.; Crossley, J. G.; Orpen, A. G.; Rieger, A. L.; Rieger, P. H. *J. Chem. Soc., Dalton Trans.* **1996**, *0*, 3491-3502.

55. Reginato, N.; McCrory, C. T. C.; Pervitsky, D.; Li, L. J. *J. Am. Chem. Soc.* **1999**, *121*, 10217-10218.

56. Darnault, C.; Volbeda, A.; Kim, E. J.; Legrand, P.; Vernede, X.; Lindahl, P. A.; Fontecilla-Camps, J. C. *Nat. Struct. Mol. Biol.* **2003**, *10*, 271-279.

57. Huang, W.; Jia, J.; Cummings, J.; Nelson, M.; Schneider, G.; Lindqvist, Y. *Structure* **1997**, *5*, 691-699.

58. Denny, J. A.; Darensbourg, M. Y. *Chem. Rev.* **2015**.

59. Miller, M. L.; Ibrahim, S. A.; Golden, M. L.; Darensbourg, M. Y. *Inorg. Chem.* **2003**, *42*, 2999-3007.

60. Hung, M.-C.; Tsai, M.-C.; Lee, G.-H.; Liaw, W.-F. *Inorg. Chem.* **2006**, *45*, 6041-6047.

61. Hsieh, C. H.; Chupik, R. B.; Brothers, S. M.; Hall, M. B.; Darensbourg, M. Y. *Dalton Trans.* **2011**, *40*, 6047-6053.

62. Pinder, T. A.; Montalvo, S. K.; Hsieh, C. H.; Lunsford, A. M.; Bethel, R. D.; Pierce, B. S.; Darensbourg, M. Y. *Inorg. Chem.* **2014**, *53*, 9095-9105.

63. Anderson, J. S.; Hieber, W.; Mitarbeitern *Z. Anorg. Allg. Chem.* **1932**, *208*, 238-248.

64. Rauchfuss, T. B.; Weatherill, T. D. *Inorg. Chem.* **1982**, *21*, 827-830.

65. Hsieh, C. H.; Darensbourg, M. Y. *J. Am. Chem. Soc.* **2010**, *132*, 14118-14125.

66. Hsieh, C. H.; Chupik, R. B.; Pinder, T. A.; Darensbourg, M. Y. *Polyhedron* **2013**, *58*, 151-155.

67. Chiang, C. Y.; Miller, M. L.; Reibenspies, J. H.; Darensbourg, M. Y. *J. Am. Chem. Soc.* **2004**, *126*, 10867-10874.

68. Chiang, C. Y.; Darensbourg, M. Y. *J. Biol. Inorg. Chem.* **2006**, *11*, 359-370.

69. Li, L. J. *Comments Inorg. Chem.* **2002**, *23*, 335-353.

70. Hopkinson, M. N.; Richter, C.; Schedler, M.; Glorius, F. *Nature* **2014**, *510*, 485-496.

71. Riener, K.; Haslinger, S.; Raba, A.; Hogerl, M. P.; Cokoja, M.; Herrmann, W. A.; Kuhn, F. E. *Chem. Rev.* **2014**, *114*, 5215-5272.

72. Jenkins, R. M.; Singleton, M. L.; Leamer, L. A.; Reibenspies, J. H.; Darensbourg, M. Y. *Inorg. Chem.* **2010**, *49*, 5503-5514.

73. Hess, J. L.; Hsieh, C. H.; Brothers, S. M.; Hall, M. B.; Darensbourg, M. Y. *J. Am. Chem. Soc.* **2011**, *133*, 20426-20434.

74. Chaudhuri, P.; Karpenstein, I.; Winter, M.; Lengen, M.; Butzlaff, C.; Bill, E.; Trautwein, A. X.; Floerke, U.; Haupt, H. J. *Inorg. Chem.* **1993**, *32*, 888-894.

75. Chong, K. S.; Rettig, S. J.; Storr, A.; Trotter, J. *Can. J. Chem.* **1979**, *57*, 3119-3125.

76. Holloway, L. R.; Clough, A. J.; Li, J. Y.; Tao, E. L.; Tao, F. M.; Li, L. J. *Polyhedron* **2014**, *70*, 29-38.

77. Pierpont, C. G.; Eisenber.R *Inorg. Chem.* **1972**, *11*, 1088-1093.

78. Hayton, T. W.; McNeil, W. S.; Patrick, B. O.; Legzdins, P. *J. Am. Chem. Soc.* **2003**, *125*, 12935-12944.

79. Dillinger, S. A. T.; Schmalle, H. W.; Fox, T.; Berke, H. *Dalton Trans.* **2007**, 3562-3571.

80. *APEX2*, version 2009.7-0; Bruker AXS Inc.: Madison, WI, 2007.

81. *SAINTPLUS*: *Program for Reduction of Area Detector Data*, version 6.63; Bruker AXS Inc.: Madison, WI, 2007.

82. Sheldrick, G. M. *SADABS*: *Program for Absorption Correction of Area Detector Frames*; Bruker AXS Inc.: Madison, WI, 2001.

83. Sheldrick, G. M. *SHELXS-97: Program for Crystal Structure Solution*; Universität Göttingen: Göttingen, Germany, 1997.

84. Sheldrick, G. M. *SHELXL-97: Program for Crystal Structure Refinement*; Universität Göttingen: Göttingen, Germany, 1997.

85. Mercury: Macrae, C. F.; Edgington, P. R.; McCabe, P.; Pidcock, E.; Shields, G. P.; Taylor, R.; Towler, M.; van de Streek, J. *J. Appl. Crystallogr.* **2006**, *39*, 453–457.

86. Connelly, N. G.; Gardner, C. *J. Chem. Soc., Dalton Trans.* **1976**, 1525-1527.

87. Gardiner, M. G.; Herrmann, W. A.; Reisinger, C.-P.; Schwarz, J.; Spiegler, M. *J. Organomet. Chem.* **1999**, *572*, 239-247.

88. Field, L. R.; Wilhelm, E.; Battino, R. *J. Chem. Thermodyn.* **1974**, *6*, 237-243.

89. Park, J.; Yi, X.; Gasem, K. A. M.; Robinson, R. L., Jr. *J. Chem. Eng. Data* **1995**, *40*, 245-247.

90. Chiang, C.-Y.; Lee, J.; Dalrymple, C.; Sarahan, M. C.; Reibenspies, J. H.; Darensbourg, M. Y. *Inorg. Chem.* **2005**, *44*, 9007-9016.

91. Ingleson, M. J.; Layfield, R. A. *Chem. Commun.* **2012**, *48*, 3579-3589.

92. Grubbs, R. H. *Angew. Chem. Int. Ed.* **2006**, *45*, 3760-3765.

93. McGibbon, G. A.; Heinemann, C.; Lavorato, D. J.; Schwarz, H. *Angew. Chem. Int. Ed.* **1997**, *36*, 1478-1481.

94. Sini, G.; Eisenstein, O.; Crabtree, R. H. *Inorg. Chem.* **2002**, *41*, 602-604.

95. Ruiz, J.; Perandones, B. F. *J. Am. Chem. Soc.* **2007**, *129*, 9298-9299.

96. Huertos, M. A.; Pérez, J.; Riera, L.; Díaz, J.; López, R. *Angew. Chem. Int. Ed.* **2010**, *49*, 6409-6412.

97. Brill, M.; Díaz, J.; Huertos, M. A.; López, R.; Pérez, J.; Riera, L. *Chem. Eur. J.* **2011**, *17*, 8584-8595.

98. Häller, L. J. L.; Page, M. J.; Erhardt, S.; Macgregor, S. A.; Mahon, M. F.; Naser, M. A.; Vélez, A.; Whittlesey, M. K. *J. Am. Chem. Soc.* **2010**, *132*, 18408-18416.

99. Ruiz, J.; Berros, A.; Perandones, B. F.; Vivanco, M. *Dalton Trans.* **2009**, 6999-7007.

100. Ruiz, J.; Perandones, B. F.; Van der Maelen, J. F.; García-Granda, S. *Organometallics* **2010**, *29*, 4639-4642.

101. Baker, M. V.; Barnard, P. J.; Brayshaw, S. K.; Hickey, J. L.; Skelton, B. W.; White, A. H. *Dalton Trans.* **2005**, 37-43.

102. Han, Y.; Huynh, H. V.; Tan, G. K. *Organometallics* **2007**, *26*, 6447-6452.

103. Tomson, N. C.; Crimmin, M. R.; Petrenko, T.; Rosebrugh, L. E.; Sproules, S.; Boyd, W. C.; Bergman, R. G.; DeBeer, S.; Toste, F. D.; Wieghardt, K. *J. Am. Chem. Soc.* **2011**, *133*, 18785-18801.

104. Beck, W.; Fehlhammer, W. P. *Z. Anorg. Allg. Chem.* **2010**, *636*, 157-162.

105. Vanin, A. F. *Nitric Oxide* **2009**, *21*, 1-13.

106. Hayton, T. W.; Legzdins, P.; Sharp, W. B. *Chem. Rev.* **2002**, *102*, 935-992.

107. Ford, P. C.; Lorkovic, I. M. *Chem. Rev.* **2002**, *102*, 993-1018.

108. Boese, M.; Mordvintcev, P. I.; Vanin, A. F.; Busse, R.; Mulsch, A. *J. Biol. Chem.* **1995**, *270*, 29244-29249.

109. Ding, H.; Demple, B. *Proc. Natl. Acad. Sci. U.S.A.* **2000**, *97*, 5146-5150.

110. Albano, V. G.; Araneo, A.; Bellon, P. L.; Ciani, G.; Manassero, M. *J. Organomet. Chem.* **1974**, *67*, 413-422.

111. Chen, C.-H.; Ho, Y.-C.; Lee, G.-H. *J. Organomet. Chem.* **2009**, *694*, 3395-3400.

112. Jo, D. H.; Chiou, Y. M.; Que, L. *Inorg. Chem.* **2001**, *40*, 3181-3190.

113. Motterlini, R.; Otterbein, L. E. *Nat. Rev. Drug Discov.* **2010**, *9*, 728-743.

114. Wu, L.; Wang, R. *Pharmacol Rev.* **2005**, *57*, 585-630.

115. Kajimura, M.; Fukuda, R.; Bateman, R. M.; Yamamoto, T.; Suematsu, M. *Antioxid. Redox Sign.* **2010**, *13*, 157-192.

116. Szabo, C. *Sci. Transl. Med.* **2010**, *2*.

117. Mann, B. E.; Motterlini, R. *Chem. Commun.* **2007**, 4197-4208.

118. Crabtree, R. H. *The organometallic chemistry of the transition metals*; Wiley: New York, 1988.

119. Stamler, J. S.; Singel, D. J.; Loscalzo, J. *Science* **1992**, *258*, 1898-1902.

120. Jordan, R. B. *Reaction mechanisms of inorganic and organometallic systems* Oxford University Press: Oxford; New York, 2007.

121. Leffler, J. E.; Grunwald, E. *Rates and equilibria of organic reactions*, Dover Publications, 1963.

122. Kraihanzel, C. S.; Cotton, F. A. *Inorg. Chem.* **1963**, *2*, 533-540.

123. Cotton, F. A. *Inorg. Chem.* **1964**, *3*, 702-711.

124. Antonello, S.; Benassi, R.; Gavioli, G.; Taddei, F.; Maran, F. *J. Am. Chem. Soc.* **2002**, *124*, 7529-7538.

125. Antonello, S.; Daasbjerg, K.; Jensen, H.; Taddei, F.; Maran, F. *J. Am. Chem. Soc.* **2003**, *125*, 14905-14916.

126. Daasbjerg, K.; Jensen, H.; Benassi, R.; Taddei, F.; Antonello, S.; Gennaro, A.; Maran, F. *J. Am. Chem. Soc.* **1999**, *121*, 1750-1751.

127. Ji, C.; Goddard, J. D.; Houmam, A. *J. Am. Chem. Soc.* **2004**, *126*, 8076-8077.

128. Hammond, G. S. *J. Am. Chem. Soc.* **1955**, *77*, 334-338.

129. Hartinger, C. G.; Nazarov, A. A.; Ashraf, S. M.; Dyson, P. J.; Keppler, B. K. *Curr. Med. Chem.* **2008**, *15*, 2574-2591.

130. Gottschaldt, M.; Schubert, U. S. *Chem. Eur. J.* **2009**, *15*, 1548-1557.

131. Zhang, H. L.; Ma, Y.; Sun, X. L. *Med. Res. Rev.* **2010**, *30*, 270-289.

132. Sharon, N.; Lis, H. *Sci. Am.* **1993**, *268*, 82-89.

133. Kean, W. F.; Hart, L.; Buchman, W. W. *Brit. J. Rheumatol.* **1997**, *36*, 560-572.

134. Mjos, K. D.; Orvig, C. *Chem. Rev.* **2014**, *114*, 4540-4563.

135. McKeage, M. J.; Maharaj, L.; Berners-Price, S. J. *Coord. Chem. Rev.* **2002**, *232*, 127-135.

136. Raubenheimer, H. G.; Cronje, S. *Chem. Soc. Rev.* **2008**, *37*, 1998-2011.

137. Richter-Addo, G. B.; Hodge, S. J.; Yi, G.-B.; Khan, M. A.; Ma, T.; Van Caemelbecke, E.; Guo, N.; Kadish, K. M. *Inorg. Chem.* **1996**, *35*, 6530-6538.

138. Hess, J. L.; Conder, H. L.; Green, K. N.; Darensbourg, M. Y. *Inorg. Chem.* **2008**, *47*, 2056-2063.

139. Purser, S.; Moore, P. R.; Swallow, S.; Gouverneur, V. *Chem. Soc. Rev.* **2008**, *37*, 320-330.

140. Maschauer, S.; Prante, O. *Biomed. Res. Int.* **2014**, *2014*, 214748.

141. Szabo, C.; Ischiropoulos, H.; Radi, R. *Nat. Rev. Drug Discov.* **2007**, *6*, 662-680.

142. Lappin, A. G.; McAuley, A. *J. Chem. Soc., Dalton Trans.* **1978**, 1606-1609.

143. Neuba, A.; Haase, R.; Meyer-Klaucke, W.; Flörke, U.; Henkel, G. *Angew. Chem. Int. Ed.* **2012**, *51*, 1714-1718.

144. Furukawa, Y.; Torres, A. S.; O'Halloran, T. V. *EMBO J.* **2004**, *23*, 2872-2881.

145. Wang, X.; Sundberg, E. B.; Li, L.; Kantardjieff, K. A.; Herron, S. R.; Lim, M.; Ford, P. C. *Chem. Commun.* **2005**, 477-479.

146. Kolks, G.; Lippard, S. J.; Waszczak, J. V.; Lilienthal, H. R. *J. Am. Chem. Soc.* **1982**, *104*, 717-725.

147. Nishioka, T.; Shibata, T.; Kinoshita, I. *Organometallics* **2007**, *26*, 1126-1128.

148. Tewes, F.; Schlecker, A.; Harms, K.; Glorius, F. *J. Organomet. Chem.* **2007**, *692*, 4593-4602.

149. Shi, J. C.; Lei, N.; Tong, Q. S.; Peng, Y. R.; Wei, J. F.; Jia, L. *Eur. J. Inorg. Chem.* **2007**, 2221-2224.

150. Kascatan-Nebioglu, A.; Melaiye, A.; Hindi, K.; Durmus, S.; Panzner, M. J.; Hogue, L. A.; Mallett, R. J.; Hovis, C. E.; Coughenour, M.; Crosby, S. D.; Milsted, A.; Ely, D. L.; Tessier, C. A.; Cannon, C. L.; Youngs, W. J. *J. Med. Chem.* **2006**, *49*, 6811-6818.

151. Kascatan-Nebioglu, A.; Panzner, M. J.; Garrison, J. C.; Tessier, C. A.; Youngs, W. J. *Organometallics* **2004**, *23*, 1928-1931.

152. Hu, J. J.; Bai, S. Q.; Yeh, H. H.; Young, D. J.; Chi, Y.; Hor, T. S. A. *Dalton Trans.* **2011**, *40*, 4402-4406.

153. Coneski, P. N.; Schoenfisch, M. H. *Chem. Soc. Rev.* **2012**, *41*, 3753-3758.